DOE Environmental Management Science Program
Final Report

Project Title: **DNAPL Surface Chemistry: Its Impact on DNAPL Distribution in the Vadose Zone and its Manipulation to Enhance Remediation**

EMSP Project Number: 70035

Primary EM Problem Area: Subsurface Contamination

Principal Investigators:

Lead PI: Dr. Susan E. Powers
Clarkson University
Potsdam NY 13699-5710
315-268-6542 (PN)
315-268-7985 (FN)
sep@clarkson.edu

Co-PI: Dr. Stefan Grimberg
Clarkson University
Potsdam NY 13699-5710
315-268-6490 (PN)
grimberg@clarkson.edu

Co-PI: Dr. Miles E. Denham
Westinghouse Savannah River Company
Building 773-42A
Aiken SC 29808
803-725-5521 (PN)
miles.denham@srs.gov

Additional Researchers: Sang-Il Hwang, Post Doctoral Research Associate
Kamel Omrane, M.S. Candidate
Thomas Doty, M.S. candidate
John Cianci, M.S. candidate
M. R. Millings, WSRC Employee

Date: June 15, 2003

Prepared for the U.S. Department of Energy Under Contracts Nos.
DE-FG07-99ER15006 and DE-AC09-96SR18500

Disclaimers

Any opinions, findings, and conclusions or recommendations expressed in this material are those of the authors and do not necessarily reflect the views of the Department of Energy.

Executive Summary

A three-year collaborative research project between researchers at Clarkson University and Westinghouse Savannah River Company allowed concurrent field and laboratory research to provided an improved understanding of the distribution of DNAPL (dense non-aqueous phase liquid) in the vadose zone at the A-14 outfall area at the Savannah River Site (SRS) and the causes and significance of this distribution. It is very clear that the chemical and biological heterogeneities at this site are critically important and could be unique to the waste streams discharged at DOE facilities. The near surface soils were highly weathered and had a higher surface area that expected. Discharge of a wide range of acid, base and aluminum complexes could have contributed to these observations. DNAPL collected from the M-area basin was acidic and had a very low interfacial tension. The interfacial tension could also have been reduced through microbial activity. Anaerobic microorganisms present at the site produce biosurfactants and/or biopolymers that contribute to a reduced IFT when stressed by the presence of oxygen.

The reduction in interfacial tension observed through biological activity and the DNAPL composition could both have a significant affect on the flow and remediation of DNAPL in the subsurface. Reduced interfacial tensions allow the DNAPL to enter fine-grained media. Thus, either the DNAPL IFT or biological activity could have promoted the entry of DNAPL into fine-grained layers at SRS. The significance of this was apparent from our field characterization of the DNAPL distribution at SRS relative to soil vapor extraction (SVE) remediation efforts. Strata with a higher fraction of finer material were correlated to higher DNAPL concentrations, suggesting that the SVE system was less effective in removing DNAPL in these layers. Heterogeneity in the vadose zone creates microscopic areas where dissolved oxygen concentrations are extremely low, allowing for anaerobic organisms to proliferate. Operational changes in the SVE system due to seasonal fluctuations may have impacted dissolved oxygen levels in the vadose zone, thereby exposing the anaerobic cells to varying concentrations of oxygen. It is conceivable, therefore, that microbial activity at the A-14 Outfall Area affected the distribution of DNAPL.

The data presented here suggest that heterogeneity in the subsurface has resulted in heterogeneous removal of DNAPL. Yet, in this case the heterogeneity is not readily apparent from bulk sediment properties but required characterization of surface chemistry, mineralogy and bacterial data on a microscale. These results emphasize the complexity of the system and the need to integrate field and laboratory based studies into these types of investigations.

Table of Contents

List of Figures

List of Tables

Project Report

1.0 Research basis and objectives

The remediation of DNAPLs in subsurface environments is often limited by the heterogeneous distribution of the organic fluid. The fraction of DNAPL that is in the high conductivity regions of the subsurface can often be recovered relatively easily, although DNAPL in lower conductivity regions is much more difficult to extract, either through direct pumping or remediation measures based on interface mass transfer. The distribution of DNAPL within the vadose zone is affected by a complex interplay of heterogeneities in the porous matrix and the interfacial properties defining the interactions among all fluid and solid phases. Decreasing the interfacial tension between a DNAPL and water in the vadose zone could change the spreading of the DNAPL, thereby increase the surface area for mass transfer and the effectiveness of soil vapor extraction remediation.

Interfacial properties in the vadose zone are affected by the presence of surface-active materials. Complex NAPL mixtures that include petroleum-based constituents often contain surface-active compounds that can decrease interfacial tensions or alter the wetting properties of the system (Powers *et al*., 1996). Increasing the biological activity can also alter the interfacial phenomena governing multiphase flow. Chlorinated solvents such as TCE can be degraded in an aerobic environment through co-metabolism, potentially leading to the production of surface-active biological exudates. Similarly, higher chlorinated compounds such as PCE are degraded in an anaerobic environment, which could lead to the production of surface-active compounds. Adhesion of the microorganisms themselves at interfaces could also reduce capillary forces.

The primary hypothesis of this work was that surface-active chemicals and/or microorganisms present in the unsaturated zone can significantly alter interfacial phenomena governing the migration of DNAPLs, thereby affecting the accessibility of a DNAPL during remediation efforts. The surface-active materials are present in complex NAPL mixtures and are produced through microbial metabolic processes. The overall goal of this research was to understand the role of and changes in interfacial phenomena on the accessibility of DNAPL in the vadose zone.

Four objectives have been defined to meet this overall goal.

1. Understand and quantify the interfacial properties of DNAPLs in response to biological activity or the presence of surface-active constituents within the DNAPL mixture or aqueous phase.
2. Identify conditions under which CT and TCE co-metabolizing cultures affect interfacial properties through the production of surface-active materials or by adhering at NAPL interfaces.
3. Quantify the net effects associated with DNAPL surface chemistry on phenomena governing multiphase flow in the unsaturated zone and remediation efforts.
4. Examine the role of surface chemistry on the distribution of DNAPL in a field setting.

2.0 Research Approach

A multi-task approach involving experimental measurements at both laboratory and field scales was designed to meet the objectives of this research (Figure 2.1). Materials for this research were chosen to be applicable to vadose zone contamination problems at the Savannah River site (SRS). This research offered a unique opportunity to develop our fundamental understanding of the fate of DNAPLs in the vadose zone through both laboratory scale testing and evaluation of field samples collected at SRS. The fieldwork provides a detailed assessment of the distribution of DNAPL in the subsurface as a function of microbial populations, mineral characterization, and heterogeneous grain size distribution. Concurrent

laboratory testing provided an understanding of the fundamental mechanisms governing these distributions.

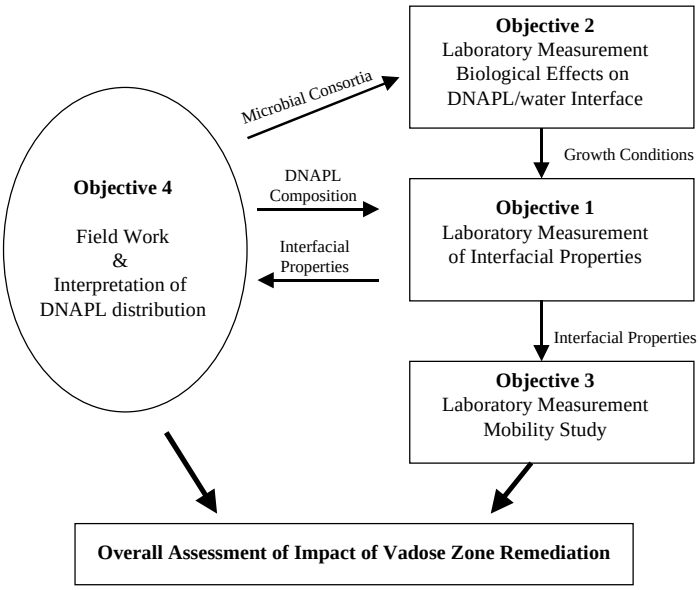

Figure 2.1: Approach for meeting the objectives of this research grant

The close coupling between lab and field provides deeper understanding of NAPL behavior in the vadose zone. This understanding could, in turn, be used to develop strategies better suited to target NAPL remediation for such fine-grained layers. Initial stages of the research focused on well-characterized materials with a shift to SRS site-specific media as the fundamental processes became better understood.

3.0 Activities Completed to Meet the Objectives

Researchers at Clarkson University (CU) and SRS completed the research conducted under this grant between September 15, 1999 and March 14, 2003. Laboratory work was conducted both at CU (in support of objectives 1-3) and SRS (objective 4). Two rounds of fieldwork at SRS provided samples for analysis and provided a quantitative assessment of the distribution of microbial activity and DNAPL as a function of stratigraphy and mineral composition in the vadose zone at the M-area and A-14 outfall area (Figure 3.1)

Table 3.1 provides an overview of the work completed to meet the stated objectives. As our work progressed, the tasks and findings for objectives 1 and 2 merged and are treated here in a single section. The scope of our work was also modified to focus primarily on SRS issues. Thus, our original intent to study interfacial tension changes associated with carbon tetrachloride degrading organisms was changed to focus on a bacterial population of PCE/TCE degraders isolated from SRS sediments. For objective 3, our work focused on multiphase flow rather than remediation efforts due to the unrealistic laboratory set up that could not incorporate all of the physical, chemical and biological heterogeneities that were observed to limit remediation efforts at SRS. Overall, these changes provided an opportunity to focus most specifically on the issues associated with SRS.

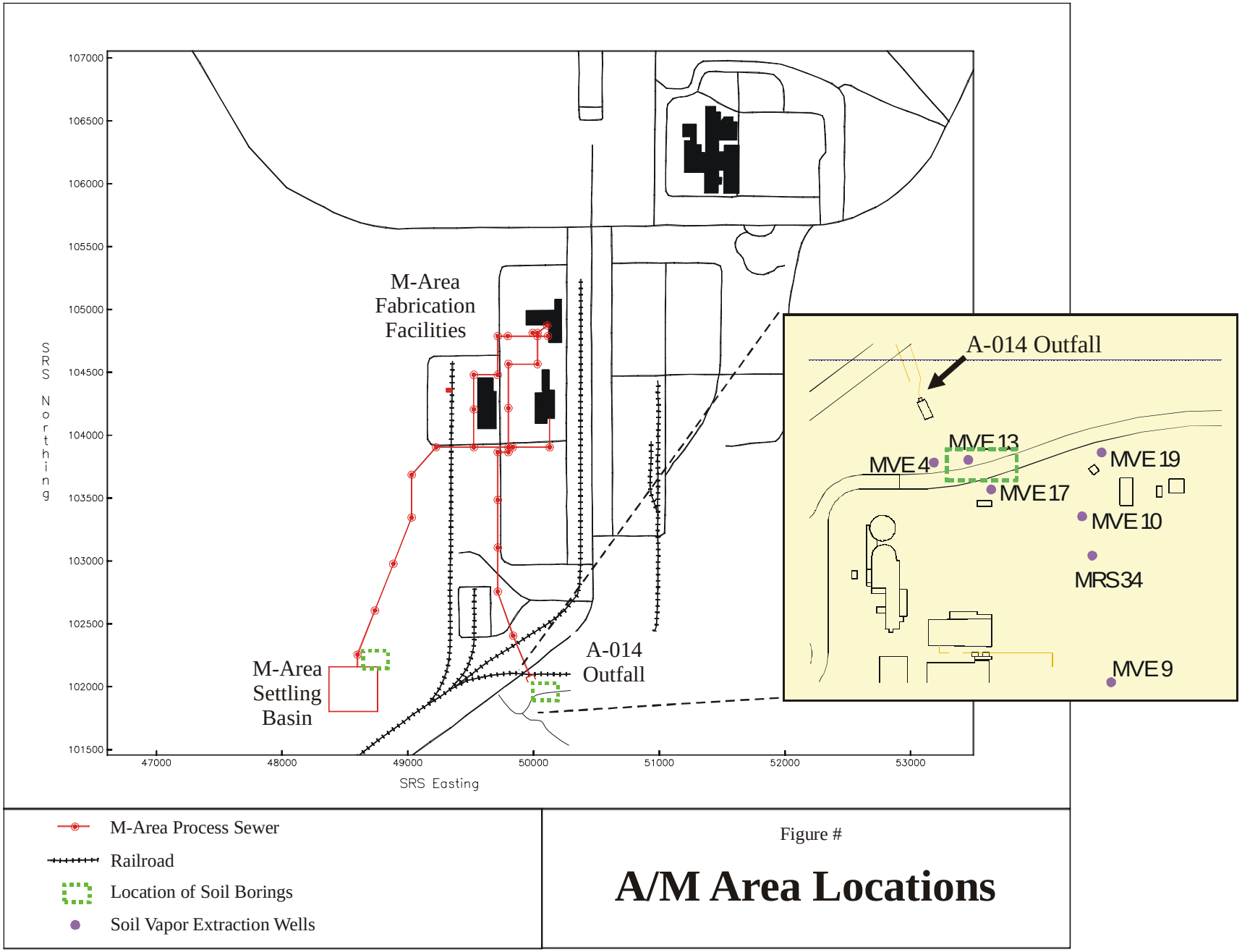

Figure 3.1: SRS site layout

Table 3.1: Work completed to meet stated objectives

Objective	Related Activities	Deviations from Initial Proposals
1. Understand and quantify the interfacial properties of DNAPLs in response to biological activity or the presence of surface-active constituents within the DNAPL mixture or aqueous phase. 2. Identify conditions under which CT and TCE co-metabolizing cultures affect interfacial properties through the production of surface-active materials or by adhering at NAPL interfaces.	Surface (ST) and interfacial tension (IFT) measured for two microbial cultures over a range of growth conditions. Adhesion properties measured for two PCE-degrading microbial cultures over a range of growth conditions. Surface/Interfacial tension measured for SRS DNAPL and a range of synthetic DNAPL mixtures	MATH assay adhesion tests were used to assess microbial adhesion and cell hydrophobicity rather than the originally proposed contact angle measurements CT degradation and associated changes in interfacial properties were not assessed in order to focus most closely on SRS issues Additional efforts were extended to begin to characterize the DNAPL because of its very low interfacial tension
3. Quantify the net effects associated with DNAPL surface chemistry on phenomena governing multiphase flow in the unsaturated zone and remediation efforts.	Experimental apparatus designed, built and used to quantify the distribution of DNAPL/water and contaminated water/air in 2-D micromodel. Experimental apparatus designed, built and used to quantify permeability-saturation-pressure (k-S-P) relationships for DNAPL/water and contaminated water/air. (Note – no experiments were completed under active remediation efforts) Mathematical development of models describing pressure saturation curves from grain size distributions were developed	Difficulties in the experimental approach with anaerobic bacteria prevented us from using microorganisms directly in either of these systems. We instead used fluids with IFTs that were representative of the range of those observed in microbial systems. Results of micromodel experiments were assessed at a larger scale than proposed in order to utilize a fractal model to interpret differences in fluid migration and distribution as a function of wetting and IFT Based on review of field results, volatilization column experiments were not conducted. It would be difficult to represent the significance of DNNAPL accessibility in fine grained media in column experiments.

Table 3.1: Work completed to meet stated objectives (con't)

4. Examine the role of surface chemistry on the distribution of DNAPL in a field setting.	Two rounds of drilling/sample collection completed at the SRS site. Samples characterized for VOCs, microbial activity, grain size distribution, mineralogy, and surface area. Quantitative sample characteristics correlated to better understand DNAPL distribution related to microbial growth and grain size distribution.	Due to a change of PI at SRS, the focus of this work was more on the soil mineralogy and chemistry rather than fractures within the clay. This change was discussed and approved when the SRS contract was initiated in 1999.

4.0 Significant Findings

Research conducted as part of this EMSP project provided us with an improved understanding of the distribution of DNAPL in the vadose zone at the A-14 outfall area at the Savannah River Site (SRS) and the causes and significance of this distribution. It is very clear that the chemical and biological heterogeneities at this site are critically important. The very low interfacial tension of the SRS DNAPL (< 2 mN/m) and the higher than expected weathering and surface area of the porous media could both be attributed to the discharge of a wide variety of materials at this site. Waste streams to the A-014 Outfall also included metal hydroxide precipitates, acids, caustics, and industrial lubricants and cleaning compounds. Wide swings in the pH associated with these wastes could have contributed to the unique characteristics that were observed at this site.

Biological activity was also observed to reduce the surface tension of water and interfacial tension between a solvent and water. The most notable reductions occurred when anaerobic PCE degrading communities were stressed with dissolved oxygen or PCE. Relative to experimental controls, the surface tension (ST) decreased by as much as 11% and the interfacial tension (IFT) by as much as 43% at dissolved oxygen concentrations of 1.5 mg/L. ST decreased by 15% when the PCE concentration was close to its solubility limit. The much more significant decline in IFT relative to ST in the presence of oxygen as a stressor suggested that biosurfactant production was not the only mechanism responsible for these declines. Based on a series of control experiments and the nature of our experiments, we concluded that the production of biopolymers and coagulation of biotic or abiotic colloidal materials to a size sufficient to promote gravity settling could be responsible for the significant decline in the IFT.

The reduction in interfacial tension observed through biological activity and the DNAPL composition could both have a significant affect on the flow and remediation of DNAPL in the subsurface. Micromodel and multi-step outflow experiments both showed the significance of the reduced interfacial tension. As expected, the entry pressure of the DNAPL is much lower when the IFT is decreased, allowing it to enter finer grained media. Thus, either the DNAPL IFT or biological activity could have promoted the entry of DNAPL into fine-grained layers at SRS. The relative surface area of residual DNAPL in a two-fluid system is also higher at low IFT due to differences in the capillary entrapment processes. There were no observed changes in the relative permeability as a function of variable IFT.

The significance of DNAPL entry into finer grained media was apparent from our field characterization of the DNAPL distribution at SRS relative to soil vapor extraction (SVE) remediation efforts. Strata with a higher fraction of finer material were correlated to higher DNAPL concentrations, suggesting that the SVE system was less effective in removing DNAPL from these layers. Since the surface area of the soil declined gradually in both cores as a function of depth but the d50 remained similar, the observed weathering processes dominate at the top 20 feet of the soil cores. Concurrently, bacterial concentrations were highest at high DNAPL concentrations (>22 ft depth). Heterogeneity in the vadose zone creates microscopic areas where dissolved oxygen concentrations are extremely low, allowing for anaerobic organisms to proliferate. Operational changes in the SVE system due to seasonal fluctuations may have impacted dissolved oxygen levels in the vadose zone, thereby exposing the anaerobic cells to varying concentrations of oxygen. It is conceivable, therefore, that microbial activity at the A-14 Outfall Area affected the distribution of DNAPL.

The data presented here suggest that heterogeneity in the subsurface has resulted in heterogeneous removal of DNAPL. Yet, in this case the heterogeneity is not readily apparent from bulk sediment properties but required characterization of surface chemistry, mineralogy and bacterial data on a microscale. These results emphasize the complexity of the system and the need to integrate field and laboratory based studies into these types of investigations.

Details supporting these findings have been disseminated through a variety of papers and presentations (Section 5.0) and are summarized in Sections 6.0 – 8.0.

5.0 Research Products

5.1 Papers:

Grimberg, S.J., S.E. Powers, M. Denham, K. Chen, (2000) "Field Study to Correlate Chlorinated Solvent Concentrations and Microbial Distributions in the Unsaturated Zone." Published In: *Proceedings*, ACS Division of Environmental Chemistry, (Washington DC, August 2000), 40(2): 348-352.

Hwang, S., and S.E. Powers, (2003) "Estimating Unique Soil Hydraulic Parameters from Multi-Step Outflow Experiments with Sandy Media." *Adv. Water Res*. 26(4): 445-456.

Hwang, S.I. and S.E. Powers, (2003) "Lognormal Distribution Model for Estimating Soil Water Retention Curves for Sandy Soils." *Soil Science*, 168(3): 156-166.

Hwang, S., and S.E. Powers, "Dependence of water retention and unsaturated hydraulic conductivity characteristics on particle size distribution models." (in press *Soil Sci. Soc. Am. J*.)

Denham, M.E., S.J. Grimberg, M. R. Millings, S.E. Powers. "Vadose zone DNAPL distributions relative to physical, chemical and biological sources of heterogeneity at a field site." *Submitted to* J. Cont. Hydrology.

Hwang, S.I. and S.E. Powers, "Effects of variable interfacial properties on capillary pressure-saturation-relative permeability relationships for two-fluid systems." In preparation for submission to the *J. Contam. Hydrol*.

Cianci, J., S.I. Hwang and S.E. Powers, "Fractal Analysis to Evaluate Two-phase Fluid Distributions in Glass Bead Micromodels." In preparation for submission to *J. Contam. Hydrol*.

Doty, T., K. Omrane, S.E. Powers, S.J. Grimberg, The Role of PCE Degrading Microorganisms on DNAPL Interfacial Properties**.** In preparation.

5.2 Presentations at Conferences:

Cianci, J., S.I. Hwang and S.E. Powers, "Photo-visualization Study Illustrating the Effects of Interfacial Properties on Multiphase Flow in Glass Bead Micromodels." Poster presented at the Spring Annual Meeting of the American Geophysical Union. Boston MA, June, 2001.

Hwang, S.I., and S.E. Powers, "Using a Multi-step Outflow Technique to Estimate k-S-P Parameters for Contaminated Solutions." Poster presented at the Spring Annual Meeting of the American Geophysical Union. Boston MA, June, 2001.

Hwang, S.I., and S.E. Powers, "Using a Multi-Step Outflow Technique to Estimate Unsaturated Hydraulic Conductivity Function for Quartz Sands With Variable Interfacial Properties." Presented at the AGU Fall Meeting, San Francisco CA, December 2001.

Omrane, K., S.E. Powers, S.J. Grimberg, "Factors contributing to the low interfacial tension of the Savannah River DNAPL." *Presented* at the 76th ACS Colloid and Surface Science Symposium, Ann Arbor MI, June, 2002.

Doty, T, S.J. Grimberg, The Role Of Microorganisms On DNAPL Interfacial Properties And Transport. Abstract 289, *Presented* at the 3rd International Conference on Remediation of Chlorinated and Recalcitrant Compounds, Monterey, CA, May 20 – 23, 2002.

Hime, J., A. Crandall, S.J. Grimberg, Optimal Conditions for TCE Bioremediation. *Presented* at the 74th Annual Winter Meeting of the New York Water Environment Association, February 5, 2002, New York City, NY. (Received 2nd place award for student presentation)

5.3 Invited Lectures

Grimberg, S.J. (2003) Bacteria/DNAPL Interactions and Their Role on DNAPL Interfacial Properties. Presented to the Department of Inorganic, Analytical and Applied Chemistry, University of Geneva, Switzerland, June 6, 2003.

Grimberg, S.J. (2003) The role of microorganisms on DNAPL interfacial properties and DNAPL distribution. Presented under the Environmental Sciences Series of the EAWAG, Switzerland, May 23, 2003.

Grimberg, S.J. (2001) The Role of Microorganisms on DNAPL Interfacial Properties. Cornell University, Ithaca, NY, December 6, 2001.

Powers, S.E., S.J. Grimberg, M. Borkovec, and M. Denham (2000) DNAPL Surface Chemistry: Its Impact on DNAPL Distribution in the Vadose Zone and its Manipulation to Enhance Remediation. Presented at the Vadose Zone Workshop, Richland, WA, November 28-30, 2000.

Powers, S.E., S.J. Grimberg, M. Borkovec, and M. Denham (2000) DNAPL Surface Chemistry: Its Impact on DNAPL Distribution in the Vadose Zone and its Manipulation to Enhance Remediation. Presented at the Vadose Zone Workshop, Atlanta, GA, April 25-28, 2000.

Powers, S.E., S.J. Grimberg, M. Borkovec, and M. Denham (1999) DNAPL Surface Chemistry: Its Impact on DNAPL Distribution in the Vadose Zone and its Manipulation to Enhance Remediation. Presented at the Vadose Zone Workshop, Richland, WA, November 16-18, 1999.

5.4 Graduate Thesis

John A. Cianci (2002), Fractal Analysis to Evaluate the Interfacial Property Effects of Two-Phase Flow in Porous Media, Masters Thesis, Clarkson University, Potsdam NY.

Tom Doty (2003), The Role of Microorganisms on DNAPL Interfacial Properties and Distribution**,** Masters Thesis, Clarkson University, Potsdam NY.

Kamel Omrane (2003), Factors affecting the interfacial properties in the subsurface at the Savannah River Site, Masters Thesis, Clarkson University, Potsdam NY.

5.5 Undergraduate Research Reports

Effects of Nutrient Conditions on the Adhesion of Desulfuromonas chloroethinica by Contact Angle Measurement, Kathleen D. Gallagher, 2000.

Favorable Growth Conditions for TCE Bioremediation at Savannah River Site, Jeremiah Shackelford, 2000.

6.0 Research details - Objective 4

6.1 Objective

"Examine the role of surface chemistry on the distribution of DNAPL in a field setting."

(note – the findings from the field work help to lay a foundation for laboratory work. Thus, we present these results in detail first)

6.2 Description of the Field Site

The history of DNAPL contamination and remediation efforts at the DOE Savannah River Site (SRS) illustrates the importance of chemical and biological heterogeneities on the DNAPL distribution and remediation efficiencies.

SRS is situated along the Savannah River in west-central South Carolina. It is located in the Atlantic Coastal Plain physiographic province approximately 40 km (25 mi) southeast of the fall line, the boundary between the Coastal Plain and Piedmont provinces. The Coastal Plain is underlain by a seaward dipping wedge of unconsolidated and semi-consolidated sediments. The upper units of the Coastal Plain sediments in the A-14 Area of the SRS include the Upland Unit and the Tabacco Road Sand, both of which consist of alternating sands and fine-grained units (Eddy et al. 1991; Eddy-Dilek et al. 1993). The water table lies in the range of 40 to 43 m (130 to 140 ft). Substantial variation exists between the permeability of the sandy and clayey subunits.

SRS used and released chlorinated solvents and other chemicals to the subsurface during operations from the early 1950's through the mid 1980's. Solvents, primarily trichloroethylene (TCE), tetrachloroethylene (PCE), and 1,1,1-trichloroethane (1,1,1-TCA), were used in degreasing processes in facilities that fabricated reactor fuel and target assemblies for nuclear reactors. It has been estimated that 13 million pounds of chlorinated degreasing solvents were used. Of this total, 1.5 million pounds of solvent were estimated to have been released to the A-014 Outfall (Marine and Bledsoe, 1984; Looney et al., 1992).

In addition to the chlorinated solvents, waste streams to the A-014 Outfall also included metal hydroxide precipitates (e.g. aluminum, uranium, nickel and lead), acids (e.g. nitric, phosphoric, boric and sulfuric), caustics (e.g. sodium hydroxide), and industrial lubricant (e.g. lead oil) and cleaning compounds (Pickett et al., 1987; Jackson et al., 1996). Variations in operation schedules together with changes in products used through time resulted in varying waste stream chemistries and volumes discharged to outfall.

Dissolved solvents were detected in the ground water in 1981. Beginning in 1987, soil vapor extraction was implemented in various stages for vadose remediation within the A/M Area (Jackson et al., 1999). At the A-014 Outfall the soil vapor extraction system currently consists of seven wells screened at various depths within the vadose zone. More specifically, MVE-13, MVE-17, and MVE-19 target shallow contaminants (16-26 feet below land surface) close to the outfall whereas MVE-4, MVE-9, MVE-10, and MRS-34 are screened deeper within the vadose zone. Table 6.1 lists the wells, their installation dates, and approximate depths of their screen zones. The efficiency of the soil vapor extraction efforts was less than expected. Preliminary analysis suggested that this was due to the migration of the DNAPL into small pores (BHI, 1996). For better accessibility and recovery of the DNAPL in the SRS contaminated sand, it is therefore essential to understand factors governing DNAPL mobility in the subsurface.

Table 6.1: Wells used for SVE (see Figure 3.1 for locations)

Well ID	Well Installation Date	Approximate Screen Zone (ft bls)
MVE-4	9/1990	54-115
MVE-9	3/1994	35-102
MVE-10	3/1994	43-109
MVE-13	4/1999	17-27
MVE-17	4/1999	16-26
MVE-19	4/1999	14-24
MRS-34	4/2000	95-115

6.3 Methods

In March 2000 four soil borings were collected from the A/M-Area, two from the M-Area Settling Basin and two from the A-014 Outfall, using hollow stem augers and split spoons. Depth discrete sediment samples were collected at approximately 1-foot intervals for TCE, PCE and microbial analysis. Based on these analytical results, two additional soil borings were collected at the A-014 Outfall in May 2001 using direct push/rotary hammer (GeoProbe®) techniques. This method was used to collect continuous core samples in 4-foot long, 1¾ -inch diameter polycarbonate sleeves (Gregg In-Situ MacroCore™). Once collected the polycarbonate sleeves were split and depth discrete soil samples were collected at approximately 1-foot intervals for TCE, PCE and microbial analysis. The two soil borings (SB-01 and MHS-03) with the highest concentrations of TCE and PCE were chosen for more extensive analyses to investigate the interrelations between soil properties that may be important to DNAPL accumulation and remediation. Photos from this activity are included in Figures 6.1 and 6.2.

Chlorinated Solvent Analysis. The method for TCE and PCE analysis is a modified version of EPA Method 5021 and has been an effective analytical technique used in environmental characterization at SRS since 1991. The method involved collecting a plug of sediment (approximately 2 cm^3) from the core using a modified plastic syringe. The plug was placed in a 22-mL headspace vial with 5 mL of pure deionized water. The glass vial was then sealed with a crimped Teflon-lined septum top for headspace analysis. Duplicate samples were collected at each sample depth. For analysis of chlorinated solvents in liquid media, 1 mL of media was placed in a 7-mL headspace vial and sealed with a crimped Teflon-lined septum top for headspace analysis. Volatile analysis was performed using a Hewlett Packard 5890 or 6890 Series II gas chromatograph with electron capture (ECD) and flame ionization (FID) detectors in parallel with an automated headspace sampler at 70°C. A DB-5 capillary column (60 meters long, 0.25 mm inside diameter, and a 0.25-µm film thickness; J&W Scientific) was used to analyze chlorinated compounds. The temperature program was as follows: Injector temperature and detector temperature were kept constant at 250ºC and 300ºC, respectively. The initial column temperature of 40ºC was maintained for 2 minutes, followed by a 10ºC /min increase to 220ºC, at which point the temperature was then increased at a rate of 40ºC /min to 300ºC. The resulting overall run time was 22 minutes. Residence time of PCE was approximately 10 min using this method.

Microbial Enumeration Method. Bacterial concentrations in the soil core were measured in 1-foot intervals by removing 3 cm^3 soil plugs using sterile technique. The soil plugs were immediately stored at 4ºC and shipped daily for analysis at Clarkson University. Soil samples collected during the first sampling event were analyzed using the acridine orange direct count method (AODC), while the LIVE/DEAD *Bac*Light staining kit (Molecular Probes, Inc., Eugene, OR) was used for samples from the

second sampling event. The *Bac*Light kit contains two fluorescent dyes: SYTO 9, a green stain that generally labels all bacteria in a population – those with intact membranes and those with damaged membranes; and propidium iodide, a red stain that penetrates only bacteria with damaged membranes, causing a reduction in the SYTO 9 stain fluorescence. Approximately 5 mg of soil were mixed for 4 minutes with a mixture of 10-mL particle-free water and 0.01% stain. The sample was then filtered through a non-fluorescent 0.2-µm polycarbonate filter and bacterial cells were counted at 1250X magnification using a fluorescent microscope (Model BX-50, Olympus Inc.). Controls included particle-free water and sterilized soils. For each slide 20 fields were counted four times. All samples were analyzed in triplicate. Sample standard deviations were calculated for each measurement.

Figure 6.1: Photograph showing hollow stem augering at the A-14 Outfall.

Figure 6.2: Photograph showing sampling of split spoon core.

Biodegradation experiments. Soil samples from the most contaminated depths were used as inoculants in microcosm experiments to test for the presence of organisms that co-metabolize TCE and reductively dechlorinate PCE and TCE. Soil samples were suspended in mineral media appropriate for the respective redox conditions (Gerhadt et al. 1994). For the aerobic experiments, soil slurries (1 gram soil in 30 mL of media) were set up for a range of carbon sources (phenol, formate, acetate and toluene) to investigate what conditions would stimulate TCE co-metabolism. Both nitrate and ammonia were used (final concentrations 1 g/L) as potential nitrogen sources in the media. Microcosms were incubated at 30°C on an orbital shaker at 100 rpm. TCE concentrations in the headspace were monitored over time.

Methods for Detailed Soil Core Characterization. Analyses of soil properties for the two soil borings included grain size distribution, surface area, bulk chemistry, bulk mineralogy, soil pH, petrographic and scanning electron microscopy and gravimetric moisture. Grain size analyses were conducted according to an internal SRTC dry sieving procedure (Manual WSRC-L14.1, Procedure 2-43 Rev. 1, issued 10/30/92) with modifications to sieve sizes and disposition of samples. Surface area was determined by the BET nitrogen adsorption method using a Micromeritics ASAP2010 (Accelerated Surface Area and Pore volume analyzer) precision gas adsorption instrument. For bulk chemistry analysis, sediment samples were fused in a lithium tetraborate/lithium fluoride mixed flux, and a Rigaku 3271 wavelength dispersive x-ray fluorescence spectrometer was used to determine the elemental compositions. Bulk mineralogy of ground sediment samples was analyzed using a Siemens D500 diffractometer by step scanning over the 2Θ ranges of 3-70° with a step size of 0.02° and a dwell time of 1s. Soil pH was determined using ASTM Standard Test Method for pH of Soils (ASTM D4972-01). Petrographic thin sections made using standard commercial methods were examined using Leitz and Zeiss petrographic microscopes. Sediments were also analyzed using a Cambridge 250 scanning electron microscope to determine mineral morphology and distribution. Gravimetric moisture was determined by weight difference before and after oven drying.

6.4 Results

General Core Properties. Figure 6.3 shows sediment properties plotted as a function of depth for sediment borings SB-01 and MHS-03 at the A-014 Outfall. In general, sediment surface area and moisture content decrease with depth. Iron and aluminum concentrations also decrease with depth because they are associated with the fine-grained matrix of the sediments (data not shown). In both sediment borings the median grain size (d_{50}) increases gradually with depth and is largest in the depth interval from 18-23 feet. In sediment boring SB-01 this corresponds to a significant decrease in the concentrations of TCE and PCE. This also corresponds with the screened sections of the SVE extraction wells MVE 13 and 17 (Table 6.1), which were closest to SB-01. This pattern is not observed in sediment boring MHS-03; TCE and PCE concentrations are nearly constant with depth. Below 23 feet, d_{50} decreases with depth, indicating the presence of smaller particles. For homogenous particles the observed decreasing surface area in this depth range, however, would indicate an increase in particle size. This implies that an additional mechanism - other than variation in particle size - must be responsible for the observed decrease in surface area with depth.

TCE and PCE Concentrations. The one parameter for which there is a marked difference between the two sediment cores is solvent concentration. The highest concentrations in these cores are indicative of the presence of DNAPL. Samples with PCE concentrations larger than 45 mg/kg were considered to contain DNAPL (based on PCE solubility, a soil bulk density of 1.6 g/cm^3, and a water saturation of 0.75). TCE concentration in all sampled cores were at least one order of magnitude lower than measured PCE concentrations. Earlier analysis of the SRS DNAPL revealed an approximate composition of 80 % PCE (by vol) versus 20 % TCE. The concentrations of PCE and TCE in boring MHS-03 are relatively constant (10^3 mg/kg for PCE and 10^1 mg/kg for TCE) throughout the upper sampled depth interval (less than 27 ft. depth). Between a depth of 27 to 34 ft., PCE and TCE concentrations decreased gradually to 10^{-1} mg/kg and 10^{-3} mg/kg, respectively. In contrast, PCE and TCE concentrations varied by six and four orders of magnitude, respectively, throughout core SB-01. Concentrations gradually increased down to a depth of 17 feet to 10^4 mg/kg and 10^1 mg/kg for PCE and TCE respectively, followed by a sharp decrease in PCE and TCE concentrations at a depth interval of 17.5 to 25.0 feet in boring SB-01. This depth interval corresponds to the screen intervals of the shallow vapor extraction wells (Table 6.1), suggesting DNAPL removal within this depth interval at this core. This depth interval also corresponds to the increase in the median grain size in both borings, suggesting that the SVE efficiently removed most DNAPL at this depth. Below a depth of 25 feet in boring SB-01 concentrations initially increase sharply before they gradually decline to 10^{-1} and 10^{-2} mg/kg PCE and TCE, respectively, at a depth of 30 feet.

Bacterial distribution. Total bacterial concentrations varied in both cores by more than two orders of magnitude. Bacterial concentrations in core MHS-03 are about one order magnitude lower than in core SB-01. This difference is due to the selectivity of the analytical tests that were employed. For core MHS-03 we used a modified acridine orange direct counting method (AODC), while for core SB-01 the more sensitive LIVE/DEAD *Bac*Light stain was used, which allowed for detection of more cells in that core.

Bacterial cell concentrations in core MHS-03 remained low down to a depth of 22 feet. The relatively low cell concentrations may have been due to the higher amount of fines present in the top portion of the core, which would limit pore size. While the median grain size remained relatively constant at 0.3 mm for the top 15 feet, the surface area decreased gradually with depth, indicating a decreasing concentration of fine particulates throughout the depth of the boring (Figure 6.3). An order of magnitude increase in cell concentration was observed below 22 feet. The logarithm of cell concentrations were positively correlated with observed TCE and PCE concentrations in that interval (Figure 6.4).

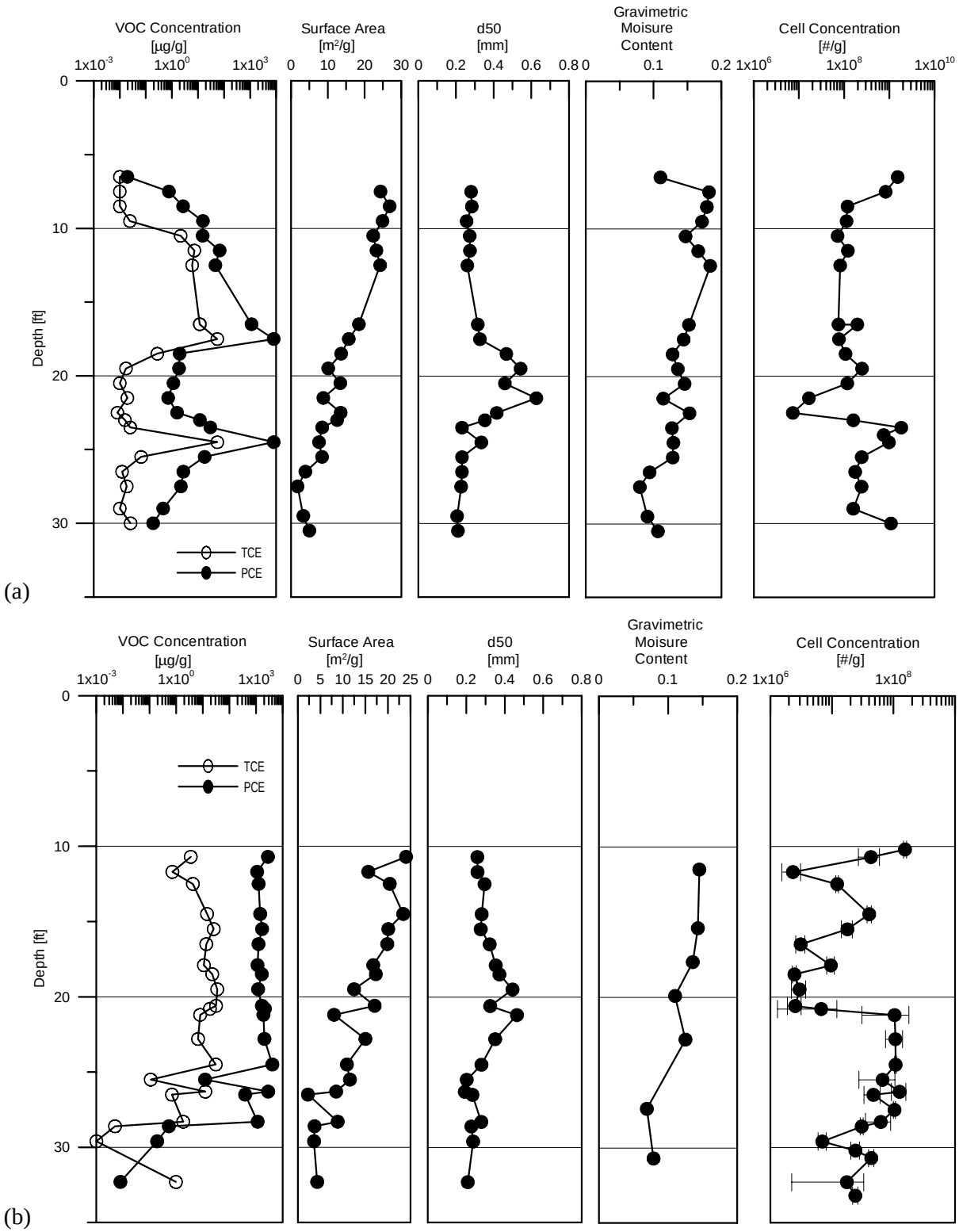

Figure 6.3: Characterization of soil borings SB-01 (a) and MHS-03 (b).

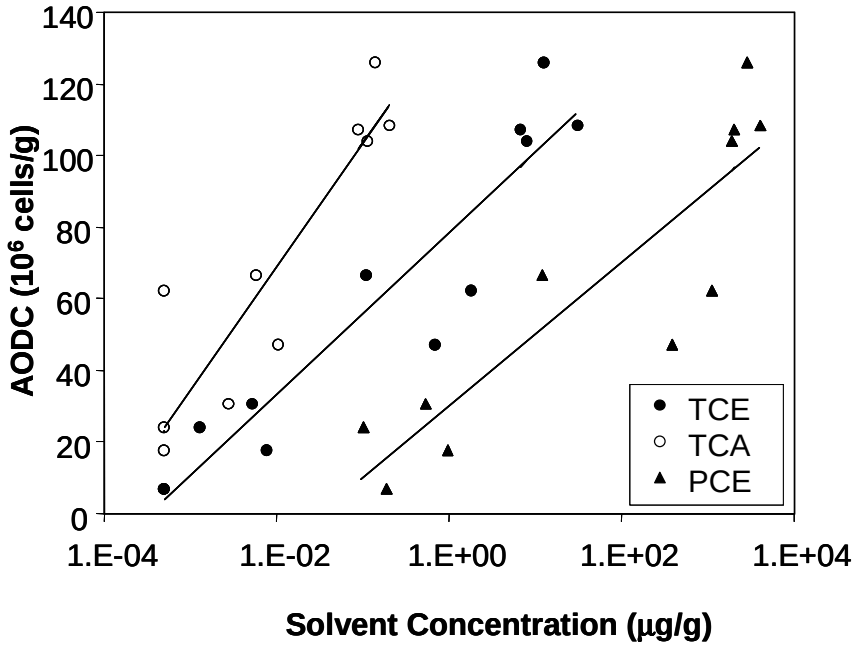

Figure 6.4: Cell Concentration as a function of VOC concentrations in boring MHS-03 below 20 feet.

Similarly, cell concentrations in core SB-01 also remained constant over the first 20 feet. Fine-grained porous media in this section again seemed to limit the distribution of cells. As shown in Figure 6.3 for MHS-03, cell concentrations in this boring were also correlated with contaminant concentrations below 20 feet ($r^2 = 0.91$, n = 10; correlation not shown). In this deeper segment the soil pore spaces seemed sufficiently large to allow for growth to occur. In the coarser grained layer where efficient removal of DNAPL due to the active SVE system occurred (depth ~22 ft), bacterial concentrations were lowest at 8×10^6 cell/g. The gravimetric soil moisture content in that region was measured to be 18 %, not significantly different than in other core sections. Desiccation due to the SVE operation therefore cannot explain the low bacterial concentrations in this apparently well-aerated soil section.

Further characterization of the microbial community revealed that the community was capable of co-metabolizing TCE under aerobic conditions as well as reductively dechlorinating PCE and TCE under anaerobic conditions (Doty et al, in preparation). Microcosm experiments using soil from various sections of both cores under aerobic conditions revealed the most rapid TCE degradation using phenol as a primary carbon and energy source. No TCE biodegradation relative to an un-inoculated control was observed using either acetate or sodium formate as carbon sources, while some biodegradation was observed when toluene and nitrate were used as carbon and nitrogen sources, respectively. Biodegradation rates of TCE in phenol-amended microcosms were independent of the nitrogen source and were equal to 0.3 mg TCE/g soil/day. In the anaerobic samples PCE disappearance and the concurrent appearance of TCE, DCE and VC were observed after 14 days of incubation (Doty et al., in preparation). However, no biodegradation rates were quantified for that system.

Grain Size: The sediments in the top 30 feet near the A-14 Outfall can be classified as coarse to fine grain sands with minor fine-grained material. For this study, fine-grained material is defined as the silt and clay fraction (<0.075 mm). This fraction varies from 4.4 to 15.7 wt % in boring SB-01 and from 5.3 to 13.8 wt. % in boring MHS-03. A much greater variation is observed in the relative abundances of the sand-sized fractions. Figure 6.5 shows grain size in both borings classified as medium to coarse sand (>0.25 mm), very fine to fine sand (0.075-0.25 mm), and fine-grained material (<0.075 mm). The largest

variation in grain size is from the medium/coarse sand compared to very fine/fine sand. Much of this variation is associated with an increase in the coarse/medium fraction at a depth interval of 17.5 to 23.5 feet in sediment boring SB-01. A similar feature occurs in sediment boring MHS-03 at a depth interval of 15.5 to 25.5 feet.

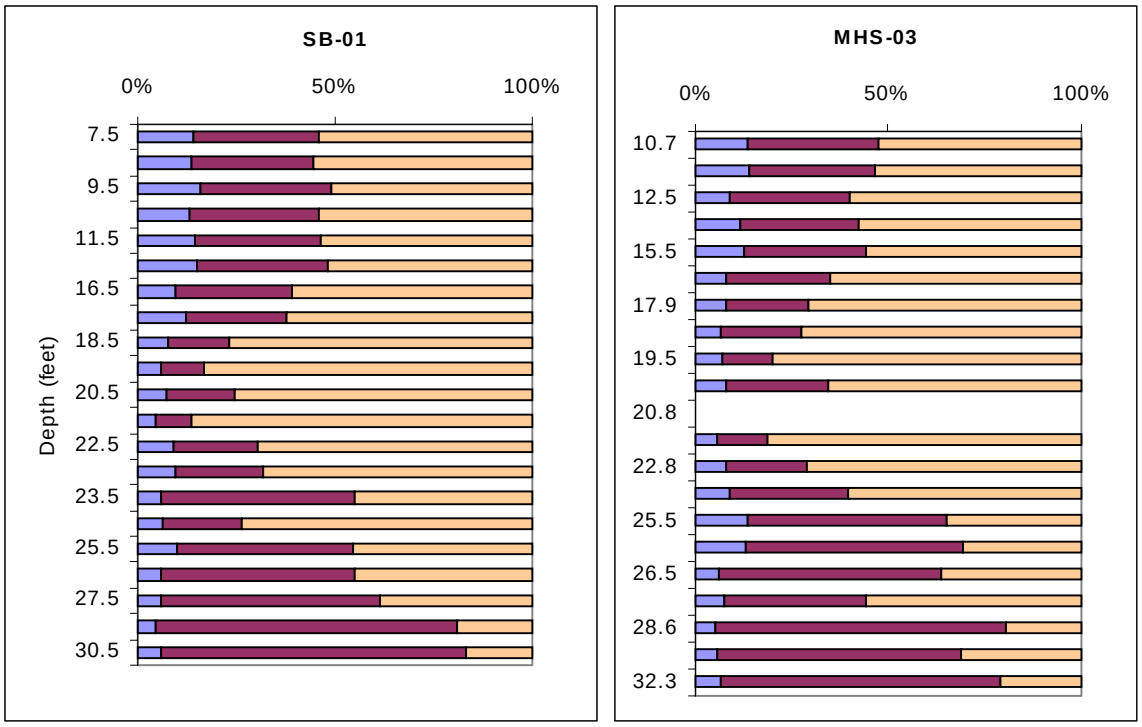

Figure 6.5: Plots of grain size variation with depth. Blue bars represent fine grained material (< 0.075 mm), maroon bars represent very fine to fine grained sand (between 0.075 and 0.25 mm), tan bars represent medium to coarse sand (> 0.25 mm).

Mineralogy/Chemistry: The mineralogy of the sediment borings, as determined by powder x-ray diffraction, is dominated by quartz, kaolinite, and hematite. This is consistent with the bulk chemistry determined by x-ray fluorescence spectroscopy. Figure 6.6 shows Si, Al, and Fe x-ray fluorescence data plotted as the fraction of quartz, kaolinite, and hematite in the sediments. The observed pattern is typical of SRS sediments that are composed of quartz sand with a pore-filling matrix of fine-grained kaolinite and hematite. The linear trend of the A-14 Outfall data indicates that the fraction of hematite (0.18) to kaolinite (0.82) is relatively constant across most of the samples. Thus, variations in bulk chemistry are the result of variations in the amount of matrix relative to quartz, rather than variations in the mineralogy of the matrix. This may have implications for DNAPL migration because it suggests that the pH at which the net surface charge on the matrix is zero is constant throughout the sediment column.

There are other trends in the chemical composition of these samples that are useful to note. Figures 6.7 and 6.8 suggest that the A-14 Outfall samples may be enriched in iron relative to aluminum over other SRS samples. The titanium to iron ratios of A-14 Outfall samples are at the lower range of those observed in SRS samples. In contrast, the titanium to aluminum ratios appear higher than in other SRS samples (Figure 6.9). Natural weathering processes should not alter the relative concentrations of titanium, iron, and aluminum because these elements all tend to be conserved at normal groundwater pH and oxidizing conditions. Thus, differences in A-14 Outfall ratios from other SRS samples would suggest that there are differences in depositional mineralogy or that the corrosive chemistry often disposed at the A-14 Outfall altered the ratios.

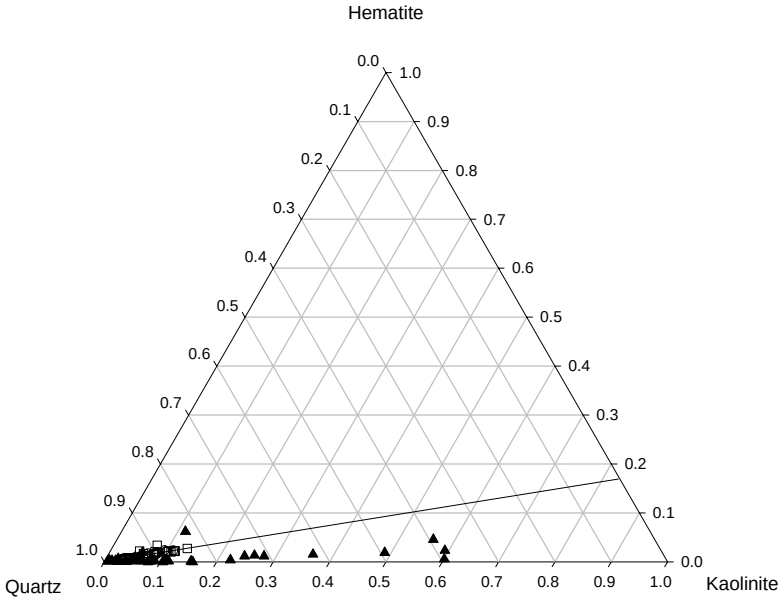

Figure 6.6: Ternary diagram of x-ray fluorescence data plotted as fraction of quartz, kaolinite, and hematite. Open circles are samples from SB-01, open squares are from MHS-03, triangles are from background cores P-16, P-28, and P-30 (Strom and Kaback, 1992).

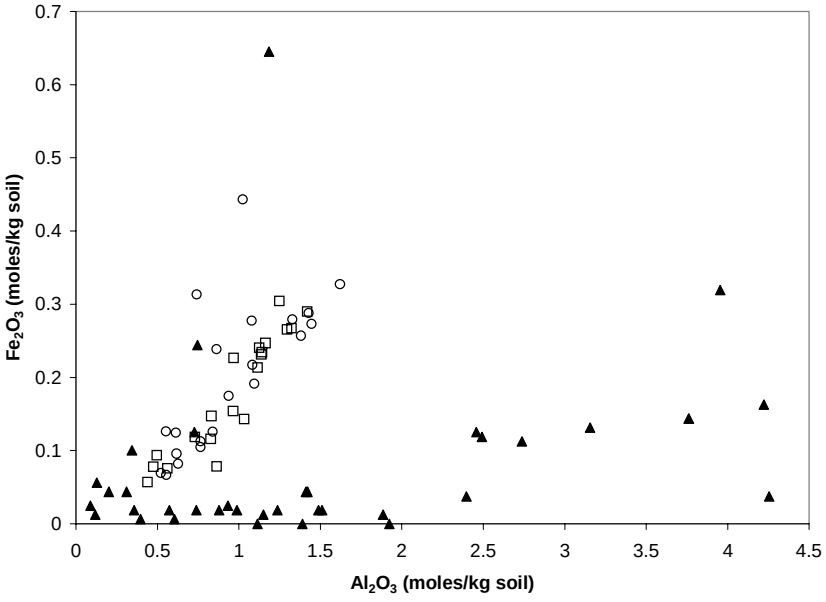

Figure 6.7: Fe_2O_3 versus Al_2O_3 (moles/kg). Open circles are samples from SB-01, open squares are from MHS-03, triangles are from background cores P-16, P-28, and P-30 (Strom and Kaback, 1992).

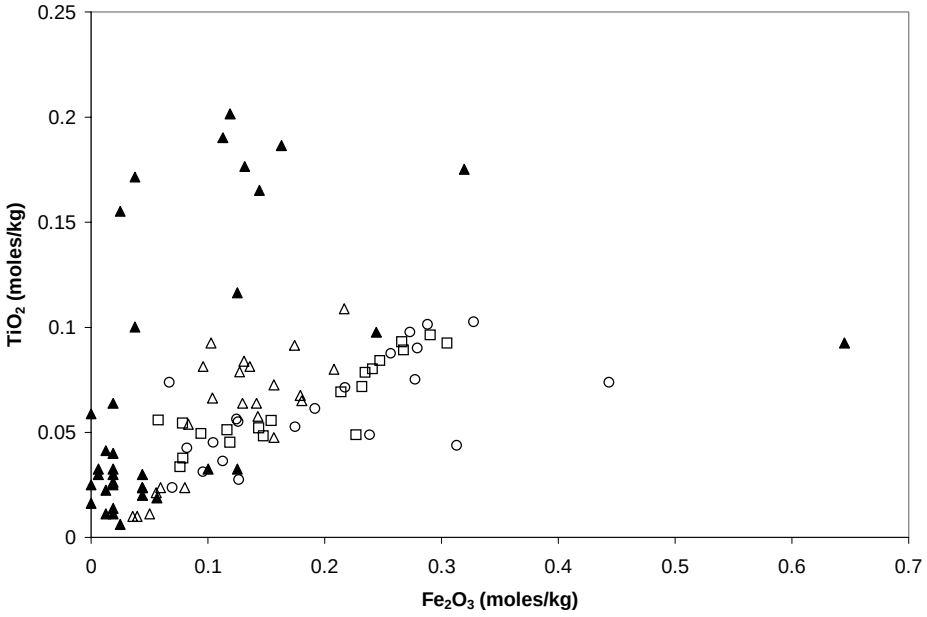

Figure 6.8: TiO2 versus Fe2O3 (moles/kg). Open circles are samples from SB-01, open squares are from MHS-03, closed triangles are from background cores P-16, P-28, and P-30 (Strom and Kaback, 1992), open triangles are from shallow A/M Area cores reported in Denham et al. (1999).

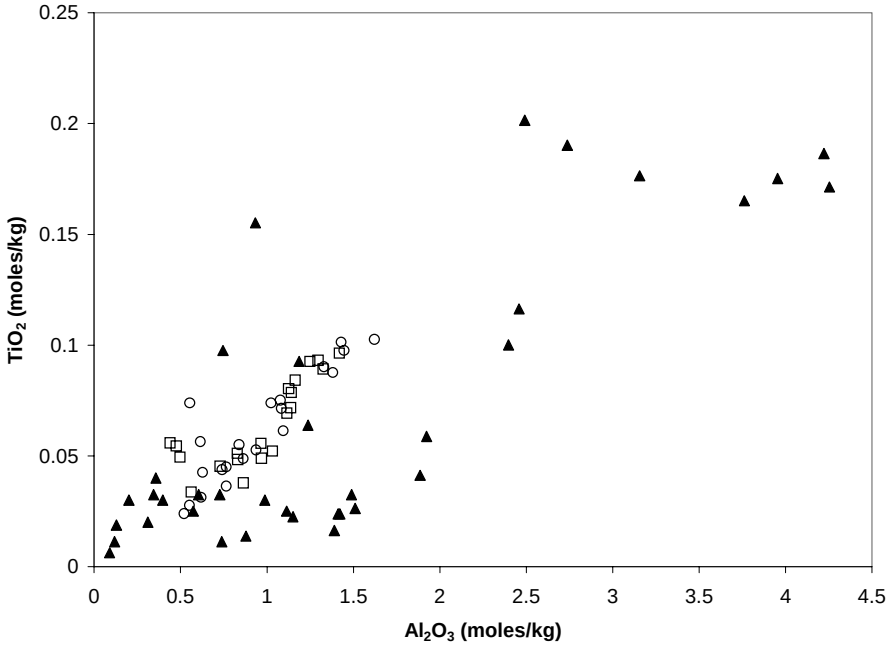

Figure 6.9: TiO_2 versus Al_2O_3 (moles/kg). Open circles are samples from SB-01, open squares are from MHS-03, triangles are from background cores P-16, P-28, and P-30 (Strom and Kaback, 1992).

Sediment samples from SRS, including those from the A-14 Outfall, show an excess of aluminum over an ideal mixture of quartz and kaolinite. Figure 6.10 shows the Al_2O_3 concentrations plotted versus the SiO_2 concentrations for A-14 Outfall samples and SRS background samples. The solid line represents the trend for a mixture of quartz and kaolinite. Samples that plot above this line have an excess of aluminum that is probably the result of the highly weathered nature of South Carolina coastal plain sediments. Under these weathering conditions kaolinite typically weathers to gibbsite because of preferential leaching of silica. However, it is noteworthy that the A-14 Outfall samples tend to show less excess aluminum than other SRS samples. Again, this could be the result of different depositional mineralogy or the effect of corrosive solutions disposed at the A-14 Outfall.

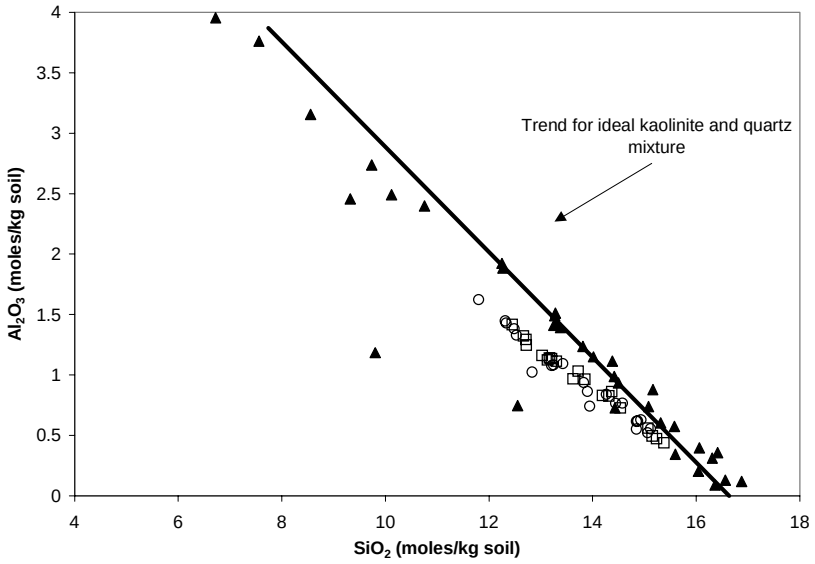

Figure 6.10: Al_2O_3 versus SiO_2 (moles/kg). Open circles are samples from SB-01, open squares are from MHS-03, triangles are from background cores P-16, P-28, and P-30 (Strom and Kaback, 1992).

The potential effect of corrosive solutions on sediment chemistry can be examined by comparing solubilities of pertinent phases. Figure 6.11 shows the calculated solubilities of kaolinite and gibbsite versus pH. At normal groundwater conditions (pH between 5 and 7) gibbsite is the less soluble phase, indicating that kaolinite will ultimately weather to gibbsite. The solubilities converge at alkaline conditions suggesting that disposed alkaline solutions would not alter the aluminum silica ratios of a mixture of quartz, kaolinite, and gibbsite. Conversely, at acidic conditions kaolinite becomes less soluble than gibbsite and gibbsite may dissolve relative to kaolinite. This would result in removal of some of the excess aluminum formed during weathering. Hematite is less soluble than both kaolinite and gibbsite at all oxidizing conditions. Therefore, corrosive solutions could leach aluminum relative to iron resulting in elevated iron to aluminum ratios.

The compositional trends observed in the A-14 Outfall samples are consistent with exposure to acidic fluids, but these trends must be viewed with caution. The SRS background samples are from depth intervals extending to 755 feet compared to the maximum depth of 32.3 feet for the A-14 Outfall samples. In addition, the background samples come from cores collected over a large area. These factors enhance the possibility that the trends observed are the result of depositional differences. Furthermore, it has not been demonstrated here that these trends are statistically valid. Until those analyses are completed, the

compositional trends merely raise interesting possibilities rather than prove that disposed acid changed the nature of the sediments at the A-14 Outfall.

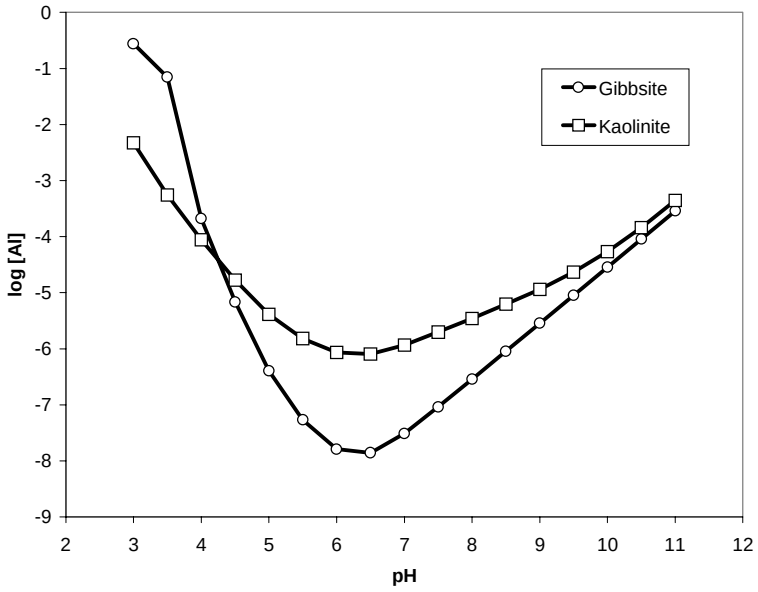

Figure 6.11: Solubility of gibbsite and kaolinite versus pH. Solubility expressed as total dissolved aluminum.

Surface Area: The fine-grained fraction in most sediments and soils is the dominant contributor to surface area. This holds true for samples from the A-14 Outfall. Figure 6.12 shows a comparison of the relationship between surface area and percent fine-grained material in A-14 Outfall samples and other studies. Samples from the A-14 Outfall have a significantly steeper slope than the other sets of samples. This suggests that the fine-grained matrix in A-14 Outfall samples has a higher specific surface area than the fine-grained material in the other studies reported here. Extrapolating the regression line for A-14 Outfall samples to 100% fine-grained matrix, yields a specific surface area of 151 m^2/g for this matrix. Given that the extrapolation is from a narrow range of values near the origin, a reasonable range of specific surface area values would be 100 to 200 m^2/g. This is higher than many other studies, but is in the range of values reported for kaolinitic tropical soil by Chorover and Sposito (1995).

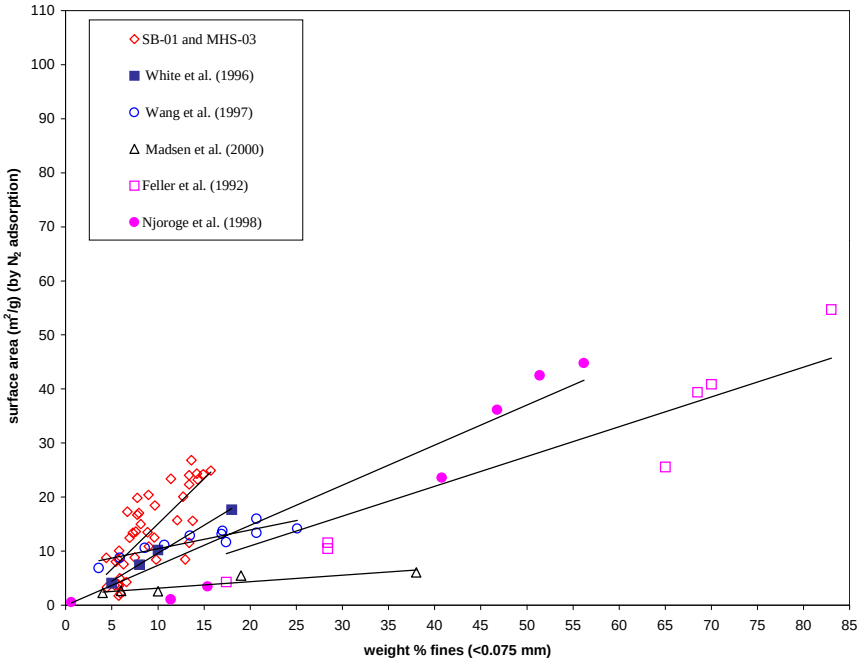

Figure 6.12: Specific surface area versus wt.% fines for A-14 Outfall samples compared to samples from other studies.

To examine the relationship of mineralogy to specific surface area, it was assumed that the total surface area is the sum of the surface area contributed by each mineral phase. Thus, the following equation allows surface areas to be calculated from mineralogical composition and values of specific surface for each mineral phase.

$$SA_{total} = SA_k * f_k + SA_h * f_h + SA_q * f_q$$

In this equation the total surface area of a sample (SA_{total}) is equal to the sum of the individual specific surface areas of kaolinite, hematite, and quartz (SA_k, SA_h, and SA_q respectively) times the fraction of each mineral in the sample (f_k, f_h, and f_q). Midpoints in the ranges of specific surface area values reported by Langmuir (1997) were used for each mineral (Table 6.2).

Table 6.2: Specific surface areas for various minerals from Langmuir (1997).

Mineral	**Specific Surface Area (m^2/g)**
Kaolinite	24
Hematite	2
Quartz	0.14

The fraction of each mineral was calculated from bulk chemical compositions of A-14 Outfall samples. Figure 6.13 shows how these calculated values relate to measured values. There is a strong linear trend in the calculated versus measured values, but it is well below the 1:1 line. This suggests that the model for calculating specific surface areas is valid, but that at least one phase used in the calculations has a specific surface area significantly higher than that reported in the literature. Of the three minerals, kaolinite requires the minimum increase in specific surface area values to give reasonable calculated values. The solid symbols in Figure 6.13 are the result of using a specific surface area for kaolinite of 200 m^2/g, rather

than 24 m^2/g. The specific surface area of hematite would have to be about 900 m^2/g to achieve a similar result.

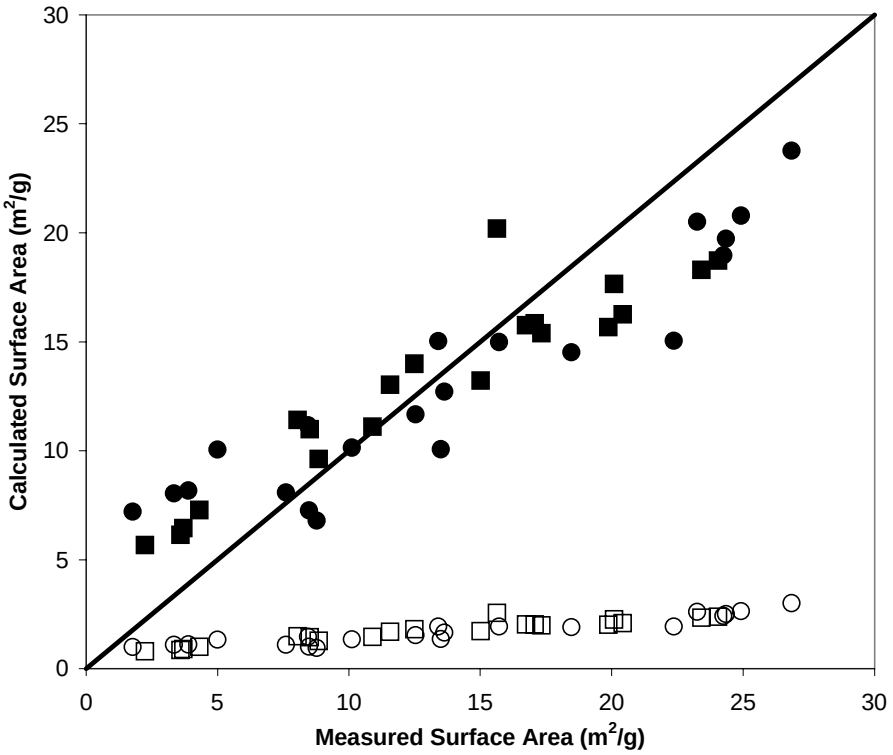

Figure 6.13: Calculated versus measured surface areas using the model discussed in the text.

Weathering tends to increase the specific surface area of natural sands. This may be because of an increase in surface roughness (White et al., 1996) or an increase in porosity from mineral dissolution (Kieffer et al., 1999). Yet, relatively pure Georgia kaolinite used in experiments by Huertas et al. (1998) had a specific surface area of only 8.16 m^2/g. A large difference in grain size could explain the difference between this value and specific surface areas of fine-grained matrix in A-14 Outfall samples. But, this difference may also be consistent with exposure of the A-14 Outfall samples to corrosive solutions. Both acidic and caustic solutions may increase microporosity in kaolinite. Likewise, incongruent dissolution of kaolinite in acid may result in an amorphous silica gel at the surface (Xie and Walther, 1992). The specific surface areas of such gels are high; Langmuir (1997) reports literature values ranging up to 292 m^2/g.

Textures revealed in scanning electron photomicrographs are consistent with high specific surface areas for A-14 Outfall samples. Figures 6.14 and 6.15 show the abundance of microporosity and microstructures in the fine-grained matrix. The presence of highly weathered grains also contributes to surface area (Figure 6.16). It should also be noted that micro-scale heterogeneties in the distribution of matrix complicate interpretation and prediction of behavior of fluids in these samples. For example, Figures 6.17 and 6.18 show very different distribution of matrix in two samples. The sample in Figure 6.18 may have a higher specific surface area as measured in the laboratory, but the surface area in contact with migrating fluids in the subsurface may actually be less than that in Figure 6.17.

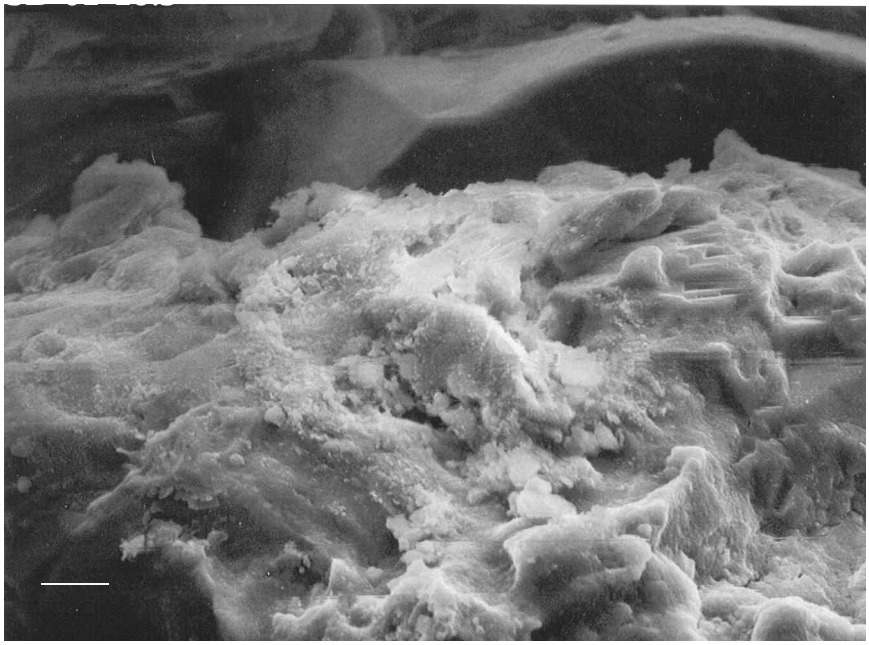

Figure 6.14: Scanning electron photomicrograph of sample SB-01-16.5.

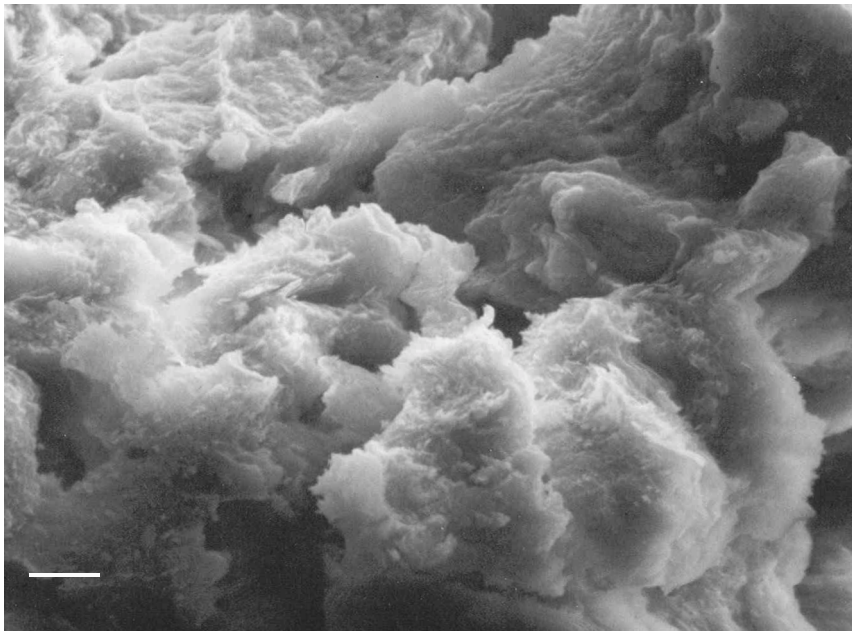

Figure 6.15: Scanning electron photomicrograph of sample SB-01-23.5.

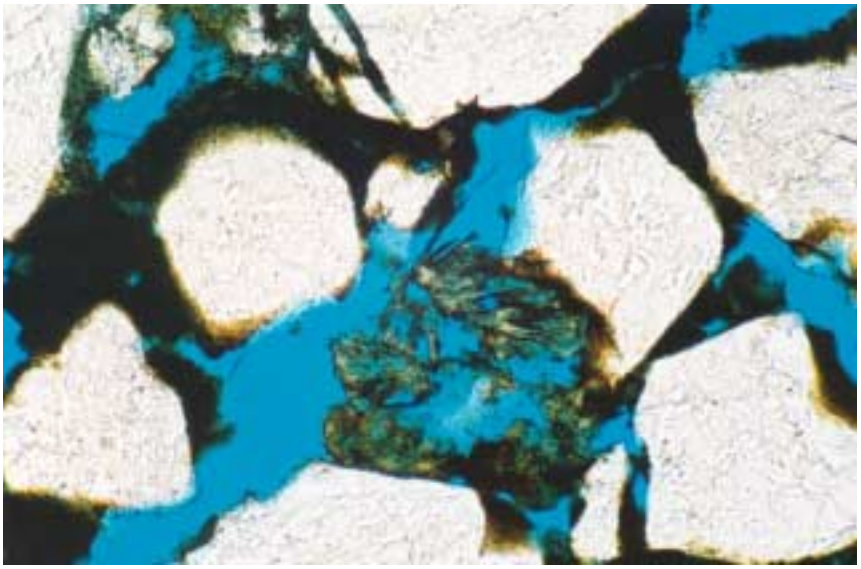

Figure 6.16: Thin-section photomicrograph of SB-01 sediment showing weathered grain. White grains are quartz, fine grained matrix is brown to black, porosity is blue. Scale is about 200 um across the bottom.

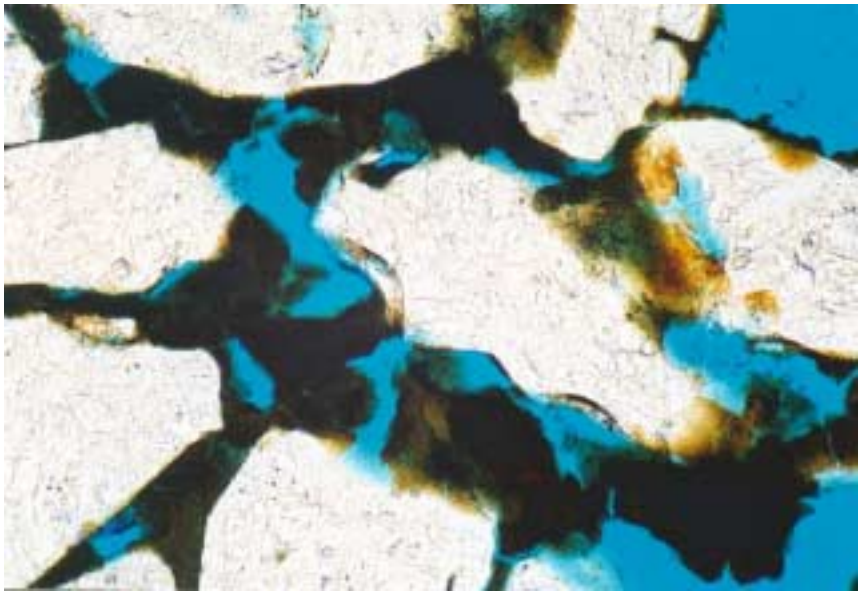

Figure 6.17: Thin-section photomicrograph showing typical texture of SB-01 sediment. White grains are quartz, fine-grained matrix is brown to black, porosity is blue. Scale is about 200 um across the bottom.

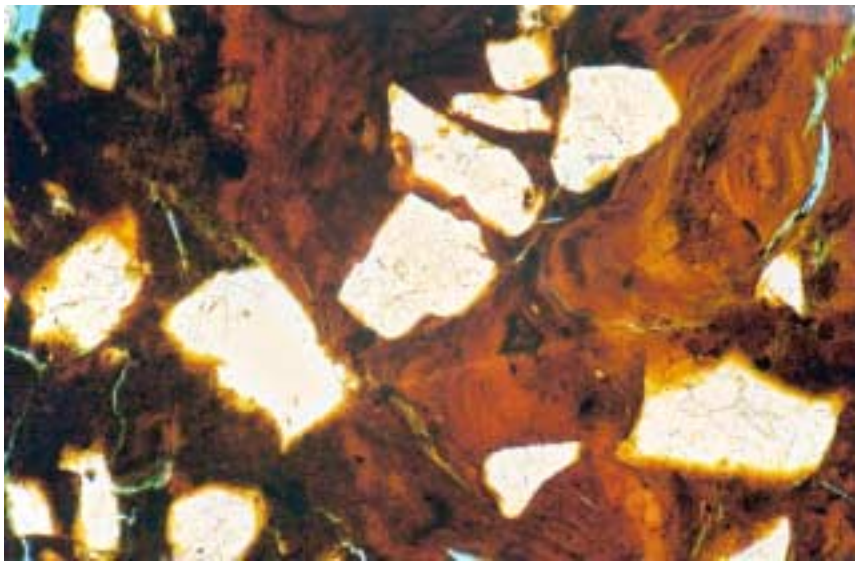

Figure 6.18: Thin-section photomicrograph of cemented nodule in SB-01. White grains are quartz, fine grained matrix is brown to black, porosity is blue. Scale is about 200 um across the bottom.

6.5 Conclusions

In summary, the measured abiotic soil properties seem to indicate that the soil in the A-014 Outfall Area has been extensively weathered, which may have contributed to the observed DNAPL presence in fine-grained material at this location. Textures revealed in scanning electron photomicrographs corroborate the high specific surface area measurements for A-014 Outfall samples. It should also be noted that micro-scale heterogeneties in the distribution of the matrix complicate interpretation and prediction of fluid behavior in these samples.

Since the surface area of the soil declined gradually in both cores as a function of depth but the d_{50} remained similar (with the exception of the 20-25 feet interval in core SB-01) the observed weathering processes dominate at the top 20 feet of the soil cores. Concurrently, bacterial concentrations were relatively low at the top 20 feet and at least one order of magnitude higher below 22 feet. At this depth the bacterial concentrations were highest at high DNAPL concentrations. Furthermore, tests indicated that the microbial consortium was capable of co-metabolizing TCE under aerobic conditions as well as degrading PCE via reductive dechlorination pathways (Doty, 2003). A range of organisms has been known to produce biosurfactants that either reduce the toxicity or enhance the bioavailability of sparsely soluble substrates. However, neither TCE- nor PCE- degrading organisms have been reported to produce biosurfactants. Under environmental stress some microorganisms excrete metabolic by-products that may exhibit surface-active properties. Doty et al. (submitted) has shown that two anaerobic PCE-degrading enrichment cultures will reduce the TCE/mineral media interfacial tension up to 43% when stressed by introducing oxygen at 1.5 mg/L. Heterogeneity in the vadose zone creates microscopic areas where dissolved oxygen concentrations are extremely low, allowing for anaerobic organisms to proliferate. Operational changes in the SVE system due to seasonal fluctuations may have impacted dissolved oxygen levels in the vadose zone, thereby exposing the anaerobic cells to varying concentrations of oxygen. It is conceivable, therefore, that microbial activity at the A-14 Outfall Area affected the distribution of DNAPL.

The data presented here suggest that heterogeneity in the subsurface has resulted in heterogeneous removal of DNAPL. Yet, in this case the heterogeneity is not readily apparent from bulk sediment

properties but required characterization of surface chemistry, mineralogy and bacterial data on a microscale. The data presented here provide important information for designing realistic laboratory and modeling studies of DNAPL behavior in coastal plain sediments. In particular, they emphasize the complexity of the system and the need to integrate field-based studies into these types of investigations.

7.0 Research details - Objectives 1 – 2

7.1 Objectives

- Understand and quantify the interfacial properties of DNAPLs in response to biological activity or the presence of surface-active constituents within the DNAPL mixture or aqueous phase.
- Identify conditions under which PCE and TCE co-metabolizing cultures affect interfacial properties through the production of surface-active materials or by adhering at NAPL interfaces.

Note – in the following sections, the work related to these objectives is broken into two parts – those related to the abiotic factors (DNAPL and porous medium composition) and those related to biological activity.

7.2 General Approach and Methods

Interfacial tension measurements were conducted for all samples prepared including biotic (SRS and synthetic DNAPL) and abiotic samples (bacteria stressed with oxygen). Wettability measurements were conducted for the abiotic samples and the adhesion tests for the bacteria samples at different dissolved oxygen concentration. Surface charge characterizations were performed for sand particles, SRS DNAPL emulsion, and bacteria cells stressed with oxygen.

Interfacial tension and surface tension measurements

All interfacial tension (IFT) and surface tension (ST) measurements were conducted using the Du Nouy ring method. A ring tensiometer (Fisher surface tensionmat, model 21) was used to determine the surface and interfacial tension of all fluid systems. A 20 ml sample of aqueous phase was introduced in a beaker, and 20 ml of the DNAPL was then introduced carefully below the aqueous phase using a syringe. The interfacial tension and surface tension measurements were then conducted according to the ASTM method at room temperature ($25\pm1\ ^{0}C$) (ASTM, 1991). The surface tension at the air/water interface was measured first. The same samples were kept under the hood in the same beakers covered with parafilm for the 24 and 48 hours measurements.

Electrophoretic mobility measurements

Electrophoretic mobility was measured using the Zeta PALS instrument (Phase Analysis Light Scattering, Brookhaven Instruments Corporation). The Zeta PALS instrument utilizes phase analysis light scattering to determine the electrophoretic mobility of charged colloidal suspensions. An appropriate volume of each sample described below was injected into a disposable cuvette to measure the electrophoretic mobility. For more accurate results, every measurement was based on 10 runs and at least 20 cycles for each run. Electrophoretic mobility was measured for three types of samples.

1- Bacteria samples were prepared by making colloidal suspension of 1ml of bacteria cell at a concentration of $9.37x10^{8}$ cells/ml into 15 ml of 0.01 M KCl solution under aerobic conditions. The pH was than adjusted using either diluted KOH or HCl depending on the pH target.

2- After equilibrating the SRS DNAPL with de-ionized water at a volume ratio of 1/2 The DNAPL colloidal emulsions were prepared by mixing 100µl of the emulsion in 15ml of 0.01 M KCL solution. The pH was than adjusted with either KOH or HCl depending upon the pH target.

3- The sand colloidal suspensions were prepared by vigorously mixing 1g of sand in 50ml of DI water, and let the big particles settle for 20 minutes. A 100µl volume was taken from the top of the sand and suspended in 15ml of 0.01 M KCL solution. The pH was than adjusted with either KOH or HCl depending upon the pH target.

7.3 Methods – Abiotic Factors

Materials

A DNAPL sample from the Savannah River site and synthetic DNAPL mixtures were used in this research. 99.5% trichloroethylene (Sigma Aldrich Co) was used as the DNAPL in all synthetic DNAPL mixture. 99% tributylphosphate (Sigma Aldrich Co) and 90% Dibutyl butylphosphonate (Sigma Aldrich Co) were used as representative for the surfactants used by the DOE facility in the plutonium production process to make the synthetic DNAPL. Hydraulic oil received from the SRS site was also used in the synthetic DNAPL matrix.

Different DNAPL compositions were tested for any interfacial tension or wetting conditions changes. Table 7.1 summarizes the mixtures tested. Interfacial tension was also measured as a function of TBP or DBBP dissolved in TCE at concentrations ranging from 0.16 to 3%.

Table 7.1: Synthetic DNAPL compositions tested

TCE Mass %	Oil Mass %	TBP Mass %	DBBP Mass %
100	0	0	0
0	100	0	0
95	5	0	0
95	0	5	0
90	10	0	0
90	2.5	2.5	5
90	5	5	0

De-ionized water was used in all aqueous phase solutions preparations. The Orion PH meter model 420A was used in all aqueous titrations, non-aqueous titrations, and pH adjustments. The pH was adjusted with 0.1N HNO_3 and 0.1N KOH solutions. Ionic strength was measured using a Cole Parmer conductimeter model 014816-61 and adjusted using the 99% NaCl (Fisher Scientific) from 0.01 to 0.1 M.

Quartz sand was donated by U.S silica (Ottawa, IL) and was sieved to obtain the 0.425-0.60 mm fraction diameter. The sand was cleaned by placing it in a glass beaker, soaking it with concentrated HNO_3 (50%), then washing it several times with acetone and water, and finally drying it at 103 ^{0}C for 24 hours.

Three SRS sand samples were received from the SRS site in May 2001. They were taken from the core number SB-3 at different heights in the subsurface. Two different types of sand were used in our experiments due to their different mineral surface composition. The first one was clay taken at 11’ 5”-13’5” height and the yellow sand taken at 40’6”41’2” height.

The goethite-coated sand was prepared by the procedure described by Scheidegger et al. (1992). 100 mg of goethite was mixed with 10 ml of 99% $NaNO_3$ (Fisher Scientific Co) solution in a 50-ml vial at a fixed ionic strength 0.1M and pH = 6.5. After shaking the mixture for 24 hours in order to obtain a homogenous suspension, 2.5 g of silica sand was added. The mixture was mixed for another 24 hours. After the settling of the sand grains, the pH of the supernatant was measured, and the sand was re-suspended in a 0.01M $NaNO_3$ solution with an ionic strength and a pH similar to the reaction medium. Finally, the goethite-coated sand was washed with a 0.01M $NaNO_3$ solution then with pure water.

Methods - Wettability

Bottle test experiments are the fastest and the easiest way to evaluate the wettability changes the for a given porous media/DNAPL/aqueous phase system for various pHs and ionic strengths. The method is based on equilibrating DNAPL and aqueous phase in the presence of a porous media (Powers et al.,

1996). To start the bottle test experiments, the aqueous phase was added to 15g dry sand placed in a 40-ml glass vial. The aqueous phase added was the equivalent of 25% of the pores volume.

The bulk density and the sand porosity were measured at the laboratory and found to be 1.78 g/cm^3 and 0.327 respectively (McDowell, 2002). 5ml of DNAPL was then added into the bottom of the vial using a syringe until it reached the sand surface. Oil red-O (electrophoresis grade, Fisher scientific Co) or Oil Blue-N dye (Fisher scientific Co) was added to the DNAPL when needed for clear observation at concentration of 0.1g/l. The bottles were mixed thoroughly 3 times a day for three days. Finally an excess of aqueous phase was added. In case of wetting or intermediate wetting conditions, the sand was considered completely or partially attached to the sand grains respectively; otherwise it is a water-wet condition.

Non-aqueous potentiometric titration

Acid number was determined using a non-aqueous potentiometric titration following the method used by (Bruss and Wyld, 1957; and Zheng and Powers, 2003). Separate glass and indicating electrodes were used to improve the accuracy of the electromotive force reading. The reference electrode was an inverted sleeve junction type calomel (model 39420, Beckman, Fullerton CA) and the indicating electrode was a glass electrode (model 39322, Beckman, Fullerton CA). Saturated $NaClO_4$ in 2-propanol was used as the electrolyte. The DNAPL was diluted in methyl isobutyl ketone (98.5%, Fisher Scientific Co), which is known to be a versatile solvent (Bruss and Wyld, 1957). The titrant used was tetrabutylammonium hydroxide (Fisher Scientific Co).

Before beginning the acid number titration, 120 ml of MIBK was introduced into a 250-ml glass beaker, and 1 ml of the DNAPL was than added under a continuous stirring. To help minimize external interference, a copper cage around the beaker and a Styrofoam block on the top of the stirrer were used as insulation.

In case of non-aqueous titration of a strong acid or base, the curve obtained shows very well defined inflection points, but this is not the case when weak acids or bases are being titrated. Zheng and Powers (1999) showed that a very well defined inflection point was obtained when dodecylamine (strong base) was titrated but it was not the case when pyridine (weak base) was titrated. Therefore, a spiking reagent was added to enhance the inflection of the titration curves. Stearic acid was previously found to be appropriate (Zheng and Powers, 2003) and used as the spiking reagent in all titrations.

To begin the titration, both electrodes were prepared following a standard test method (ASTM, 1996) then inserted into the solution. A 10-ml precision pipette with a 0.05-ml graduation was used with its tip kept under the surface of the solution to introduce the titrant in the beaker. The titrant was added at different volumes depending upon the rate of change of the reading. The derivative of the emf vs. time curve was calculated for an easy determination the inflection point for each titration. To determine the actual normality of the titrant, tetrabutylammonium hydroxide in MIBK was titrated using a known amount of 2-nitrophenol dissolved in MIBK. The acid number was calculated using the following equation

Nuclear magnetic resonance (NMR)

NMR spectroscopy is a analytical technique used to characterize and determine the structure of functional groups using common elements such as hydrogen. In this research project, NMR was used to determine the presence of any acid functional group in the SRS DNAPL that would be detected by looking at the presence of hydrogen atom.

SRS DNAPL samples for NMR spectroscopy were prepared by dissolving 5 mg of DNAPL in 0.6 ml of deuterated chloroform (99.9% Fisher scientific). The solution was then placed in a 5-mm NMR tube and analyzed using the Bruker Avance NMR model DMX 400.

7.4 Results – Abiotic Factors

Surface and interfacial tension

The surface and interfacial tension of the SRS DNAPL was measured after equilibrating the DNAPL with the aqueous phase at different pH values. The average values and the standard deviations (STD) are presented in the following table.

Table 7.2: SRS DNAPL interfacial and surface tension (±one standard deviation)

pH	IFT (dynes/cm) [a]	ST (dynes/cm) [b]
3.3	1.8±0.5	36.1±2.5
6.3	1.2±0.2	39.8±0.9
8.8	1.1±1.3	32.8±1.5

a Measured at the DNAPL/water interface
b Measured at the water/air interface

It is clear from Table 7.2 that the SRS DNAPL has a low interfacial tension at different pHs, when compared to the interfacial tension of pure TCE (34.5 dynes/cm) and pure PCE (47.5 dynes/cm) at the water interface. This may indicate the presence of surface-active compounds. These surface-active compounds could be either produced by microbial activity in the subsurface or initially present in the DNAPL mixture released by the DOE facility. The presence of organic acids in the DNAPL could cause the reduced interfacial tension (Lord, 1997; Zheng and Powers, 2003).

If present in sufficient amount, organic acids or bases could change pH after partioning into the aqueous phase. In order to see the effect of the SRS DNAPL in changing the water pH, 10 ml of the SRS DNAPL was equilibrated with 20 ml of de-ionized water at different pH values, and the final pH of the de-ionized water was measured (Table 7.3). The final pH of the de-ionized water decreased from 6.3 to 3.8, and for the water adjusted to a pH of 9.8 decreased to pH 8. Conversely, the pH of the aqueous phase at an initial pH 2.7 did not show any changes. The results were a clear indication that the SRS DNAPL contains acid that partitions into the aqueous phase. This may be responsible for the low interfacial tension of the SRS DNAPL measured

Table 7.3: SRS DNAPL equilibrated with DI water

Initial pH	Final pH
9.8	8
6.3*	3.8
2.7	2.7

The surfactants TBP and DBBP, and the hydraulic oil used during the plutonium production process at the DOE facility could possibly be present in the SRS DNAPL mixture, and might have contributed to its low interfacial tension. For this reason, a matrix of synthetic DNAPL was made using different compositions of TBP, DBBP, and the hydraulic oil. TCE was used as the DNAPL in all samples, and de-ionized water as the aqueous phase. The effect of TBP and DBBP on the interfacial tension of TCE was measured as a function of their concentrations in TCE. The results are shown in Figure 7-1. The TCE-water interfacial tension decreased from 35 dynes/cm with no surfactants added to 26 dynes/cm (25% reduction) when DBBP was added at 3%. The non-ionic surfactants TBP and DBBP reduced the interfacial tension of the DNAPL, but not to the low value measured for the SRS DNAPL, even at high concentrations.

The low interfacial tension of the hydraulic oil at the oil-water interface (12.2 dynes/cm, Table 7.4) could also contribute to the low IFT of the SRS DNAPL. Studies have shown that interactions among surfactant molecules, DNAPL molecules, and water molecules are important factors in lowering the interfacial tension (Zhang et al., 2002). Therefore, synthetic DNAPL mixtures were prepared using different combinations of TBP, DBBP and the hydraulic oil to identify their effect on the interfacial tension (Table 7.4). TBP and DBBP dissolved in the DNAPL (TCE) did not have a significant effect on the interfacial tension. In addition, the results indicate that adding hydraulic oil to the TCE, TBP and the DBBP mixture doesn't not have a significant effect on the interfacial tension either. Presence of 5% of TBP lowered the interfacial tension to 25.3 dynes/cm and adding 5% of the hydraulic oil to 5% TBP lowered the interfacial tension only to 21.5 dynes/cm. Similar interfacial tension values (21 dynes/cm) were obtained in the presence of a high concentration of the hydraulic oil, and a mixture of TBP, DBBP and the hydraulic oil (Table 7.4).

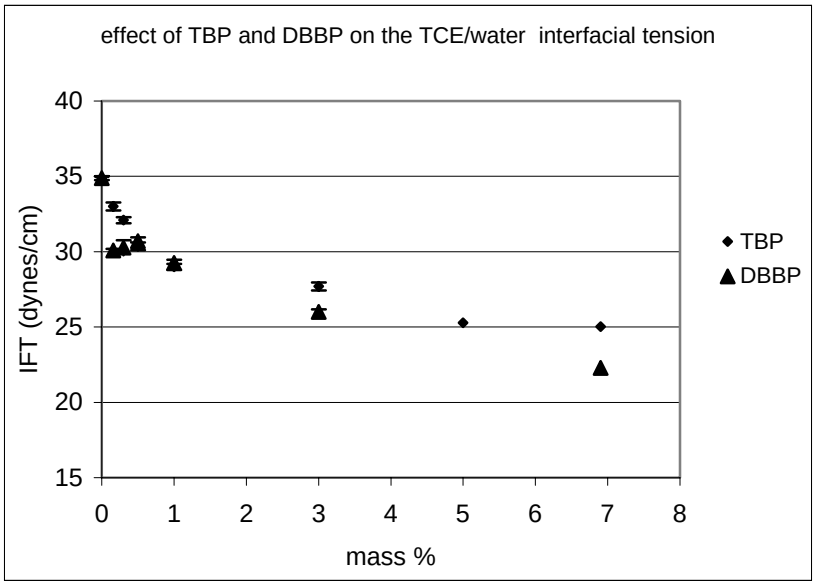

Figure 7.1: Effect of TBP and DBBP on the TCE/water interfacial tension

Table 7.4: Interfacial tension of a matrix of synthetic DNAPL

TCE Mass %	Oil Mass %	TBP Mass %	DBBP Mass %	IFT± one standard deviation (dynes/cm)
100	0	0	0	34.9±0.1
0	100	0	0	12.2±0.8
95	5	0	0	23.3±0.6
95	0	5	0	25.3±0.3
90	10	0	0	21.6±0.5
90	2.5	2.5	5	21.3±0.1
90	5	5	0	21.5±0.1

Characterizing Acidic Components

Aqueous titration

In order to quantify the acid(s) that have partioned into the de-ionized water, a titration of that aqueous phase was conducted using sodium hydroxide (Figure 7.2). A 200-µl volume of 1N HCl was added as a spiking agent to enhance the infection point, which was then subtracted from the total acid in the solution. The amount of the acid extracted from the SRS DNAPL was titrated using a 0.1 NaOH solution. The results showed 0.3 moles acid/L were extracted from the DNAPL into the aqueous phase.

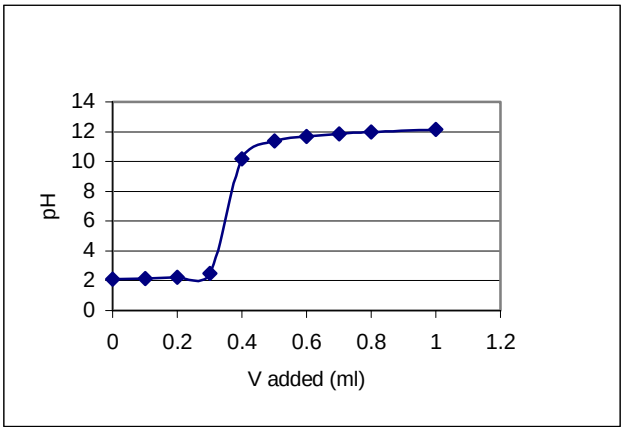

Figure 7.2: Aqueous titration for the de-ionized water equilibrated with SRS DNAPL

This concentration may not reflect the total acid present in the DNAPL, because it shows only the acids partioned into the aqueous phase. Therefore, non-aqueous potentiometric titration was the best way to directly titrate the total amount of acid present in the DNAPL.

Non-aqueous titration

The non-aqueous potentiometric titration conducted showed that the SRS DNAPL contained a significant amount of acid (4 mg KOH/mg of sample) (Figure 7.3). This amount of acid may be responsible for the low interfacial tension measured for the DNAPL. Zheng and Powers (2003) also studied the effect of acid number on the interfacial tension of different fossil fuel derived NAPLs. They found that the interfacial tension decrease with increasing the acid number. For example, a creosote sample with an acid number of 3.24 had an interfacial tension less than 10 dynes/cm. Hoeiland et al. (2001) also showed the same correlation between the acid number and the decrease in the interfacial tension. Potentiometric titration of TBP and DBBP dissolved in MIBK and the hydraulic oil dissolved in the same solvent, showed almost no acid present in the system (Table 7.5), which indicates that neither the surfactants TBP and DBBP nor the hydraulic oil can account for the acidic characteristics of the SRS DNAPL.

Table 7.5: Acid numbers for the SRS DNAPL, TBP, DBBP and the hydraulic oil.

System	**Acid number (±Standard error)** (mg KOH/mg of sample)
SRS DNAPL dissolved in MIBK	4.06±0.81
Hydraulic oil dissolved in MIBK	0.08±0.1
2.5% TBP + 2.5% DBBP in MIBK	0.12±0.11

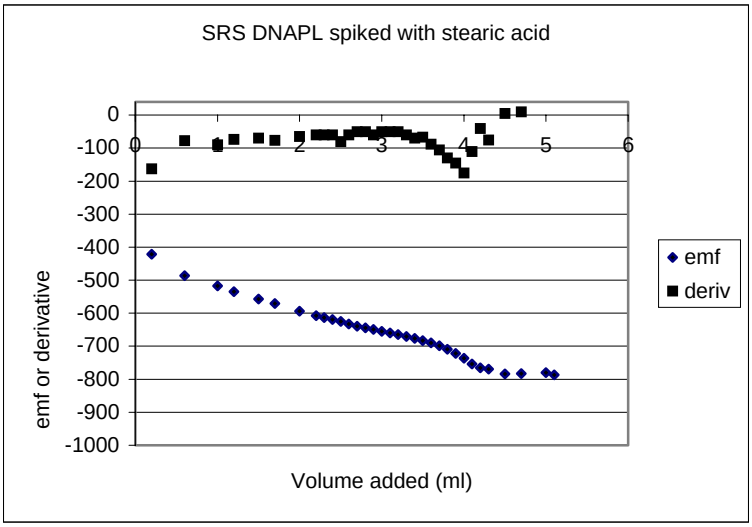

Figure 7.3: Titration of 1ml of SRS DNAPL dissolved in MIBK spiked with 0.25meq stearic acid

Wettability tests

Bottle test experiments conducted to assess any wettability changes for the quartz-TCE-Water system using a relatively high concentration of TBP over a range of ionic strength and pH values (Table 7.6). The results don't show any effect of pH, ionic strength or presence of TBP on the wettability of quartz sand, which remained water wet under all conditions tested.

The SRS DNAPL and the SRS sand (SRS clay taken at 11'5" to 13'5" and SRS sand taken at 40'6" to 43') were also used in the wettability tests over a range of pH from 2 to 10.3. No wettability changes were observed despite the low SRS DNAPL interfacial tension.

Table 7.6: The effect of TBP, ionic strength, and pH on wettability

Ionic strength	**pH**	**TBP (mass%) in TCE**	**Observation**
0.01	4.7	0	Water wet
0.01	7.2	0	Water wet
0.01	10.3	0	Water wet
0.1	4.7	5	Water wet
0.1	7.2	5	Water wet
0.1	10.3	5	Water wet
0.01	4.7	5	Water wet
0.01	7.2	5	Water wet
0.01	10.3	5	Water wet

Discussion

From the results obtained, it is clear that the low interfacial tension measured for the SRS DNAPL was not only due to the presence of TBP, DBBP or the hydraulic oil, but also due to other compounds which could be surface-active compounds present in the DNAPL mixture. The unknown history of the contamination spill at the Savannah River Site makes it difficult to know the compounds responsible for the low interfacial tension of the SRS DNAPL. It is also possible that surface-active compounds could have been produced by bacteria or resulted from other processes once disposed to the subsurface. NMR analysis conducted for the SRS DNAPL did not show any presence of Bronsted acids (H^+ donors). This indicates the possibility of presence of other types of acids without presence of protons in the functional group.

Shift in the wettability from water to oil wet condition occurs when the surface charge of two interfaces are opposite or when the van der Waals forces are sufficient enough to overcome the electrostatic repulsion force between the interfaces (Zheng et al., 2000). However, for the bottle test experiments conducted, no wettability changes were observed for any variable tested. This could be explained by the fact the attractive interaction between the water-sand and the DNAPL-water interfaces was not enough to destabilize the thin water film existing between the DNAPL and the sand which indicates that the total force is not attractive (Hirasaki, 1991). The electrostatic repulsion force between the DNAPL and the solid surface could not be overcome neither by the presence of the non-ionic surfactant (TBP), nor by changing the solution chemistry of the aqueous phase.

Similarly, which could be attributed to the same reasons, coating the quartz sand with iron oxide (α-FeOOH), which is a positively charged molecule did not change the wettability condition of the system. It is possible that the poor coating of the quartz sand (20.16 % in mass of Fe) left relatively high negative surface charges at the quartz surface; therefore, a repulsion force between the DNAPL and goethite-coated sand interfaces was strong enough to keep the water film coating the solid surface

Electrophoretic mobility of the SRS soil and DNAPL (Figure 7.4) showed negatively charged surfaces for the clay, the sand, and for the SRS DNAPL, which may explain the repulsive forces between the DNAPL and the soil. This is due to a relatively high proportion of silica at the sand surface, which has an isoelectric point at pH 2, causing a negative surface charge at the sand and clay surfaces despite the presence of aluminum and iron at the surface (Section 6).

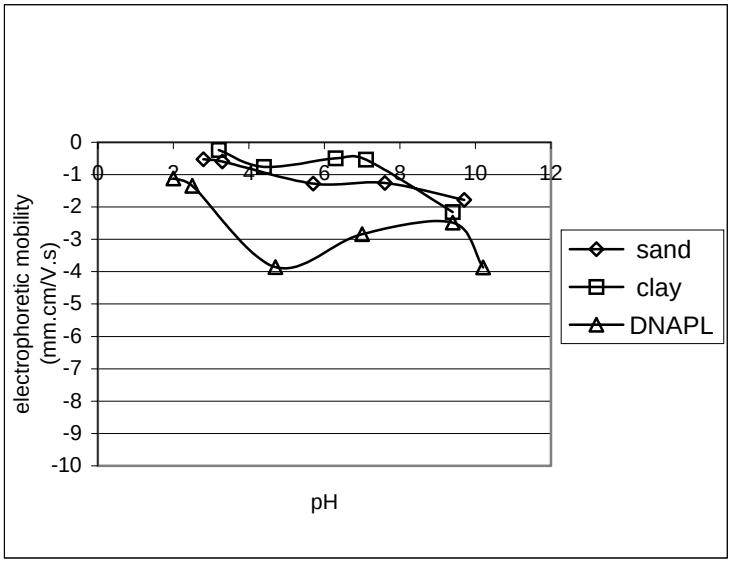

Figure 7.4: SRS soil and DNAPL electrophoretic mobility

7.5 Methods – Biological Activity

Cultures

Four different cultures were investigated with respect to their ability to effect interfacial properties. Of the four cultures three were able to degrade PCE under anaerobic conditions (Desulfuromonas chloroethinica [ATCC #70029], a butyrate fermenting enrichment culture [Gossett et al., 1997], an enrichment culture from the SRS Site) while the fourth culture consisted of an aerobic enrichment culture using soil from the SRS Outfall Area. This culture co-metabolized TCE using a range of carbon sources.

TCE-Degrading Enrichment Culture. Soil samples from the most contaminated depths were used as inoculants in microcosm experiments to test for the presence of organisms that co-metabolize TCE and that would affect interfacial properties. Soil samples were suspended in mineral media appropriate for the respective redox conditions (Gerhadt et al. 1994). For the aerobic experiments, soil slurries (1 gram soil in 30 mL media) were set up for a range of carbon sources (phenol, formate, acetate and toluene) to investigate what conditions would stimulate TCE co-metabolism. Both nitrate and ammonia were used (final concentrations 1 g/L) as potential nitrogen sources in the media. Microcosms were incubated at 30°C on an orbital shaker at 100 rpm. TCE concentrations in the headspace were monitored over time. Media surface tension and interfacial tension to TCE was measured at the conclusion of the biodegradation experiment.

Desulfuromonas choloroethinica (ATCC #70029), a gram negative, rod shaped bacterium was grown anaerobically with acetate as an electron donor and tetrachloroethylene (PCE) as the electron acceptor in minimal media (Krumholz et al., 1996). The culture was delivered freeze-dried and was revived in sulfate reducing bacteria nutrient media and incubated at 35°C for 1 week at 150 rpm (Gerhardt et al., 1994).

Butyrate Fermenting Enrichment Culture. The media for the butyrate fermenting culture, as described by DiStefano et al. (1992), is prepared as follows (Table 7.7): Media constituents 1 through 8 are added to a 10-liter vessel, which is then purged with nitrogen gas for a period of one hour. After the nitrogen purge is completed, constituents 9 and 10 are added, and a final purge consisting of 80% N_2 and 20% CO_2 is conducted for an additional 15 minutes. The pH is measured and adjusted, as necessary, to a pH of approximately 7.0, with either NaOH or HCl.

Table 7.7: Butyrate Culture Media Constituents

Constituent			Amount (g)	Final Concentration (g/L)
1	Distilled Water	H_2O	10 Liters	1 Liter
2	Ammonium Chloride	NH_4Cl	2	0.2
3	Potassium Phosphate	K_2HPO_4	1	0.1
4	Potassium Di-phosphate	KH_2PO_4	0.55	0.055
5	Magnesium Chloride	$MgCl_2.6H_2O$	2	0.2
6	Rezasurin		0.01	0.001
7	Trace Metals Solution	TMS	100 ml	10 ml
8	Ferric Chloride	$FeCl_2.4H_2O$	1	0.1
9	Sodium Bicarbonate	$NaHCO_3$	60	6
10	Sodium Sulfide	$Na_2S.9H_2O$	5	0.5

Trace metals solution consists of trace amounts of metals and salts listed in Table 7.8. After all constituents are added, the media vessel is sealed under continuous purge, to ensure anaerobic conditions.

Table 7.8: Butyrate Culture Trace Metals Solution Constituents

	Constituent		Amount (g)	Final Concentration (g/L)
1	Distilled Water	H_2O	5 Liters	1000 grams
2	Manganese Chloride	$MnCl_2.4H_2O$	0.5	0.1
3	Cobalt Chloride	$CoCl_2.6H_2O$	0.85	0.17
4	Zinc Chloride	$ZnCl_2$	0.5	0.1
5	Calcium Chloride	$CaCl_2.2H_2O$	1.255	0.251
6	Boric Acid	H_3BO_3	0.095	0.019
7	Nickel Chloride	$NiCl_2.6H_2O$	0.25	0.05
8	Sodium Molybdate	$Na_2MoO_4.2H_2O$	0.1	0.02

The culture was maintained in a 5 L stirred reactor, with a culture volume of 3 L. The culture was continually stirred at approximately 100 rpm, and was maintained at a constant temperature of 30° C. The culture was maintained in a basal medium (Table 7.7) as described by DiStefano et al. (1992), and the feeding regimen is described as follows (Smatlak et al. 1996): The culture was fed every 48 hours, during which 110 µmol (18.2 mg) of neat PCE, 440 µmol (38.8 mg) of butyric acid, and 400 µl of a 50g/l yeast extract stock solution were administered per liter of culture. Additionally, during every other feed (every fourth day), 510 µl of vitamin solution per liter of culture was dispensed to the culture. Also during every other feed, 300 ml of culture was wasted and replaced with fresh basal medium. This translates to an average cell residence time of 40 days in the reactor. The culture and all associated media were purged with a 70% N_2/30% CO_2 gas mixture, which was first passed through a titanous chloride/sodium bicarbonate/sodium citrate solution (Zehnder 1976) in order to remove any trace amounts of oxygen. The concentrations of PCE and any less chlorinated ethenes- trichloroethylene (TCE), cis- and trans- dichloroethylene (DCE), and vinyl chloride (VC) were all tracked weekly via GC analysis, as explained in greater detail below.

SRS PCE Dechlorinating Enrichment Culture. The second SRS culture examined in this study was a mixed culture created from soil samples collected from the Lagoon Area of the SRS site, and was also observed to readily dechlorinate PCE. Soil samples from eight different soil borings at the SRS site were used to seed initial culture vials. All soil samples used were taken at depths of 90 feet or greater, and considered anaerobic. These eight initial samples consisted of 15 grams of soil and 80 ml of a generic anaerobic media obtained from Hurst et al. (1997), which was anaerobically dispensed under nitrogen purge to 125 ml sample vials, and sealed under nitrogen purge. Samples were then injected with 0.8 µl of PCE, yielding an initial concentration of approximately 17 mg/l. The samples were fed a generic carbon source which was comprised of a number of compounds, all of which had been previously documented as carbon sources for a number of anaerobic dechlorinating cultures. The specific carbon sources and from whom they have been adopted is shown in Table 7.9.

Table 7.9: Constituents and their associated references

Reference Source	Constituent
Vogel and McCarty (1985) Prakash and Gupta (2000)	Acetone
Yang and McCarty (1998)	Benzoate
Fennell et al (1997); Smatlak et al. (1996)	Butyrate
Hopkins et al. (1993)	Phenol
Common Carbon Source	Yeast Ext.

The carbon sources were combined into one stock carbon source, as explained below. Every 48 hours, the SRS culture was fed a mixed carbon source, which consisted of phenol (40 mg per liter of sample), butyrate (40 mg per liter of sample), acetone (40 mg per liter of sample), benzoate (40 mg per liter of sample), and yeast extract (30 mg per liter of sample). This combination of carbon sources ensured adequate concentrations of carbon sources, enabling PCE dechlorination. This carbon source mixture was administered to the sample cultures every 48 hours. The samples were maintained on an orbital shaker at 100 rpm, and maintained at a constant temperature of 30°C. All samples were then monitored daily for decreases in PCE or the appearance of any TCE, DCE, or VC, which would indicate dechlorination, and therefore microbial activity. After a period of about 14 days, four of the samples showed significant PCE reductions. These samples were then used to seed a new culture, which included approximately 50 ml of each of the four active cultures, and 100 ml additional media, increasing total culture volume to approximately 300ml. This new culture (SRS culture) was fed the same carbon source solution and at identical concentrations as described previously for each sample culture. The SRS culture was again monitored via GC analysis, and spiked a second time with PCE, after which PCE concentrations were again observed to decrease.

Media for the SRS culture was similar, but not identical to the butyric culture media. The SRS media was obtained from Hurst et al. (1997), and is prepared as described in Table 7.10.

Table 7.10: SRS Culture Media Constituents

	Constituent		Amount (g)	Final Concentration (g/L)
1	Distilled Water	H_2O	10 Liters	1 Liter
2	Rezasurin		0.01	0.001
3	Potassium Di-phosphate	KH_2PO_4	1.38	0.138
4	Potassium Phosphate	K_2HPO_4	1.76	0.176
5	Ammonium Phosphate	$(NH_4)_2HPO_4$	0.2	0.02
6	Ammonium Chloride	NH_4Cl	2	0.2
7	Magnesium Chloride	$MgCl_2.6H_2O$	6	0.6
8	Ferric Chloride	$FeCl_2.4H_2O$	2	0.2
9	Potassium Chloride	KCl	1	0.1
10	Calcium Chloride	$CaCl_2$	1	0.1
11	Sodium Sulfide	$Na_2S.9H_2O$	1	0.1
12	Sodium Bicarbonate	$NaHCO_3$	42	4.2
13	Trace Metals Solution	TMS	100 ml	10 ml

Constituents were added one at a time, under continuous nitrogen purge. The nitrogen purge was then maintained for one hour, at which time the vessel was sealed under continuous nitrogen purge to ensure anaerobic conditions in the vessel. As with the SRS media, a trace metals solution was required in the SRS culture media. This TMS was similar to the butyrate TMS in that both contain trace amounts of metals and salts, however the individual constituents were not identical (Table 7.11). The vessels of both the butyrate and SRS cultures were similar, both in volume and purge equipment. Both vessels were sealed with a stopper apparatus, which included an airtight inlet and vent to allow for purging of the vessel contents. The inlet purge flow line included tygon tubing extending to the bottom of the vessel, with an attached gas-diffusing stone. The oulet vent consisted of open tubing extending approximately one inch beyond the bottom of the stopper, which allowed excess gas from the headspace to be vented. Both inlet and outlet vent lines included a valve immediately above the stopper, in order to maintain anaerobic conditions when purge gas was not flowing.

Table 7.11: SRS Culture Trace Metals Solution Constituents

	Constituent		**Amount (g)**	**Final Concentration (g/L)**
1	Distilled Water	H_2O	10 Liters	1 Liter
2	Potassium Iodide	KI	10	1
3	Manganese Chloride	$MnCl_2*4H_2O$	4	0.4
4	Cobalt Chloride	$CoCl_2*6H_2O$	4	0.4
5	Nickel Chloride	$NiCl_2*6H_2O$	0.5	0.05
6	Cupric Chloride	$CuCl_2$	0.5	0.05
7	Zinc Chloride	$ZnCl_2$	0.5	0.05
8	Boric Acid	H_3BO_3	0.5	0.05
9	Sodium Molybdate	$Na_2MoO_4*2H_2O$	0.5	0.05
10	Sodium Metavanadate	$NaVO_3*nH_2O$	0.5	0.05
11	Sodium Selenite	Na_2SeO_3	0.1	0.01

As with the butyrate culture, purge gases were first scrubbed of any trace amounts of oxygen by passing them through a solution of titanous chloride, sodium bicarbonate, and sodium citrate (Zehnder 1976).

Every 48 hours, the SRS culture was fed the mixed carbon source, which consisted of phenol (40 mg per liter of culture), butyrate (40 mg per liter of culture), acetone (40 mg per liter of culture), benzoate (40 mg per liter of culture), and yeast extract (30 mg per liter of culture). The culture also received 10 μmol (1.7 mg) of neat PCE per liter of culture. The samples were maintained on an orbital shaker at 100 rpm, and maintained at a constant temperature of 30°C.

Microcosm Experiment

Microcosms of all anaerobic cultures were prepared and incubated for one week, in order to observe the extent of significance of the stressor variables. All butyrate culture samples were created in 125ml sample bottles, and all SRS cultures were created in 80ml sample bottles. Due to the relatively small volume of SRS culture, all SRS samples were produced with final volumes consisting of 50% of final butyrate sample volumes, however all ratios remained constant between culture samples. All sample bottles were first sterilized in an autoclave for 25 minutes at 250°C. The sterilized bottles were submerged in DI water. Nitrogen was then used to displace the water in the bottle. The bottles were then removed from the DI bath, and immediately sealed and crimped under continuous nitrogen purge. This

process ensures an anaerobic, nitrogen atmosphere in each sample bottle. 100 ml of butyrate media was dispensed anaerobically into each of the sample bottles for the butyrate samples. Correspondingly, 50 ml of SRS media was dispensed for the SRS culture. Next, 20 ml of butyrate enrichment culture was injected to each butyrate sample bottle, and 10 ml of SRS culture injected to each SRS sample bottle. All samples were then incubated for a week at 30ºC on an orbital shaker at 100 rpm, and all were fed identical constituents at the same concentrations per liter of culture as fed to the main culture reactor, unless dictated otherwise by the variables of interest. An initial set of samples was produced with the butyrate culture following the above procedure, and to which no amendments or variables were introduced. These samples were then tested in order to serve as an original, "base-case" standard to which all other amended butyrate samples were compared. Variables are summarized in Table 7.12. This allowed a measure of the extent of significance each variable produced. The same process was conducted with the SRS culture, to act as an SRS base case scenario.

Table 7.12: Variables Tested for Anaerobic Enrichment Cultures

	Variable	**Concentration**	
Butyrate Culture	EDTA	200	mg/L
	Lactic Acid	440	µmol/L
	Propionic Acid	440	µmol/L
	Increased PCE	190	mg/L
	Dissolved O_2	0	mg/L
	Dissolved O_2	1.5	mg/L
	Dissolved O_2	2.8	mg/L
SRS Culture	Increased PCE	190	mg/L
	Dissolved O_2	0.8	mg/L
	Dissolved O_2	1.5	mg/L

Chlorinated Solvent Analysis

For analysis of chlorinated solvents in liquid media, 1 mL of media was placed in a 7 mL headspace vial and sealed with a crimped Teflon-lined septum top for headspace analysis. Volatile analysis was performed using a Hewlett Packard 5890 or 6890 Series II gas chromatograph with electron capture (ECD) and flame ionization detectors (FID) in parallel with an automated headspace sampler at 70°C. A DB-5 capillary column (60 meters long, 0.25 mm inside diameter, and a 0.25 µm film thickness; J&W Scientific) was used to analyze chlorinated compounds. The temperature program was as follows: Injector temperature and detector temperature were kept constant at 250ºC and 300ºC, respectively. The initial column temperature of 40ºC was maintained for 2 minutes, followed by a 10ºC /min increase to 220ºC, at which point the temperature was then increased at a rate of 40ºC /min to 300ºC. The resulting overall run time was 22 minutes. Residence time of PCE was approximately 10 min using this method.

Contact Angle Measurements.

Centrifuged samples of Desulfuromonas chloroethinica were resuspended in 50 mL minimal media for a final density of OD_{420} ~ 0.01. Samples were filtered through 47mm Millipore 0.2um GTTP isopore membrane filters (Fisher Scientific, NJ). Deposited cell lawns were rinsed with 40-50 mL of deionized water. Samples were dried for 15 minutes under continued vacuum pressure, followed by 30 minutes without vacuum pressure. This drying time was deemed to be sufficient because the contact angle remained constant for drying times exceeding 30 minutes during initial screening experiments. Contact angle measurements were taken on a Kruss goniometer (model G-I) using the apolar solvent, diiodomethane. 4 to 8 angles were read on each microbial lawn.

Microbial Adhesion To Hydrocarbons

The microbial adhesion to hydrocarbons (MATH) assay measures the tendency of bacteria to adhere to a hydrocarbon-water interface. This test was conducted following the method described by Rosenberg (1991). 3 ml of sample was introduced into a UV cuvette and the initial absorbance (A_0) was measured. After returning the sample to a 10ml glass vial, 500µl of TCE was than added or 0.5 g of sand was added where the adhesion of bacteria to porous media was investigated. The mixtures was thoroughly mixed for 2 minutes, and let sit for 10 minutes. The supernatant absorbance was measured (A_1) using a double beam UV/Vis scanning spectrophotometer (Perkin Elmer, 559A). The percent of adhesion was calculated using the following equation:

$$\%Adhesion = \frac{A_1 - A_0}{A_1} * 100$$

7.6 Results – Biological Activity

Four different cultures were investigated with respect to their ability to effect interfacial properties. Among the variables investigated were ionic strength (I = 0.2 to 0.01), the ammonia and EDTA concentration in the growth media, the presence of elevated PCE concentrations and the presence of dissolved oxygen. Effects on TCE/water interfacial properties were small for Desulfuromonas chloroethinica and the TCE degrading enrichment culture. The affinity of Desulfuromonas chloroethinica to diiodomethane, a hydrophobic solvent, was a dependent on culture incubation conditions (Figure 7.5). A max reduction from 45 to 35 degrees relative to the control, which was grown in the standard growth media, was obtained when the culture was incubated in a media containing excess ammoniumchloride. Other changes in the growth media, such as changing the carbon source or the dissolved trace metal concentrations through the addition of EDTA had less of an effect of changing the hydrophobicity of the bacterial cell membrane.

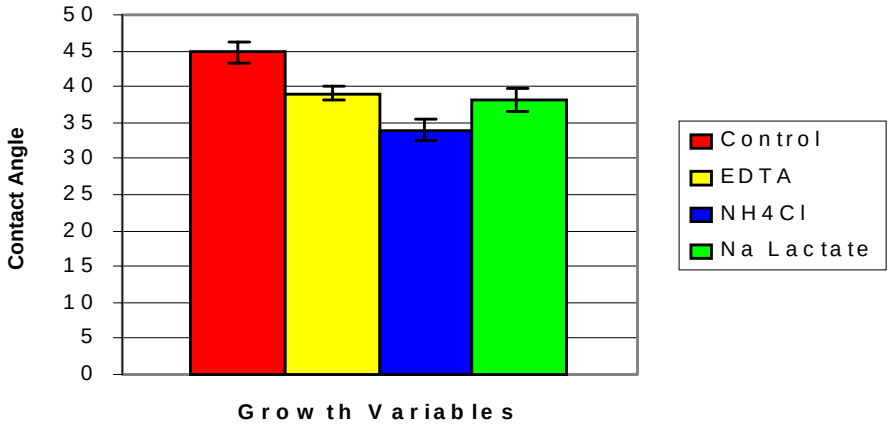

Figure 7.5: Contact angle of diiodomethane on bacterial lawn of Desulfuromonas chloroethinica. A lower contact angle is indicative of a higher affinity of the bacterial surface to the apolar solvent.

For the butyrate fermenting enrichment culture changing carbon source or trace metal concentration in the media had a minimal impact on affecting media surface tension or TCE/media interfacial tension (Table 7.13). Surface tension for both particulate media (containing bacteria) and particle-free (filtered through

0.2 µm and therefore free of bacteria) changed less than 3 dyn/cm compared to the "non-stressed" Base culture. Similarly, interfacial tensions were not affected under these growth conditions.

Table 7.13: EDTA and Carbon Source Amendments Results for Butyrate Culture

Type of Sample	**ST & IFT (dynes/cm)**			
	Base Case	**Propionic**	**Lactic**	**EDTA**
Particulate ST	66.2	68.0	68.1	69.3
Particle-Free ST	66.6	66.8	66.4	68.0
Particulate IFT	26.2	26.5	24.8	32.9
Particle-Free IFT	30.3	29.8	32.9	32.8

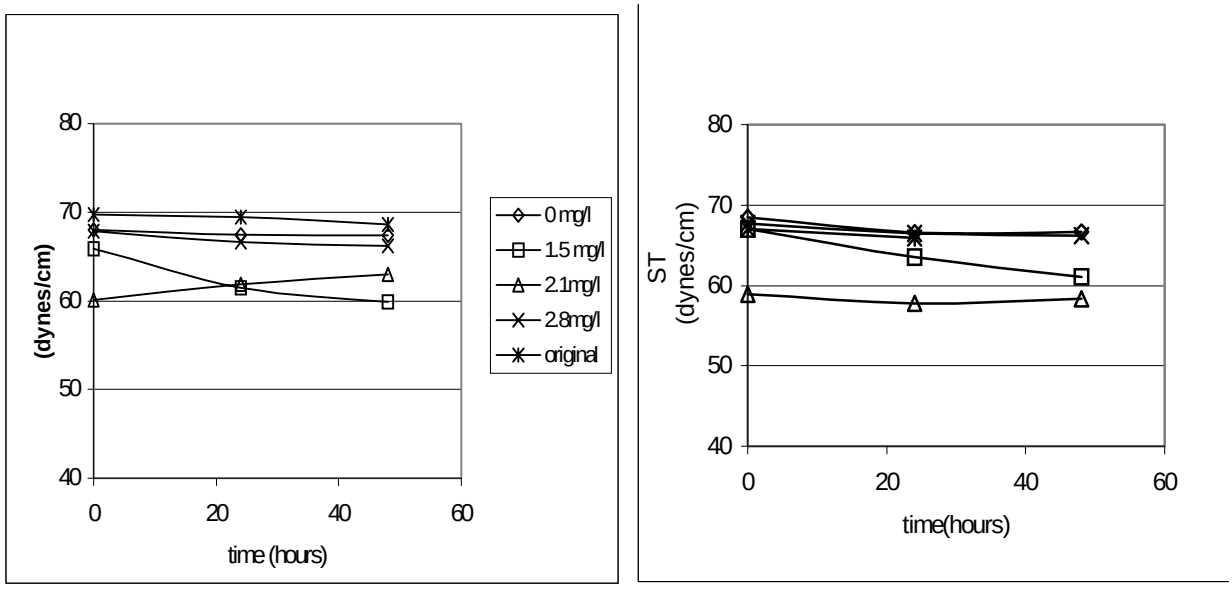

Figure 7.6: Surface tension of butyrate culture as a function of dissolved oxygen concentrations (left: particulate fraction, right: particle-free media)

When stressed with excess PCE or oxygen, the surface tension was slightly lower than that of the non-stressed culture (>58 vs. 68 dyn/cm) (Figure 7.6). Interfacial tension, however, changed significantly upon inducing stresses to the anaerobic enrichment cultures. For example, upon exposure of the culture to oxygen at 1.5 mg/L with one-week incubation, the IFT declined from 37 to 18 dyn/cm, which represents a 51% reduction relative to the sterile control (Figure 7.7). IFT measurements were conducted over a 48 hrs period to determine the dynamic processes of particulate settling and the absorption of surface-active compounds at the TCE/water interface. IFT tension in all samples declined as a function of time, which may be attributed to particulate settling. The extent of IFT decline relative to the non-stressed culture (original) however was dependent on the "stressor" concentration. Similar reductions in IFT were observed when the culture was grown in the presence of 190 mg/L PCE, which is a concentration approximately 10 times higher that is used to grow the stock culture (Figure7.7). A noteworthy point for this set of results - the surface tension decreased slightly (from 70 to 60 dyn/cm) and was not a function of equilibration time. To determine the impact of bacteria accumulating at the TCE/water interface on IFT, bacteria were removed through filtration (0.2 µm filter) prior to measuring IFT (Figure 7.7). IFT decline again over a 24-hour period and IFT reductions were similar to measurements that contained the microorganisms (Figure 7.8). Again, surface tension did not decline to a large extend for the particle-free media (Figure 7.6). A decline in surface tension in parallel to a decline

in IFT would be indicative of the biosurfactants production, since surfactants would absorb to any hydrophobic surface in the system and are not governed by settling processes. Experiments using abiotic particles at similar particle size than bacteria did not induce similar IFT changes as were observed with the biological systems (Figure 7.9). Therefore any observed effects on IFT were due to biological activity.

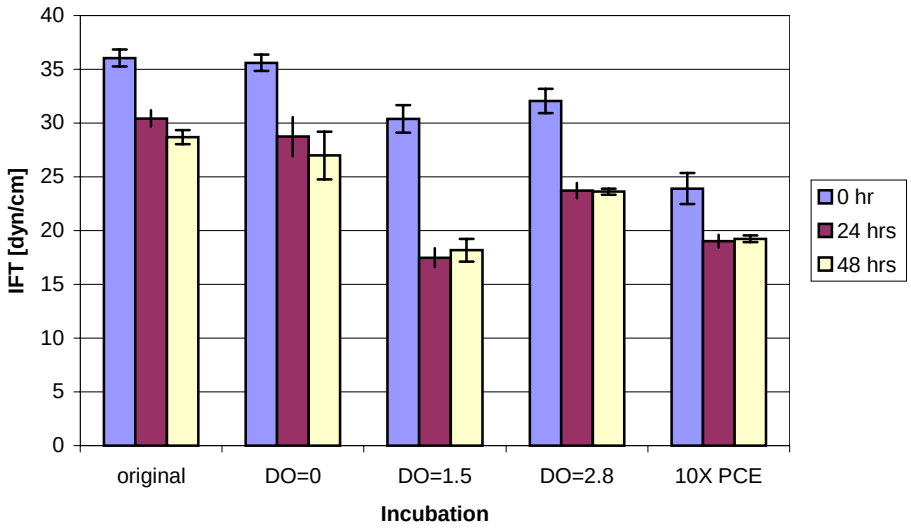

Figure 7.7: Effect of dissolved oxygen on IFT for butyrate fed culture, filtered through 1 μm to remove inorganic particulate.

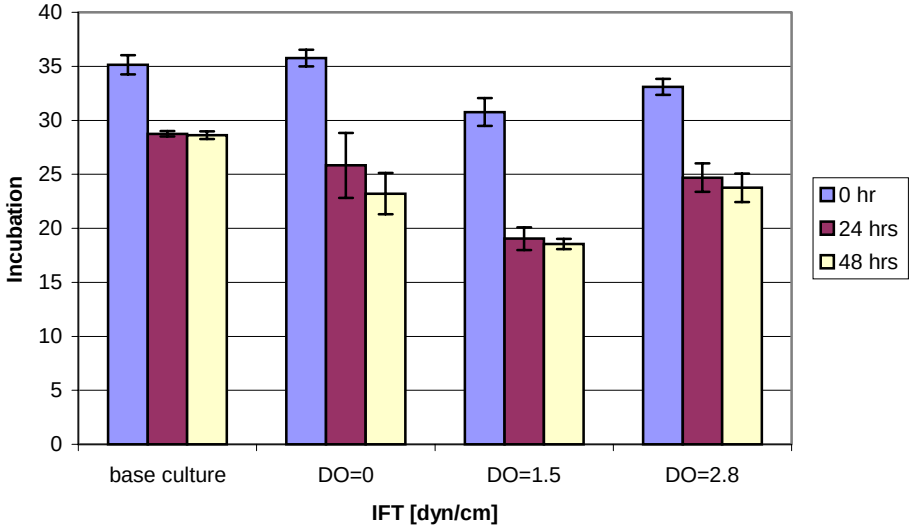

Figure 7.8: IFT of butyrate enrichment culture. “particle-free” solution.

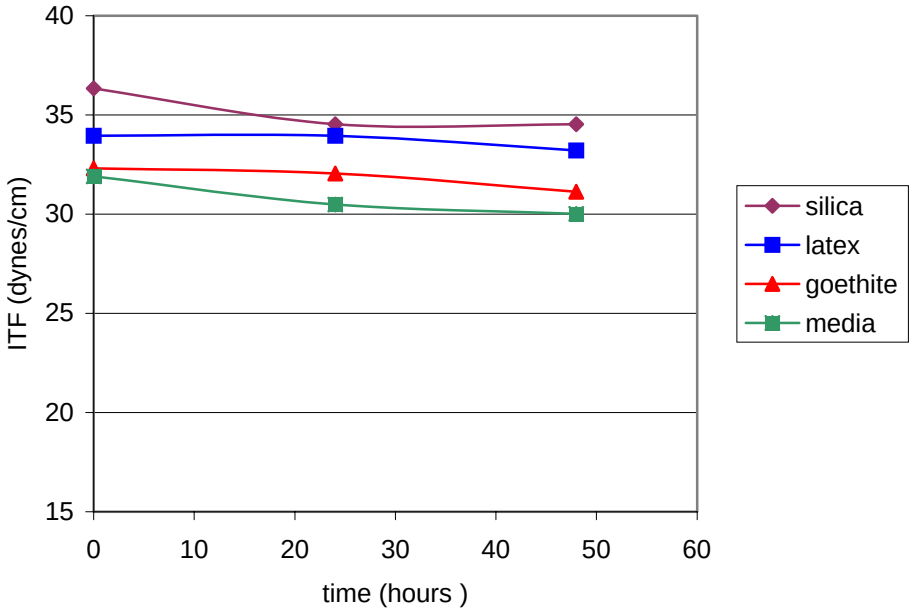

Figure 7.9. IFT between TCE and water in the presence of inorganic colloidal material.

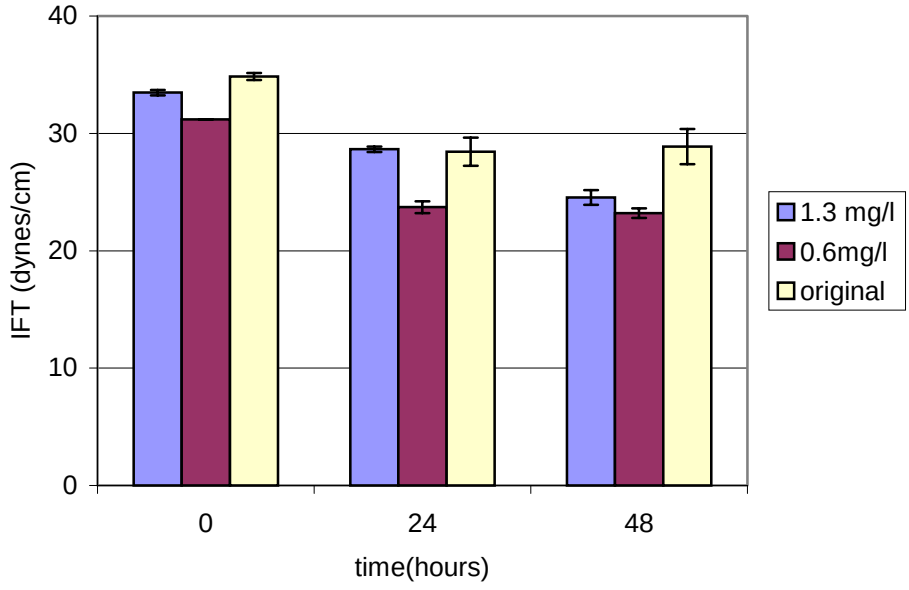

Figure 7.10: Effect of oxygen on TCE/water IFT for concentrated SRS anaerobic enrichment culture.

Similarly, the SRS enrichment culture exhibited IFT reduction when stressed with oxygen (Figure 7.10). The changes in IFT for similar oxygen levels to the butyrate culture were not a large as were observed with the butyrate fermenting culture.

To investigate the affinity of the organisms to interact directly with the TCE interface two additional characterizations were conducted: (1) Surface charge properties of the organisms as a function of "stressor" concentration and (2) MATH assay to TCE.

The electrophoretic mobility is a characterization method to determine surface charge at the bacteria cell wall (membrane). Surface charge changes is an important factor that determines the ability of the bacteria to adhere to surfaces, which might have been the case for the interfacial tension observed for the oxygen stressed bacteria. The surface charge of bacteria cells is strongly dependant on pH (Rijnaarts et al, 1995), which makes it necessary to investigate the affect of pH on the surface charge of the SRS and butyrate culture.

Electrophoretic mobility was measured for the original butyrate fermenting culture and the stressed culture at 1.5mg/l and 2.5mg/l of dissolved oxygen at different pH values, which allow different degree of protonation of the cell wall chemical groups. The electrophoretic mobility of the cells was very pH dependent (Figure 7-11). Conversely, the results indicate the iso-electric point at pH lower than 2. As was determined by previous research, the isoelectric point (IEP) is a very important factor that needs to be determined when the adhesion of bacteria is the subject of interest (Rijnaarts et al., 1995).

For the butyrate culture, the electrophoretic mobility was not significantly affected by the dissolved oxygen concentration (Figure 7.11). Conversely, the SRS culture shows a slight dependence on the DO concentration especially at pH values higher than 5 (Figure 7.12). At pH values close to 8, the electrophoretic mobility for 1.5mg/l DO was -1.86 μm cm/V s, while for the original culture was -2.61μm cm/V s. However, all surfaces at different pH values are always negatively charged. A t-test was conducted for statistical comparison of different sets of data for both butyrate culture and SRS culture. For the SRS culture, the t-test conducted for all sets of data showed that the original culture is different from the 1.5 mg./l DO, 0.5 mg/l and 0.75 mg/l DO. It showed also that 1.5 mg./l Do, 0.5 mg/l and 0.75 mg/l DO are not similar.

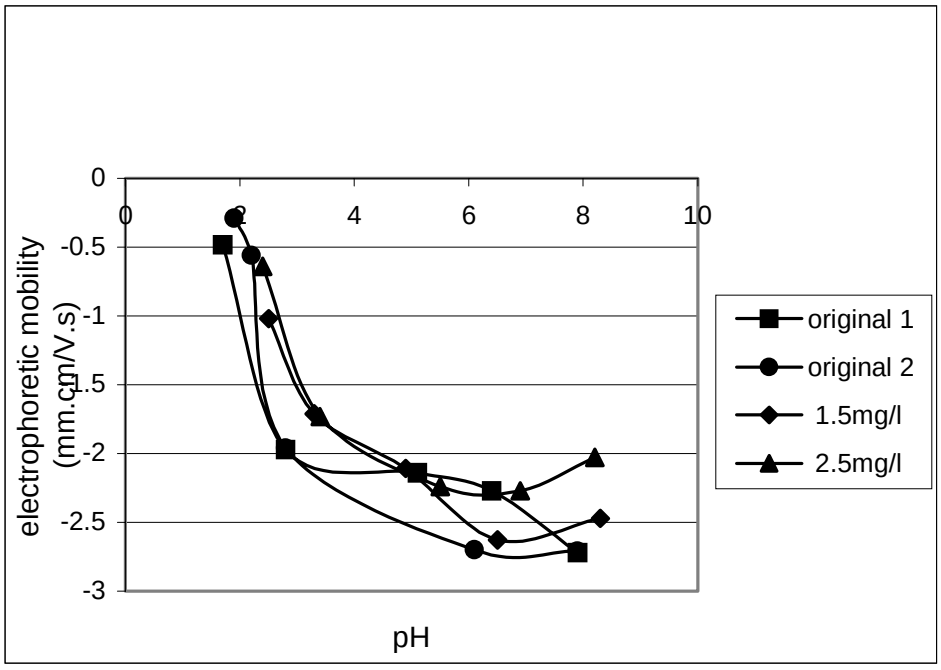

Figure 7.11: Electrophoretic mobility for butyrate fermenting bacteria stressed with oxygen and the original culture. Note: original 1 and 2 are duplicates for the culture without oxygen added.

For the Butyrate culture, the t-test results showed that the original 1 and 2 are different. The t-test also showed that the original 1 sample is different from 1.5 mg/l DO and 2.5 mg/l DO. The 1.5 mg/l DO and the 2.5 mg/l Do are also statistically different. Even so the differences seemed to be small than for the SRS enrichment culture.

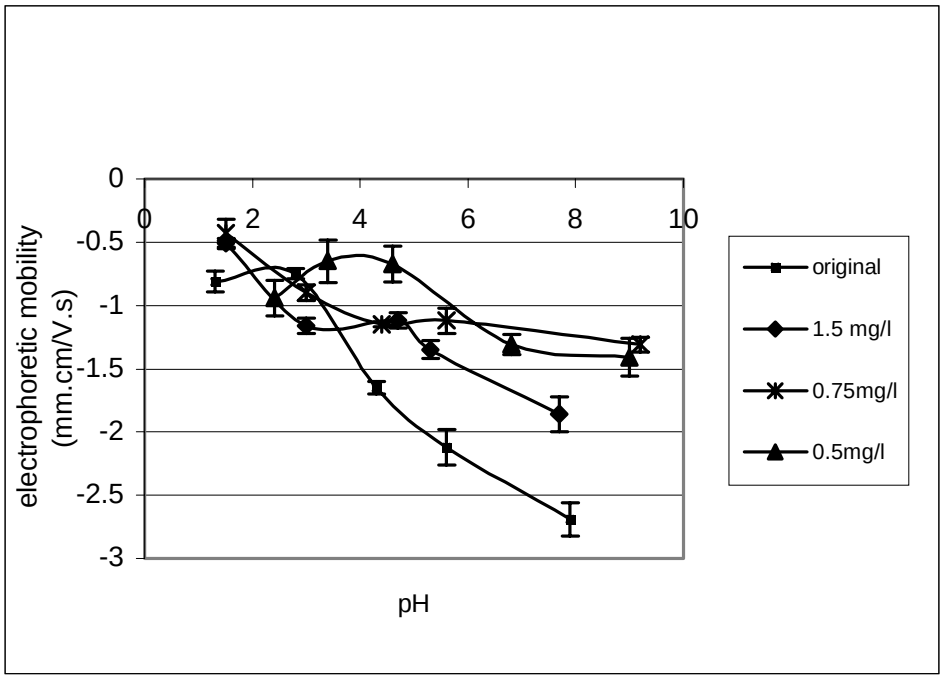

Figure 7.12: SRS culture electrophoresis mobility as a function of dissolved oxygen and pH. Electrophoretic mobility as a function of pH for the SRS culture for dissolved oxygen concentrations of 0.5, 0.75 and 1.5 were statistically different to original, non-stressed culture.

The MATH assay conducted for both the butyrate culture and the SRS culture at different DO concentrations did not show any adhesion at the TCE or sand interfaces. This is an indication that the interfacial tension reductions are not caused by direct adhesion of bacteria at the interface.

7.7 Conclusions

In summary, significant reductions in the interfacial tension were observed, both due to the DNAPL itself and biological activity. The interfacial tension of the DNAPL is extremely low and is attributed to acidic components in the DNAPL. These could have been released as part of the DNAPL following its use in the manufacturing area, or other materials could have partitioned into this solvent after its release.

Among the biological growth conditions tested (elevated concentrations of EDTA, ammonia, PCE and several levels of dissolved oxygen) induced stresses affected interfacial properties. Most significant effects for the butyrate using enrichment culture were obtained in the presence of oxygen. Table 7.14 summarizes the percent reduction in surface tension (ST) and interfacial tension (IFT) after 24 hrs for particle-free media and media that contained bacteria (particulate). ST declined up to 15 % for the media that contained bacteria while ST for the particle-free fraction was not affected. Reduction in IFT was observed for both particle-free and particulate fractions. However, IFT for the particulate fraction decreased to a greater extent. A reduction in IFT for a particle-free solution would be indicative of the presence of dissolved biosurfactants, which should also induce a reduction in ST. No significant reduction in ST for the particle-free fraction, however, was observed. The particle-free media was

generated through filtration through 0.2 μm filters. Particles smaller than 0.2 μm particles could have passed through the filter and accumulated at the TCE/water interface. Since inorganic colloidal particles did not exert similar changes in IFT than the biotic experiments we conclude that the observed effects were due to the biological activity.

We conclude that the interfacial tension reductions observed were neither due to bio-surfactant production nor to the bacteria adhesion at the interface as shown by the MATH assays. It is possible that bacteria produced polymeric compounds that have aggregated and settled or adsorbed at the TCE water interface. Klein and Dhurjati (1995) studied CheY protein aggregation kinetics in *Escherichia Coli* and showed that proteins (polymers of α-amino acids) are able to aggregate in soluble and insoluble forms, and that the aggregation was time dependent. In addition, many studies showed that proteins could be adsorbed at interfaces and reduce the interfacial tension (Beverung et al., 1999), (van der Vegt et al., 1996) and (Keshavarz et al., 1979). Furthermore, He et al., (1998) showed that bacteria under certain growth condition are able to produce polymer compounds. They showed that the Strain pseudomonas strain stutzeri coded 1317 isolated from contaminated soil was able to produce polyhydroxyalkanoates when grown in glucose and soybean oil as carbon source. Majid et al. (1999) also showed that the *Erwinia* sp. USMI-20 was found to produce poly(3-hydroxybutyrate) from either palm oil or glucose. They also found that this bacteria is able to produce the copolymer poly(3-hydroxybutyrate-*co*-3-hydroxyvalerate) using a combination of palm and another carbon source such as propionic acid but the effect of these polymers on the interfacial tension remains unclear. In addition, Lefebvre et al., (1997) studied the effect of dissolved oxygen concentration on polymer production by *Alcaligenes eutrophus* bacteria. The study showed that under low dissolved oxygen concentration and nitrogen limitation conditions, an increase of poly (3-hydroxybutyrate-co-3-hydroxyvalerate) was observed. This was likely due to the low glucose uptake caused by the low dissolved oxygen concentration (Lefebvre et al., 1997).

Time = 24 hours	**Particulate**		**Particle Free**	
Variable	**ST**	**IFT**	**ST**	**IFT**
DO = 0 mg/l	2.80	5.53	-1.01	10.16
DO = 1.5 mg/l	11.47	42.53	3.47	33.75
DO = 2.8 mg/l	4.04	22.05	-0.84	14.13
PCE = 190 mg/l	15.31	37.48		

Table 7.14: Summary of surface tension (ST) and interfacial tension (IFT) assays. Presented in the percent decline in ST of IFT relative to the stock culture.

8.0 Research Details – Objective 3

8.1 Objective

- Quantify the net effects associated with DNAPL surface chemistry on phenomena governing multiphase flow in the unsaturated zone

Note – in the following sections, the work related to this objective is broken into two parts – research conducted with micromodel experiments versus that conducted with the multi-step k-S-P (permeability-saturation-pressure) outflow experiments. Differences in the scale of measurement made in these two experimental procedures allowed us to evaluate pore scale and column scale influences of variable wetting properties and interfacial tension.

8.2 General materials

Characteristics of the fluids involved in both this investigation are presented in Table 8.1. A viscometer (Cannon-Fenske Opaque viscometer, Cannon Instrument Corp., State College, PA) was used to measure the viscosities of the fluids. Viscosity was determined according to the procedures of ASTM standard #DF445-97. Surface (interfacial) tensions were measured using a Du Nuoy ring tensiometer (Fisher Surface Tensiomat 21, Fisher Scientific, Pittsburgh, PA), according to ASTM standard #D-971.

Table 8.1: Physical properties of the investigated fluids.

	Water	10% Ethanol	50% Ethanol	Ethanol [b]	TCE[b]	SRS DNAPL	Air
Surface tension σ, (mN m^{-1})[a]	69.5	46.0	28.7	38.0	34.5	1.2	-
Surface tension ratio (-)[b]	1.00	0.64	0.40	0.0789	1.4600	*	-
Density ρ, (g cm^{-3})[c]	1.0064	0.9936	0.9374	1.09	0.5	*	0.00128[e]
Dynamic viscosity μ, (g sec^{-1} cm^{-1})[d]	0.010	0.014	0.024			*	0.00018[e]

[a] This study, measured at 22°C, using the ring tensiometer.
[b] Using the surface tension of water as reference.
[c] This study, measured at 22°C.
[d] This study, measured at 22°C.
[e] Liu et al. (1998).
* not enough sample volume for measurement

8.3 Methods – Micromodels

Micromodels were fabricated from plate glass and 0.5-mm glass beads. Image and quantitative analysis of the drainage and imbibition of fluids through these models provided an understanding of the net effect of lowered interfacial tension or altered wettability on the flow and distribution of fluids in multiphase systems. The experimental procedures used to characterize the fluids and the models, along with the methods and variables tested are outlined in this section. Various image analysis software packages were evaluated to determine the most suitable and direct approach to analyze the fluid distributions and interface characteristics of interest.

Materials

The two-fluid systems considered in our study consisted of three systems, i.e., air-water, air-ethanol solution, and DNAPL-water systems. Distilled and deionized (DDI) water that was degassed was used as aqueous phase to initially saturate the micromodel and for all other uses. Ethanol (Pharmco Products,

Brookfield, CT) was utilized for low surface tension tests. The ethanol was used at 100% or mixed with 50% water by volume for the 50% ethanol/air systems. TCE (99.5%, Sigma Aldrich Co., St. Louis, MO) was used as the DNAPL. The TCE was allowed to equilibrate with water to prevent any mass transfer effects during the experiments. A DNAPL sample taken from the Savannah River Site (SRS) was used in later experiments as the site DNAPL. The DNAPL has been characterized as 75-90% PCE with TCE as the balance.

Various dyes were tested during this investigation to clearly visualize the liquids within the micromodels. Hydrophilic and hydrophobic dyes were needed for the aqueous phase and DNAPL, respectively. Potassium indigotrisulfonate (blue) (Sigma Aldrich Co., St. Louis, MO) was chosen as the hydrophilic dye for water and used at a concentration of 100 mg/L. 30-mL samples of water were prepared due to the light-sensitivity nature of the potassium indigotrisulfonate. This chemical becomes lighter when exposed to natural or artificial light. The 30-mL samples were used immediately and extra fluid was discarded. There was no significant change in color of the water phase over the course of a drainage and imbibition experiment.

The ethanol solutions required different dyes due to differences in hydrophobicity between the 50% and 100% ethanol solutions. The 50% ethanol solutions were dyed green or blue using conventional food coloring (McCormick, Hunt Valley, MD) at a concentration of 5 drops/ 10 mL. The pure ethanol and TCE were colored with Oil Red O (Sigma Aldrich St. Louis MO) at a concentration of 0.1 g/L.

The porous medium used in these investigations was 0.5 mm-diameter glass beads (Cataphote Corporation, Jackson, MS). The glass beads were sieved in the laboratory and the 30/40 (0.42-0.6 mm) fraction was retained. 500 g of the sieved glass beads were placed in an 800-ml beaker and cleaned by soaking in 50% HNO_3 solution for 12 hours. This was followed by repeated batch washes with acetone and then DDI water. The beads were dried at 103°C in a clean oven for 48 hours. The clean beads were then again sieved in a ~0.5-mm wire mesh. The fraction of glass beads that were trapped and retained in the sieve openings was kept for use in the micromodel construction.

The wetting properties of the clean glass beads were altered to assess the effects of variable wettability on two-fluid flow. The glass beads and glass plates used in the micromodel construction had strongly water-wet characteristic in the fluid systems tested. Their wettability was altered using octadecyltrichlorosilane (OTS; Sigma-Aldrich, St. Louis, MO). The OTS-treated glass beads were obtained by placing 100 g of glass beads in a 125-mL flask with 5% solution of OTS dissolved in ethanol. The mixture was shaken for 5 hours and subsequently air-dried (Anderson et al., 1991). The micromodels were constructed with no treated or 50% OTS-treated beads by volume.

Experimental Setup and Procedure

Two dimensional glass bead micromodels were used in all experiments of this study. Glass beads were sandwiched between two 0.32-cm thick glass plates (St. Lawrence Glass Co, Massena, NY). To control multiphase flow, two capillary barriers were installed for each end of the micromodel (Figure 8.1). A NAPL-wet Teflon strip with the thickness of 0.10 mm (Small Parts Inc, Miami Lakes, FL) was secured to the bottom plate. A water-wet stainless steel strip was placed 7 cm from the Teflon strip towards the opposite edge of the glass plate. The glass beads were contained between the two barriers and the remaining model area was the fluid reservoir. The micromodel was sealed using a UV-cure adhesive (Loctite, Rocky Hill, CT). A few micromodels were created that contained 50% non-water wetting glass beads. These beads were created through their exposure to an organosilane.

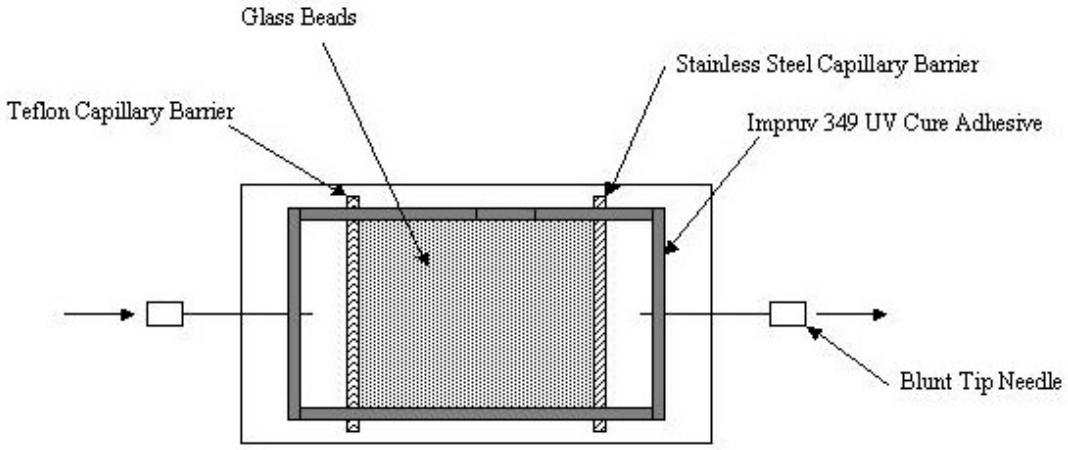

Figure 8.1: Experimental glass-bead micromodels.

The experimental setup is shown in Figure 8.2. The apparatus consisted of the micromodel, a syringe pump, and a video camera (Sony CCD-IRIS, Sony Corp., Kansas City, MO). The syringe pump was used to inject fluids through the micromodel. Live analog images of the micromodel were captured using the video camera and a manual focus lens (10X c-mount lens, Computar Inc., Commack, NY), digitized using a frame grabber board (EPX-PIXCI SV4, I-cubed Inc., Crofton, MD), and analyzed with image analysis software (EPIX XCAP-STD V2.1.010924, I-cubed Inc., Crofton, MD). Teflon and Tygon tubings were used to make the connections from the syringe pumps to the micromodel.

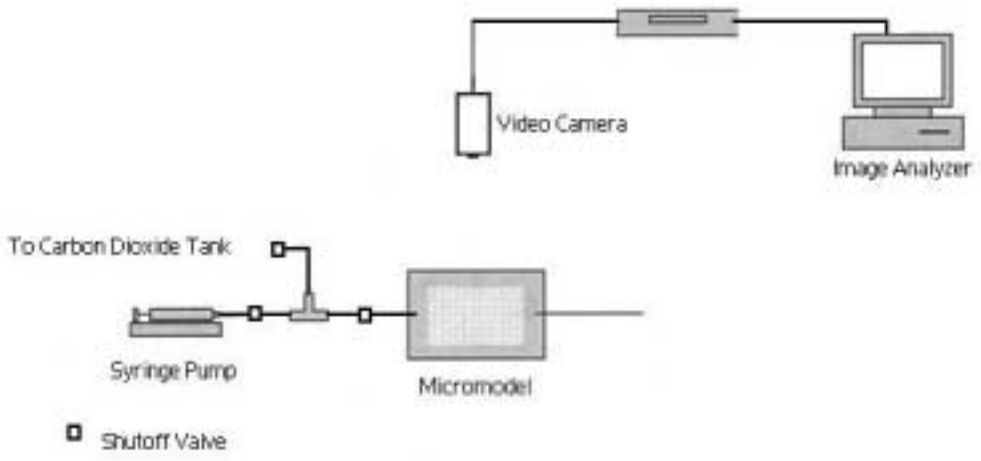

Figure 8.2: Experimental Setup (not to scale) for micromodel experiments

The micromodel was vertically oriented, flushed with carbon dioxide at a very low flow rate for 1~2 hours, and then saturated with 50 mL of degassed DDI water at a rate of 99 mL/hr. To remove any carbon dioxide dissolved water, one hundred pore volumes of water were flushed. Experimental initial conditions were set as those when the nonwetting fluid (air or DNAPL) occupies completely the fluid reservoir of the nonwetting (Teflon) capillary barrier. In the case of air-water and air-ethanol solution systems, dyed liquids were injected from the bottom to displace non-colored water within the micromodel and related tubing. Then, air was pumped into the fluid reservoir of the nonwetting (Teflon) capillary barrier in order to achieve an initial condition. In the case of DNAPL-water systems, dyed DNAPL was pumped into the nonwetting fluid reservoir for achieving an initial condition. After achieving initial conditions, the drainage event of the wetting phase was performed, and followed by imbibition. The micromodel experiments were conducted at a fixed flow rate of 1.5 mL/hr, as determined through a series of preliminary experiments. To conduct subsequent experiments, the micromodel was flushed with water and then cleaned with alternate batch washes of DDI water and acetone.

During each drainage or imbibition event, images were captured at the following times: 0 min, 2 min, 4 min, 6 min, 8 min, 10 min, 15 min, 20 min, 25 min, 30 min, and 45 min. Zero time is defined as the experimental initial condition. More frequent images were captured during the early times of each event because the invading front was the most active during these times. The images from t=6, 15, and 20 min were chosen for the image analysis. Image capturing was ceased when the displacing fluid exited the glass beads and crossed the capillary barrier.

Analysis - Determination of Fractal Dimension, Fractal Coefficient, and Interfacial Length

Image-J 1.24t (National Institute of Health, USA) was used to process the captured images, through which color images were changed to black and white images. The PROCESS function of Image-J program was used to identify the two-fluid interfaces. The determination of the bulk fluid interface length required additional image processing. The black and white image contained lakes, which are defined as entrapped pockets of the wetting fluid, and islands, which are entrapped pockets of the nonwetting fluid. Options within Image-J were used to fill in the lakes and islands, and to delineate an apparent bulk phase interface (Figure 8.3).

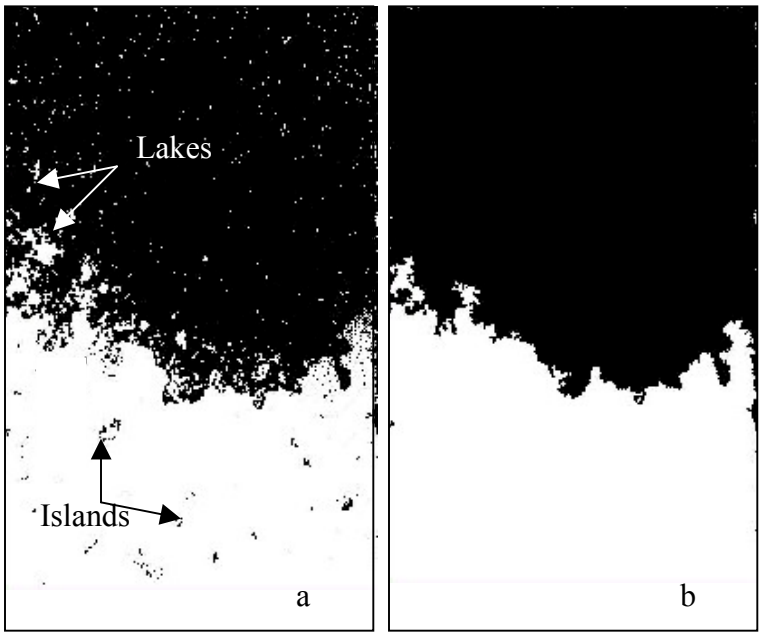

Figure 8.3: Images of water (black) imbibition before (a) and after (b) image was adjusted to isolate the bulk fluid phase.

A fractal analysis technique was employed to quantify displacement characteristics of two phase flow in glass bead micromodels. This analysis technique has been used as a quantification technique in Hele-Shaw cells as well as 2-D porous media (Smith and Zhang, 2000; Oxaal et al., 1987; Maloy et al., 1985; Nittman et al., 1985). Fractal Analysis yields two parameters: fractal dimension (D) and fractal coefficient (b).

Wetting front instability has been examined with a fractal approach as well. Smith and Zhang (2000) and Chang et al. (1994) examined finger development and wetting front instability as related to effective interfacial tension (σ^*). σ^* is the deviation from bulk interfacial tension that occurs in a porous medium due to the discrepancies between the macroscopic and microscopic interface lengths. Interfaces can be described on a macroscopic or microscopic scale, greater than pore scale or smaller than pore scale, respectively. If the curvatures that occur within a pore were taken into account when determining the interface length, it would be much greater than if the interface length were considered a straight line across the pore space, macroscopically. The interfacial coefficient (C) is defined as (Smith and Zhang, 2000):

$$C = \frac{L^*}{L} \tag{1}$$

where L is macroscopic interface length, and L^* is microscopic interface length.

The value of L^* cannot be directly measured because of the complexity of the fluid-fluid interface and is, therefore, approximated by the measured interfacial length (L_d) which depends on the measurement accuracy or observation scale (d) (Smith and Zhang, 2000). The relationship between L_d and d is presented by Mandelbrot (1982):

$$L_d(d) = ad^{1-D_S} \tag{2a}$$

where Ds is the surface fractal dimension and a is the fractal coefficient. If Eq. 2a is re-written in terms of a line fractal dimension(D_L), the resulting equation is

$$L_d(d) = ad^{-D_L} \tag{2b}$$

Dividing both sides of Eq. 2b by L yields:

$$\frac{L_d(d)}{L} = bd^{-D_L} \tag{3}$$

where b (=a/L) is time-independent fractal coefficient. The log-linear relationship presented in equation (3) is used to determine the fractal coefficient and fractal dimension based on measured values of the interface length over a range of observation scales.

At an appropriately small scale ($<d$), the actual L^* at the pore scale is the value of L_d (Smith and Zhang, 2000).

$$L^* = L_d(d^*) \tag{4}$$

where d^* is microscopic observation scale. Substituting Eqs. 2b~4 into Eq. 1 yields:

$$C = \frac{L_d(d^*)}{L} = b(d^*)^{-D_L} \tag{5}$$

The total interface length (L_t^*) is the length of the bulk fluid interface plus any interface length associated with entrapped fluid. The bulk fluid interface is the interface created by the bulk migration of the displacing fluid. As the fluid migrates through the porous medium, discontinuous globules of the displacing fluid are entrapped in the porous medium. L_t^* can be determined from Eq. 1 by:

$$L_t^* = C \times L \quad (6)$$

The bulk fluid interface length (L_c^*) is determined by applying Eqs. 5 and 6. The interface length of the entrapped fluid (L_e^*) is determined as the difference between L_t^* and L_b^*.

$$L_e^* = L_t^* - L_b^* \quad (7)$$

D_L and b in Eq. 5 were determined using the box counting method (Warfel, 1998). The default box sizes were appropriate to the micromodel scale (ranging from a single pore to smaller than the micromodel, i.e., 0.2~5 mm). The parameters D_L and b were compared for different experiments with the same micromodels and for different micromodels. Student *t*-tests, assuming equal and unequal variances, with a null hypothesis were used to determine if there were statistically significant differences between experiments.

To estimate interface lengths, the value of C was calculated from Eq. 5 using the values of D_L, b, d^*, and L. Herein, d^* was approximated by the mean particle diameter (Smith and Zhang, 2000) and L by the micromodel width. Three interface lengths (L_t^*, L_b^*, and L_e^*) were calculated using Eqs. 5 through 7. These lengths – in a 2-D system - are used in a relative sense to evaluate the effects of interfacial tension on surface area. They cannot be used in an absolute sense.

8.4 Results - Micromodels

Visual Observations

During drainage for air-aqueous phase systems, the air was introduced from the top of the micromodel. The air migrated through the porous medium in a piston like fashion. Pockets of the wetting fluid, occupying 2~5 pore spaces, were retained throughout the porous medium, especially for water (Figure 8.4), which has a much higher surface tension than ethanol (Table 8.1). Imbibition of the wetting phase showed similar results as drainage. However, the interfaces were less erratic, a characteristic which indicates a process such as gravity stabilization (Liu and Dane, 1996) moderated the flow. Water imbibed into the porous medium, entrapping the non-wetting phase (air) with such mechanisms as snapoff (Yu, 1985), wherein the wetting fluid in a pore throat causes the non-wetting phase to become disconnected from associated pores that remain filled with the non-wetting fluid. There was no apparent change in the interface with decreasing surface tension, again suggesting that the gravitational forces were dominant over the capillary forces.

For the DNAPL-water systems, the DNAPL was introduced into the porous media from the bottom of the micromodel to keep the relative density relationships consistent with that of the air-aqueous phase experiments. This simulation is analogous to water-displacing DNAPL pools in the subsurface. During the imbibition of the DNAPL, the SRS DNAPL produced a more stable interface, resulting in fewer retained regions of water (Figure 8-5). The stabilized interface was expected due to the very low IFT of the SRS DNAPL, which minimizes capillary forces governing the interface, allowing the gravitational force to become dominant. Stability is characterized by a smooth interface between the wetting and non-wetting phases. The TCE experiment produced a more erratic interface and resulted in a larger percentage of retained water. The edge effect observed in the TCE experiments could have been caused by its affinity for the glue used to build the micromodel. This edge effect was not seen with the SRS DNAPL.

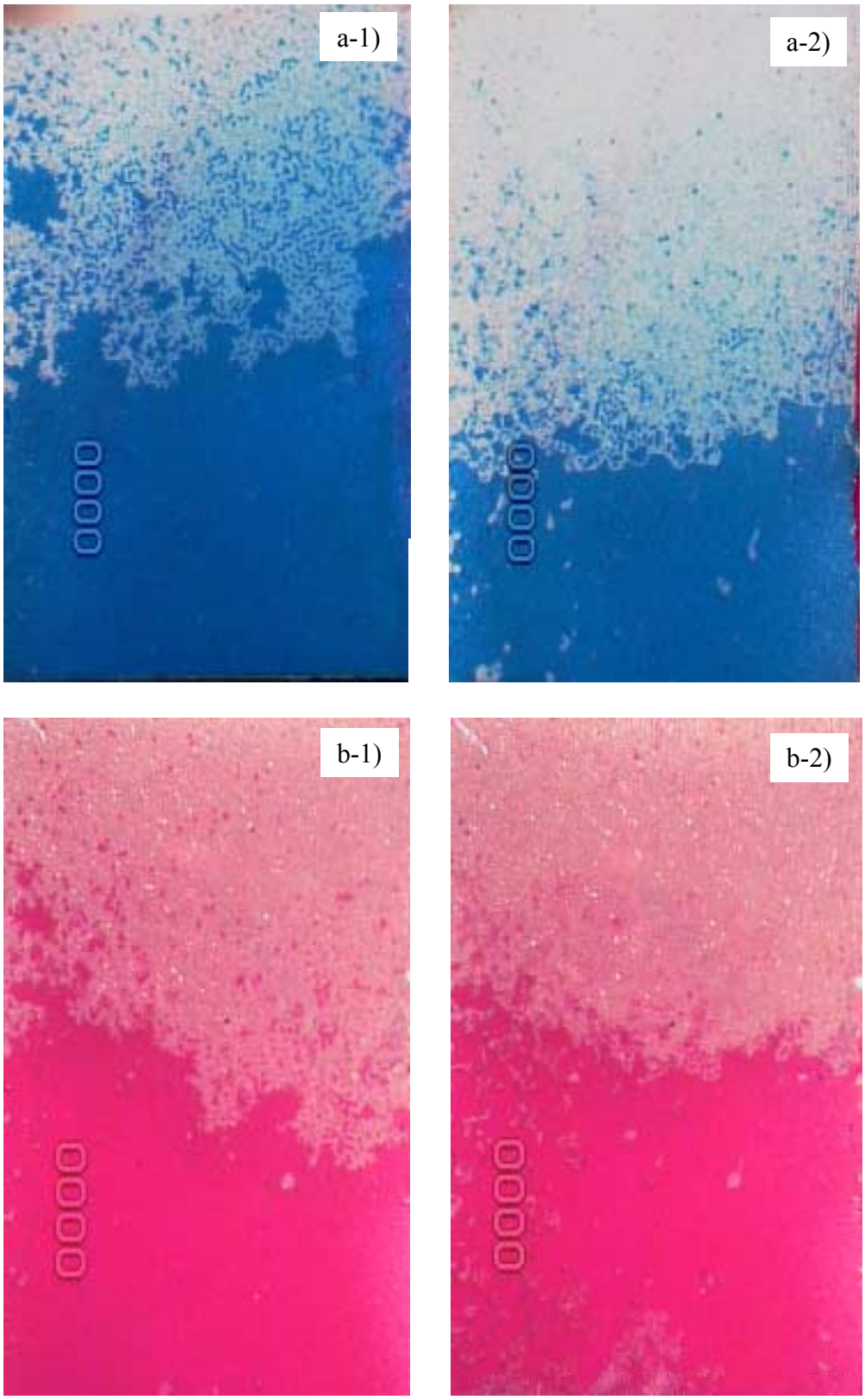

Figure 8.4: Drainage (1) and imbibition (2) patterns for micromodel experiments with water (a) and ethanol (b) as the liquid phase. All photos were taken ~15 minutes into the flow experiment.

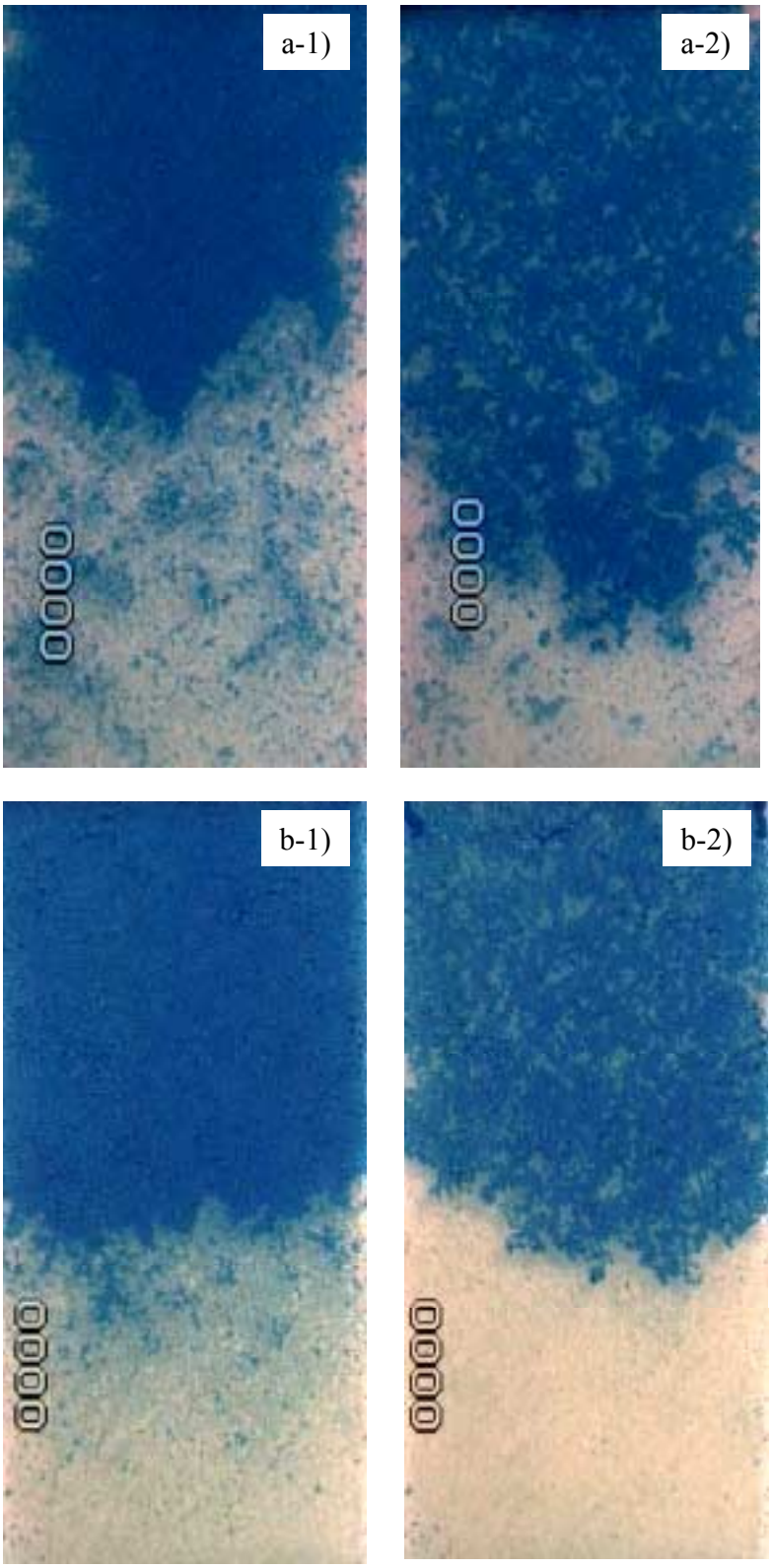

Figure 8.5: DNAPL imbibition (upward) into water (blue) (1) and DNAPL drainage (downward) (2) patterns for micromodel experiments with TCE/water (a) and SRS DNAPL/water (b). All photos were taken ~15 minutes into the flow experiment.

The imbibition of water into the micromodel (Figure 8.5 (a-2 and b-2)) yielded similar trends observed in the air-aqueous phase experiments. The SRS DNAPL appears to have a smoother interface, however, upon closer investigation, exhibited lobe-shaped and transient perturbations that are characteristic of unstable interfaces (Liu and Dane, 1996). The TCE-water interface appears to be more erratic, however the SRS DNAPL-water interface produced shorter, but thinner, fingers, characteristic of lower interfacial tension systems as noted by Smith and Zhang (2000). The finger width decreased by a factor of two, from approximately 4mm to 2mm. Similar amounts and sizes of entrapped DNAPL ganglia were observed in both cases.

Fractal Analyses

Air-fluid systems

The strong linear relationship between ln $L_d(d)/L$ and ln d (Figure 8.6) indicates that both the drainage and imbibition pathways exhibit characteristics of a fractal. Regression coefficients from these linear relationships define the fractal dimension (D_L) and fractal coefficient (b) (equation 3).

D_L values estimated in our study (Table 8.2) are representative of the range of D_L (1.31~1.64) reported by Ogawa et al. (1998). D_L decreased with decreasing surface tension during drainage. This indicates that the porous medium has less effect on the shape of the interface, which is supported by the fact that the non-wetting fluid can more readily enter smaller pores at a lower surface tension. The smaller pores are now easily accessible because their entry pressure has been decreased. During imbibition, D_L was found to remain approximately the same 1.39 and 1.44 vs. 1.41 and 1.42, with decreasing surface tension. Similar results have been reported by Smith and Zhang (2000) with the use of surfactants to reduce interfacial tension.

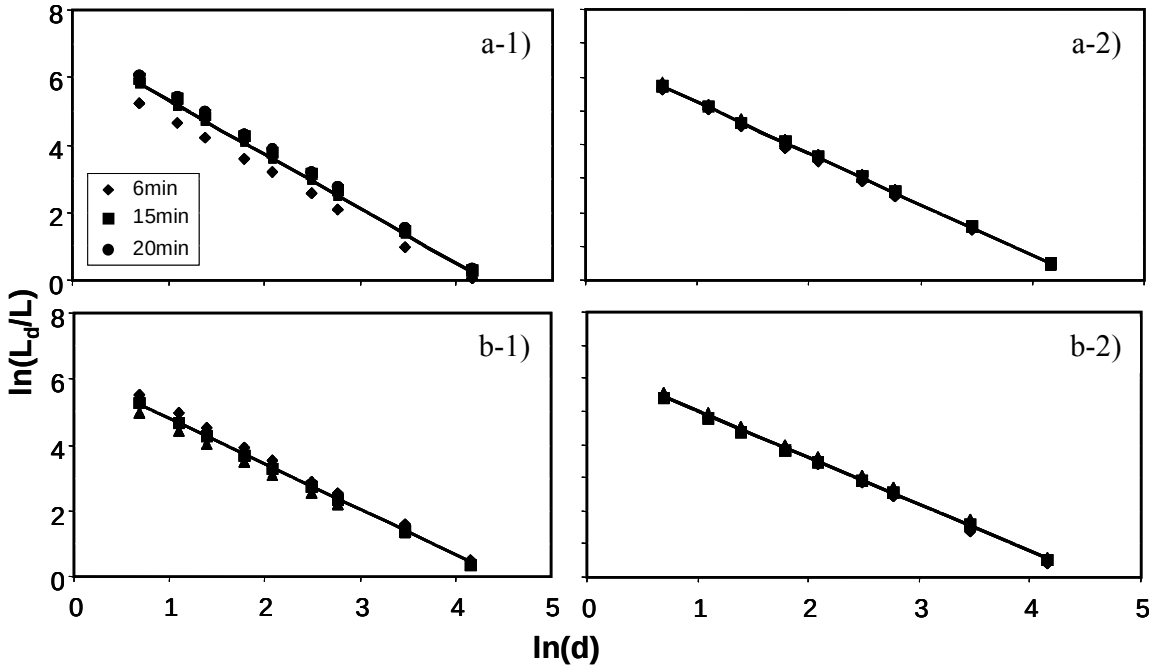

Figure 8.6: ln($L_d(d)/L$)-ln(d) relationships for air/fluid micromodels experiments. Drainage (1) and imbibition (2) with water (a) and ethanol (b) as the liquid phase. The listed times are elapsed time since overcoming the entry pressure across the capillary barrier.

Table 8.2: Fractal coefficients and dimensions for micromodel studies

Fluids			water drainage		water imbibition	
NWP	WP	ST/IFT (dynes/cm)	Fractal Dimension D (-)	Fractal Coefficient b (-)	Fractal Dimension D (-)	Fractal Coefficient b (-)
air	water	69.5	1.61 ± 0.05	6.92 ± 0.14	1.39 ± 0.03	6.19 ± 0.08
air	water	69.5	1.63 ± 0.03	6.99 ± 0.07	1.44 ± 0.03	6.27 ± 0.06
air	50% etoh	52.0	1.56 ± 0.01	6.60 ± 0.02	1.41 ± 0.02	6.00 ± 0.04
air	etoh	38.0	1.52 ± 0.01	6.80 ± 0.04	1.42 ± 0.02	6.40 ± 0.04
TCE	water	34.5	1.47 ± 0.02	6.28 ± 0.04	1.70 ± 0.05	7.39 ± 0.12
SRS DNAPL	water	1.2	1.41 ± 0.01	5.83 ± 0.03	1.73 ± 0.04	7.37 ± 0.10

The experiments produced a statistically different D_L value between drainage and imbibition paths (Table 8.2), under both high and low surface tension conditions. During drainage, the gravitational forces complement the capillary forces and further destabilize the migrating interface (Liu and Dane, 1996) and are characterized by the relatively higher D_L (1.52~1.63). The gravitational force, however, acts to minimize the capillary forces during imbibition due to the travel direction of the displacing fluid (upwards). This lead to a less erratic interface characterized by the lower D_L (1.39~1.44).

In the case of *b* values, the experiments produced similar trends to those of Smith and Zhang (2000). During drainage, *b* decreased from 6.92 ~ 6.99 to 6.6 ~ 6.8, with a decrease in surface tension. The trends observed here were determined to be statistically significant with the student *t*-test, assuming unequal variances at α=0.05. The magnitude of the observed decrease was less than that of Smith and Zhang (2000), however the relative trends remained the same. There were no measured change in *b* values with changing surface tension during imbibition. The most likely cause of this is the dominance of gravitational force over capillary force during the upward migration of the wetting fluid. The micromodel conditions that resulted in statistically significant D_L and *b* values include:

- difference between drainage and imbibition paths – low surface tension
- difference between drainage and imbibition paths – high surface tension
- difference between low and high surface tension during drainage

DNAPL-water systems

The DNAPL-water experiments were compared with two air-aqueous phase experiments, one high surface tension and one low surface tension. This combination of micromodel experiments that represents the full range of interfacial tensions that were tested in this study.

D_L and *b* values were affected by interfacial tension for both the water drainage and imbibition experiments (Table 8.2). D_L decreased from 1.61 to 1.41 with decreasing surface/interfacial tensions (water ➔ SRS DNAPL) during drainage, indicating that the porous matrix had less impact on the shape of the interface at lower interfacial tensions. The reduced interfacial tensions allow the displacing fluid to enter smaller pores that can be bypassed at higher interfacial tensions due to the high capillary pressure. *b* was found generally to decrease with decreasing interfacial tensions, indicating that the lower interfacial tension systems resulted in thinner fingers (Smith and Zhang, 2000; Chao et al., 2000). Chao et al. (2000) found that the sizes of the fingers were a function of interfacial tension and could be described by a relationship developed by Tung and Parlange (1976) and Rimmer et al. (1996).

During water imbibition, D_L and *b* increased with decreasing interfacial tension at statistically significant levels. This indicates that the porous matrix had more effect on the shape of the interface at low interfacial tensions. Gravity stabilization of the invading interface would allow the fluid to be more sensitive to variations in the porous matrix at low IFTs. This is opposite to what was observed during the drainage.

Variable wettability systems

D_L was found to decrease slightly for water drainage with a wettability change from completely water-wet to 50% fractional-wet porous medium (Table 8.3). The one exception was the case of water imbibition at the air-water system, where the D_L remained constant with the variable wettability. A more uniform fluid front, as a result of a fraction of the pores being preferentially wetted by the invading fluid, is supported by the decrease in the D_L for both IFT conditions during water drainage. The decrease of D_L in TCE-water system and constant D_L values in air-water system during water imbibition may be related to the distribution of the NAPL-wet pores in the fractional-wet medium (McDougall and Sorbie, 1995). The nonwetting phase would occupy different pores after the initial displacement of the wetting phase. McDougall and Sorbie (1995) specifically related this difference in the size of the pores that remain filled with the nonwetting fluid.

Table 8.3: Fractal dimensions and coefficients as a function of wettability

Condition	Fluids	100% Water Wet		50% Water Wet	
		D_L	b	D_L	b
water drainage	air-water	1.61±0.05	6.92±0.14	1.46±0.05	6.48±0.11
water imbibition	air-water	1.39±0.03	6.19±0.08	1.39±0.02	6.24±0.04
water drainage	TCE-water	1.47±0.02	6.28±0.04	1.42±0.03	6.36±0.07
water imbibition	TCE-water	1.7±0.05	7.39±0.12	1.61±0.02	7.31±0.06

Relative Interface Lengths

The fractal analyses performed for the DNAPL-water systems as well as air-aqueous phase systems were extended to evaluate the characteristics of the entrapped phase during displacement. Characteristics of the bulk fluid interface were isolated from the total, which also included entrapped wetting and non-wetting phases (Figure 8-3). D_L and b values of the bulk fluid interfaces remained generally constant as a function of both drainage vs. imbibition and surface/interfacial tension. In contrast, there were statistically significant differences in both of these characteristics when all of the interfaces within the micromodel were considered. This suggests that while the bulk fluid interface remains similar in all of our experiments, the interfaces associated with the fluid that is entrapped is quite different as a function of these variables.

Since most pertinent research has focused on indirect theoretical methods to estimate interfacial areas, a direct comparison of the calculated entrapped interfacial areas to literature values was not possible (Oostrom, 2001; Held, 2000). Theoretical estimations often include various assumptions about the pore geometry and focus on the bulk fluid phase, not the entrapped phase (Oostrom, 2001). The method used to calculate the relative interfacial areas in this study used the measured parameters D_L and b. During drainage, D_L based on all interfaces within the micromodel decreased with decreasing interfacial tension and b increased with decreasing surface tension. This was expected because at a lower interfacial tension, the entry pressure of smaller pores has been surpassed, allowing the displacing fluid to enter the previously bypassed pore.

The observed trends in D_L and b had a direct impact of the determination of the entrapped interface lengths of the residual wetting and nonwetting phases (Figure 8-8). Constant D_L and b values for the bulk fluid phase over the range of surface tensions tested for both drainage and imbibition lead to constant estimates of the interface length.

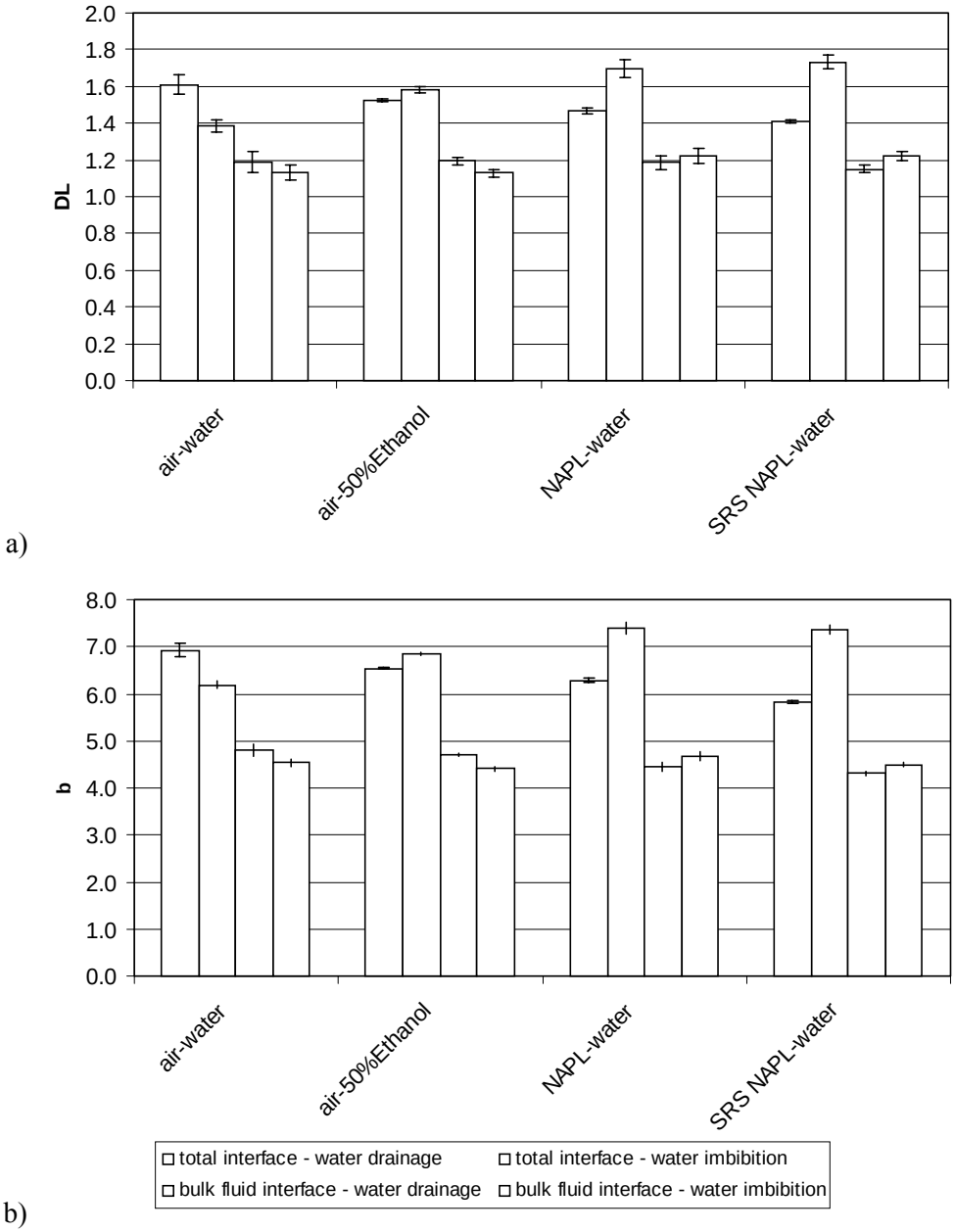

Figure 8-7: Fractal dimensions (a) and fractal coefficients (b) for all interfaces within the micromodel versus those that comprise the bulk fluid interface.

A linear regression performed over residual wetting phase interface length and residual nonwetting phase length yielded statistically different slopes when compared to the null hypothesis, m=0 (P_{value} = 0.05 and 0.03, respectively) (Figure 8-8). The bulk fluid interface lengths remained relatively constant over the range of fluids tested. The total microscopic interface is the sum of the continuous and entrapped interface lengths. It is easy to see that trends in the microscopic interface lengths are predominantly influenced by changes in the entrapped or retained interfaces rather than the continuous interface.

During drainage, the length of the entrapped wetting phase decreased by a factor of 2 with a decrease in interfacial tension of from water to almost zero. The initial displacement at high surface tension would allow the invading fluid to be very selective in the migration pathway. Smaller pores that were

characterized by high capillary pressure would cause this. As the interfacial tension decreases, the invading fluid could enter the smaller pores and ultimately decrease the entrapped phase interface length. This phenomenon was supported by the decreasing D_L values. During imbibition, the entrapped interfacial lengths of the residual non-wetting phase increased by almost a factor of two between the water-air system and the water-SS-DNAPL system. This is consistent with the fact that lower fractal coefficients produce thinner fingers with increased surface area. Little difference was observed, however, between the interface length of entrapped TCE and the SRS DNAPL. Limited supplies of the SRS DNAPL prevented replication and verification of this result.

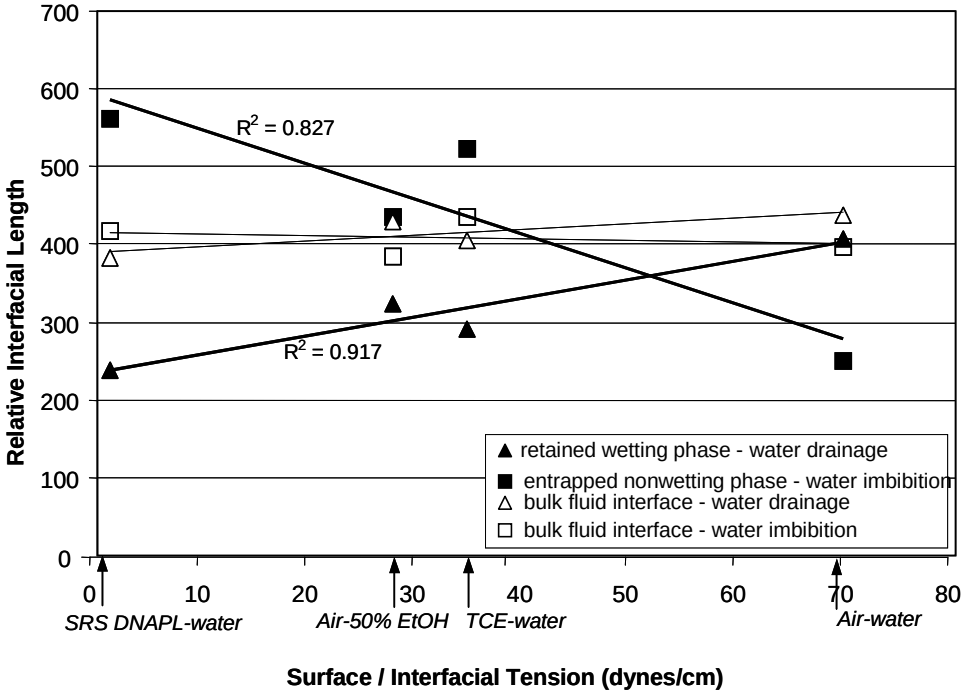

Figure 8-8: Relative length of the entrapped and bulk fluid interfaces as a function of surface/interfacial tension.

Various physical, biological, or chemical processes, such as dissolution, biodegradation, and chemical oxidation, often depend on the available interfacial area. The approach used here to estimate the interface lengths does not make any assumptions regarding the pore geometry, is directly related to the porous medium, and may prove to more accurately depict the feasibility for various remediation techniques. The wetting phase displacement and surface interfacial tension are integral in determining the appropriate remediation strategy. This characterization of the interfacial properties and displacement would indicate the efficiency of *in situ* remediation after drainage under high IFT conditions and after imbibition under low IFT conditions.

Limitations of the method

Fractal analysis was used to quantify two-phase flow in 2-D glass bead micromodels. The D_L and b values were used as indicators to describe the interfacial characteristics of each experimental condition. This method is valid as long as the interfaces have fractal characteristics over the investigation scale. The microscopic observation scale (d^*) was approximated as the mean particle diameter, as used by Smith and Zhang (2000). However, this would inherently assume any interface smaller than this scale can be measured as a straight line when, in fact, it is actually a curved interface. A smaller investigation scale would allow a more realistic description of the fluid-fluid interface in a single pore. The determination of an appropriate d^* could lead to an over- or under-prediction of the interface lengths.

A sensitivity analysis was performed to determine the significance of this assumption. Since we wished to characterize the fluid-fluid interface, changes that affect the shape often occur at a scale smaller than the particle diameter. The calculated entrapped interfacial lengths were evaluated at d^* = 0.5 mm, 0.25 mm, and, 0.2 mm. The lowest limit was established by the smallest box-size used in the box counting method to calculate D_L. The strong linear relationship between ln $L(d)/L$ and ln d supported the fact that properties of fractal still existed at this smallest investigation scale. The changes in d^* resulted in changes in the calculated entrapped interfacial lengths, however the relative trends remained the same. The calculated entrapped interface lengths all increased as d^* decreased.

These results accurately depict the relative trends in entrapped phase interfacial lengths in the micromodels. The method used to calculate the interfacial areas appears to be valid, however the appropriate d^* should be determined. The lengths calculated in this study are used for relative comparisons and cannot be use to directly estimate the interface lengths to determine mass transfer. The images used for fractal analysis must have good resolution. Improved resolution would allow a smaller investigation scale using the box counting method. The microscopic investigation scale should be evaluated to determine at what point the images lack fractal characteristics.

8.5 Methods – Multistep Outflow Experiments and Modeling

Subsurface systems have variable interfacial properties. To predict unsaturated flow and organic solute transport under different interfacial properties, we need sufficient information regarding the capillary pressure-saturation-relative permeability (*k-S-P*) relationships. Using multi-step outflow experiments, we estimated the *k-S-P* curves for two-fluid systems with variable interfacial properties (i.e., surface tension and fractional wettability). In this study, special attention was paid to the air-water P_c-S-k_r curves as affected by various fractional-wet conditions. To get variable surface tensions and fractional-wet systems, we used ethanol and mixtures of organosilane-coated sand, respectively.

Experimental Aspects

We conducted laboratory experiments to (1) determine identify hydraulic functions that were most appropriate for multi-step outflow data with inherent measurement errors; (2) determine the extent that different experimental boundary conditions affect the uniqueness of parameter sets determined for each of the hydraulic functions; and, (3) evaluate the significance of the interfacial properties of the fluids on the overall k-S-P behavior.

Multi-step outflow experiments were performed at a room temperature of 22±1^{o}C. Fluids used in the experiment were the same as in the micromodel experiments. The porous medium consisted of a quartz sand mixture (U.S. Silica Company, Ottawa, IL 61350) with grain size graded from 0.106 to 0.600 mm in diameter (d_{50} = 0.270 mm). The sand was packed into a soil column at a predetermined bulk density (1.74 g cm^{-3}). The intrinsic permeability (k) was measured on two independent soil packings using a constant-head method (Klute et al., 1986). The average measured k value was $5.0 \cdot 10^{-7} \pm 5.0 \cdot 10^{-8}$ cm^2. To get variable fractional-wet conditions for air-water system, we used mixtures of sand composed of 0, 25, 50, and 100% organosilane-coated sands. The organosilane-coated sand was obtained by adding the sands to a 5 % solution of octadecyltrichlorosilane in ethanol. Its mixture was subsequently shaken for 5 hrs, after which the sand was air-dried (Anderson et al., 1991).

A stainless steel column, 5.47-cm diameter and 3.02-cm length, was assembled with nylon membrane filter as a capillary barrier (Figure 8-9). This filter was 0.01-cm thick, with 20.0 μm pore size that provided an air entry value > 120 cm H2O (Magna Nylon Membrane Filters, Micron Separations Inc., Westborough, MA). A micro-tensiometer was constructed by gluing a high flow ceramic cup (Soil Moisture Corp., Santa Barbara, CA) to a stainless steel tube and was inserted into the middle of the soil column. The stainless steel tubing was connected to a pressure transducer (24PCBFA6G, Micro Switch, Freeport, IL) by a short piece of Tygon tubing to make a rigid connection. The transducer was connected

to the CR-10X datalogger (Campbell Scientific, Logan, UT). Water pressure head measurements were collected at 10 s intervals.

The sand was packed in the column under water while continuously stirring to establish an initial condition of complete water saturation. To minimize erosion of the sand between each experiment, a fine stainless steel mesh was placed on the top of the sample. Three multi-step outflow experiments were repeated with the same sand packing. After re-saturation for each experiment, the sample was then equilibrated through three or four small pneumatic pressure steps until an initial water saturation of approximately 83 % was attained. This initial condition was chosen to provide the initial unsaturated condition needed at the start of outflow experiment (Hopmans et al., 1992), to prevent problems measuring capillary pressure at high saturation (> 85 %) (Corey and Brooks, 1999), and to minimize water entrapment and pore water blockage phenomena due to a sudden large pressure step was applied to a near-saturated soil sample (Wildenschild et al., 2001).

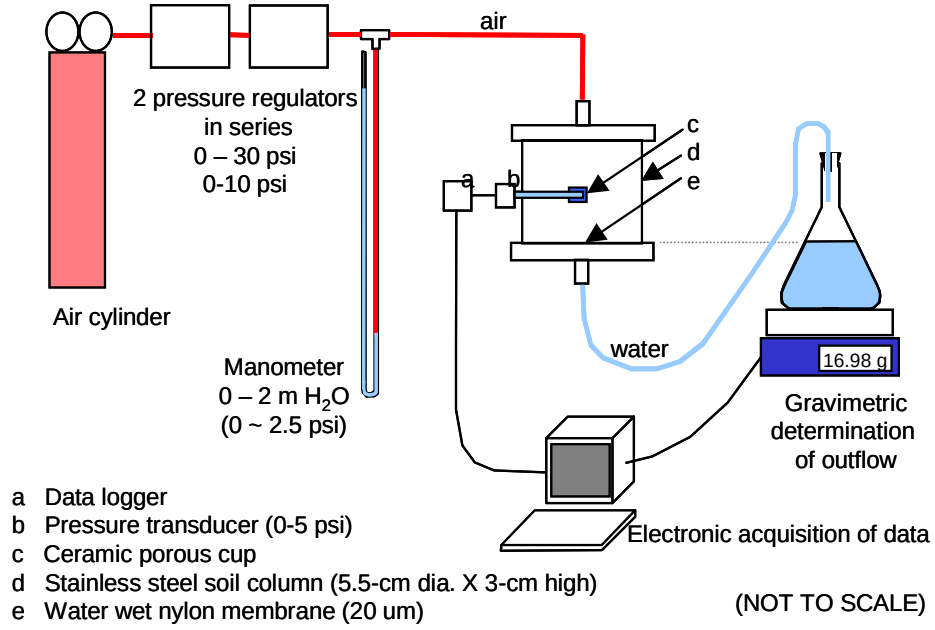

Figure 8-9: Experimental set-up for k-S-P multistep outflow experiments

Initial experiments were conducted to determine required boundary conditions for these experiments. These included:

- six pneumatic pressures were imposed on the soil sample to induce outflow with short time intervals between each successively increasing pressure increment.
- six pneumatic pressures were imposed on the soil sample as for the first case with sufficient time between each successively increasing pressure increment to allow the sample to equilibrate.
- eleven pressure steps with smaller increments were applied with sufficient time between each for equilibration.

The third set of boundary conditions was required for accurate and reproducible data and data analysis.

Data collected for each experiment included the adjustable air pressure head, which could be read with high precision (1 mm) from a water manometer; the water pressure in the middle of the cell, and water outflow for each increased pressure, which was collected in a flask on a balance and was transmitted to a computer every 10 s.

Data Analysis

Use of a numerical flow model in combination with an optimization code was required to estimate the unsaturated soil hydraulic parameters using data generated from a multi-step outflow experiment. We adopted TF-OPT of Hopmans et al. (1998), which was used previously by Liu et al.(1998) and Chen et al. (1999). The TF-OPT simulator adapted the two-fluid flow numerical model of Dr. J.L. Nieber, University of Minnesota to simulate the transient behavior of two-fluid phase flow as measured in the multi-step outflow experiments (Chen et al., 1999). To solve the governing equations, the numerical scheme of Celia and Binning (1992) was employed to achieve robust and mass conservative numerical solutions, including the modified Picard linearization algorithm of the mixed-form governing equations and a lumped finite-element approximation (Celia and Binning, 1992). Celia et al. (1990) showed that the numerical solution based on this mixed form equation was inherently mass conservative and that the lumped finite element approximation eliminated oscillations. Mass balances associated with the results from the numerical investigations conducted by Celia and Binning (1992) showed that 'even in the most computationally difficult case, the maximum mass balance error in the air phase was 0.2%, while in the water phase it is 0.003%. Celia and Binning (1992) and Chen et al. (1999) provide details of the model.

Constitutive relationships to describe the soil hydraulic properties must be selected prior to application of the numerical solution of the two-fluid flow model. In this study, we considered six soil hydraulic functions: van Genuchten-Mualem (VGM), van Genuchten-Burdine (VGB), Brooks and Corey-Mualem (BCM), Brooks and Corey-Burdine (BCB), Lognormal Distribution-Mualem (LDM), and Gardner-Mualem (GDM). Chen et al. (1999) provides additional details about each of these functions. The VGM, BCM, and LDM functions each have six fitting parameters, the VGB and BCB functions five, and the GDM function, with four, has the fewest fitting parameters. Preliminary work with both numerical experiments and multi-step outflow experimental data helped us to select the LDM model (Kosugi, 1996) for further analysis. This model, with the capillary pressure head (h_c) is the independent variable and the effective saturation (S_{ew}) and the relative permeabilities as the dependent variables (k_{rw}, k_{rn}), is given as:

Saturation: $$S_{ew} = F_n\left[\ln\left(h_m / h_c\right)/\sigma\right] \tag{8}$$

Relative Permeability: $$k_{rw} = S_{ew}^{l}\left\{F_n\left[F_n^{-n}\left(S_{ew}\right)+\sigma\right]\right\}^2 \tag{9a}$$

$$k_{rn} = \left(1-S_{ew}\right)^{l}\left\{1-F_n\left[F_n^{-n}\left(S_{ew}\right)+\sigma\right]\right\}^2 \tag{9b}$$

where $F_n(x) = 0.5erfc\left(\frac{x}{\sqrt{2}}\right)$, $S_{ew} = (\theta-\theta_r)/(\theta_s-\theta_r)$, θ is water content, θ_s is saturated water content, and θ_r is residual water content. Values are required for θ_s, θ_r, and intrinsic permeability (k). Fitting parameters include: h_m, σ and l.

8.6 Results – Multistep Outflow Experiments

Parameter Optimization Results

The inverse parameter estimation procedure was applied to multi-step outflow data for the three two-fluid pairs (air-water, 10% and 50% ethanol solutions) and three fractional-wet media (25, 50, ad 100% mass fraction of organosilane-coated sand grains), and parameters of the LDM function were optimized. Final optimized parameter sets for all systems are listed in Table 8.4.

The uncertainty in the optimized parameter values in Table 8.4 is expressed by the NSD. The NSDs for the optimized parameters were generally within just a few percent of the parameter value. The exception is the l parameter value, which describes the slope of the k_r-S curve. The NSDs up to 22% of the optimized value were observed for l, with highest uncertainties for the fractional-wet systems.

Table 8.4: Final optimized parameters with the degree of goodness-of-fit expressed by RMS and their uncertainties expressed by the NSD.

Parameters	Water	10% Ethanol	50% Ethanol	25% FW	50% FW	100% FW
h_m (cm^{-1})	31.9 (0.4)[a]	27.0 (0.7)	16.7 (1.3)	29.2 (1.1)	32.4 (2.6)	30.0 (1.1)
σ (-)	0.32 (0.9)	0.32 (1.3)	0.36 (2.5)	0.51 (1.6)	0.48 (3.1)	0.39 (1.8)
θ_r (-)	0.00 (-[b])	0.00 (-)	0.00 (-)	0.00 (-)	0.00 (-)	0.00 (-)
l (-)	2.27 (4.1)	2.32 (6.1)	2.40 (10.0)	1.92 (7.3)	1.56 (22.6)	0.80 (18.8)
RMS	0.570	0.751	1.380	0.849	1.351	1.081

[a] The number within parenthesis indicates the normalized standard deviate (NSD, %), calculated from (σ_i/b_i)*100 %, where σ_i is the standard deviation of parameter b_i as estimated from the parameter covariance matrix.

[b] Optimized parameter was close to zero, thereby providing a meaningless NSD value.

Figure 8.10 illustrates the typical comparison of measured with optimized Q and h_c for an air-water system. The good agreement between the experimentally measured and optimally simulated system responses indicates that the inversely estimated P_c-S-k_r relationships did indeed characterize the two-fluid system with variable interfacial properties investigated in our study.

Interfacial Tension Effects on k-S-P relationships

Figure 8.11 shows the associated optimized P-S curves corresponding to the parameters listed in Table 8.4. Variable ST and IFT had the expected pressure lowering impact on P-S curves, but no effect on k-S curves for the conditions tested. This result is consistent with that of Dury et al. (1998), who used water, 2%, and 6% butanol solutions as the wetting fluids with surface tension values ranged from 30.8 to 70.3 mN m^{-1}. They found that addition of butanol significantly affects the P-S curves, but had no impact on k-S curves.

Ethanol did not affect significantly θ_r (Table 8.4). We believe that this result is quite reasonable because, for sand packings with simple geometry, θ_r is primarily determined by the pore structure rather than by interfacial tension, viscosity, fluid density, or wettability (Morrow, 1970; Anderson, 1987).

The P_c-S curve for an air-ethanol solution system can be determined from that for air-water system by the modified scaling theory of Leverett (1941) using a ratio of the surface tension (Parker et al., 1987, Lenhard and Parker, 1987; Demond and Roberts, 1991). The scaling theory is defined by

$$h_{c,ae} = \left(\frac{\sigma_{ae}}{\sigma_{aw}} \right) h_{c,aw} \qquad (10)$$

where the subscript *ae* and *aw* indicate air-ethanol and air-water systems, respectively. Figure 2b shows the three P_c-S curves scaled to equivalent h_c values of the air-water system according to Eq. (7) using the surface tension values given in Table 1. Note that the scaled h_c values at a given S_{ew} were a little higher than that of air-water system and the scaled curves showed higher deviation at low S_{ew}. This deviation may be caused by limitations of the Leverett's scaling approach on surface tension only (Demond and Roberts, 1991; Dury et al., 1998).

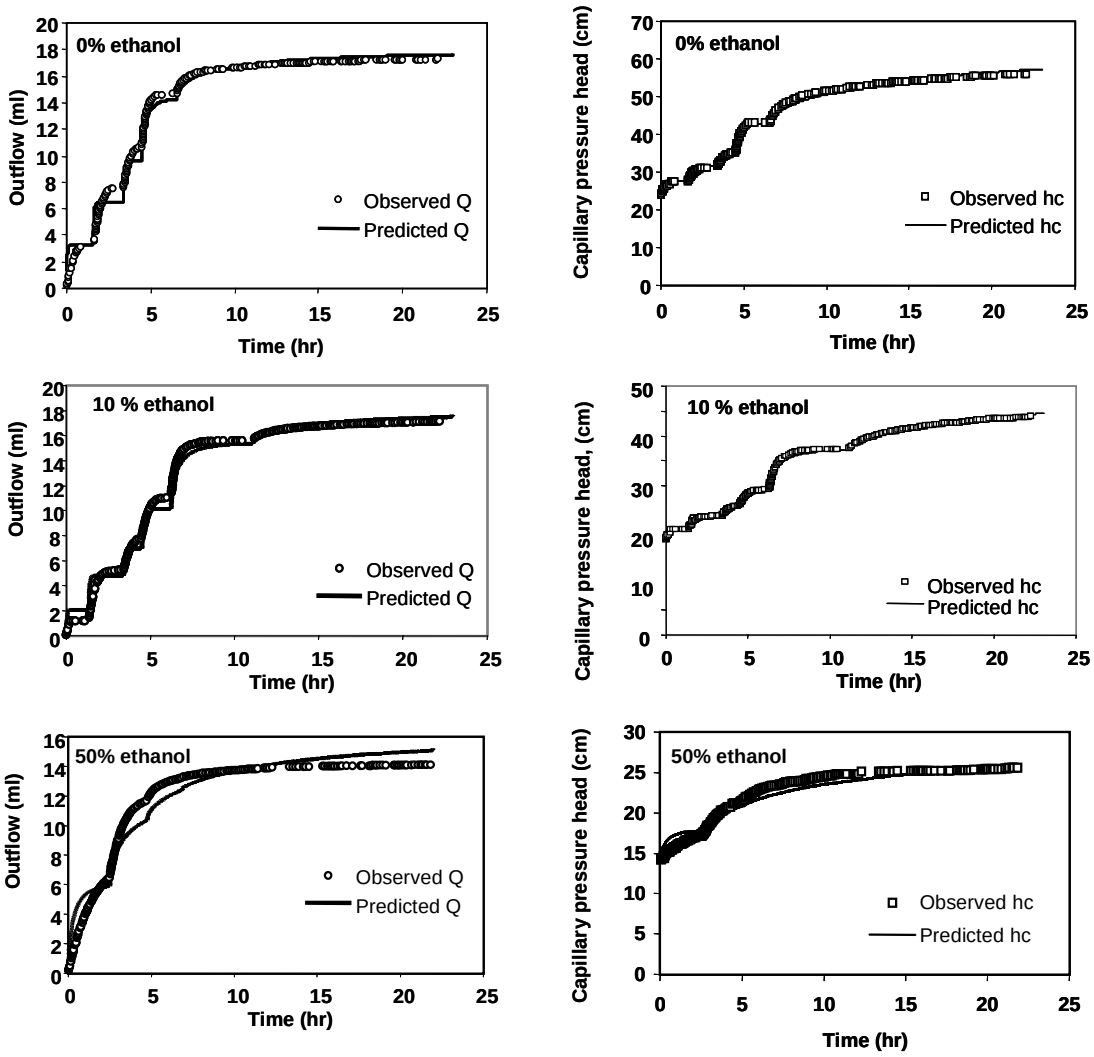

Figure 8.10: Experimental Q and P_c data from multistep outflow experiment with model curves generated by optimizing parameters in the LDM model

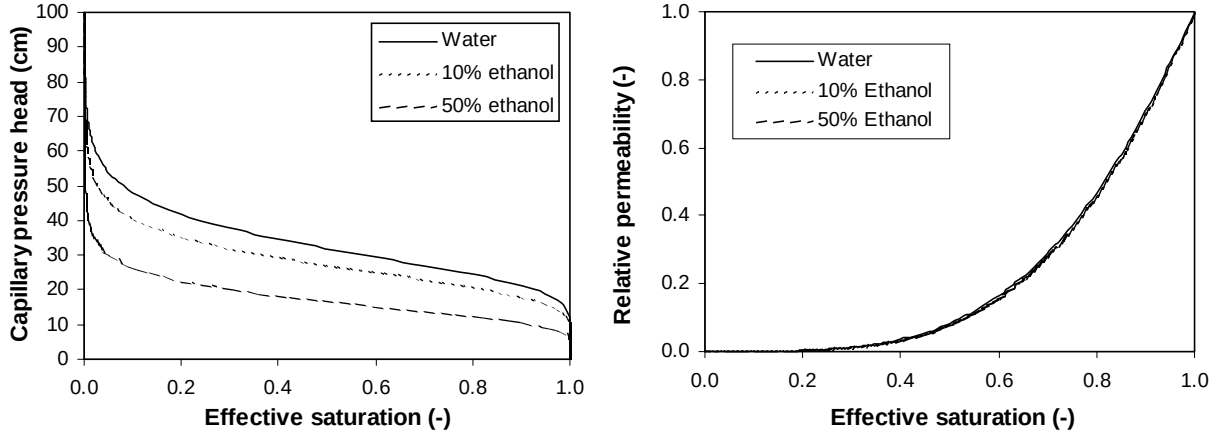

Figure 8.11: Capillary pressure and relative permeability of the wetting phase as a function of saturation – as determined by multistep outflow experiments.

Fractional Wetting Effects on k-S-P Relationships

Little consistency has existed among the experimental results investigating the effect of variable fractional-wet conditions on drainage P_c-S curves in air-water systems. Bradford and Leij (1995) found, in their measurement on primary drainage air-water P_c-S curves, that the curves for 0-50% organosilane-coated media were similar, as were the curves for the 75% and 100% media. They found that the more hydrophobic 75 and 100% media had a lower h_c at a given S_{ew}. Ustohal et al. (1998) used pure and mixtures of natural quartz sand (Qz), organosilane-coated sand (S), and Teflon PFA grains (T) for measurements of hysteretic P_c-S curves. Their drainage experimental data showed that, for Qz-S systems, pure S medium had a lower h_c at a given S_{ew} than pure Qz medium, whereas there was no distinct difference among various mixtures of Qz and S media. For Qz-T systems, the drainage P_c-S curves showed that the more hydrophobic media had a lower h_c at a given S_{ew}. Especially, for pure T medium, the drainage P_c-S curve was in the fully hydrophobic region (h_c <0). Bauters et al. (2000) and Nieber et al. (2000) conducted P_c-S measurements with 0-9% organosilane-coated media. Although Bauters et al. (2000) noted, "once water repellent soils are fully wet, the hydrophobicity disappears and thus, the drainage curves should be the same," their experimental P_c-S data in drainage condition were not the same. The curves for organosilane-coated sands were very similar. The water wettable sand had an air-entry value of about half of those for the organosilane-coated sands. Over the range of S_{ew} from about 0.4 to 0.95, the water wettable sand had a lower h_c at a given S_{ew}. More recently, Bachmann et al. (2001) investigated the effect of wettability on the drainage P_c-S curves for four sandy soils with contact angles ranged from <5^o to 110^o using soil column outflow experiments. Their estimated P_c-S curves showed no consistent trend with respect to the degree of wettability.

In this study, we found from multi-step outflow experiments that in general, at low capillary pressure heads, the decrease in water wetness causes some pores to drain more easily, whereas more water is retained in other pores at higher pressures (Figure 8.12). Especially, the water wetting sand and organosilane-coated sands curves crossed around S_{ew} ranged from 0.2 to 0.6. To ensure this result, we conducted traditional hanging column measurements for the water wetting and 50% organosilane-coated media. These results showed that the crossing happened near S_{ew} of 0.2 and there was no distinct difference between optimized P_c-S curves and traditionally measured curves, indicating that optimized P_c-S curves are quite reasonable.

Our findings show that the drainage P_c-S curves may be not significantly affected by the change of wettability. They illustrate that the nature of capillary fluid flow is not that easily described for the drainage P_c-S curves as affected by the change of wettability. The difference between ours and others mentioned above may be due to (1) the difference of grain-size and pore-size distributions, (2) use of different experimental methods where each experiment has inevitably inherent experimental errors, (3) microscale heterogeneous configuration of water-wet and non-wetting grains during experiments (Hollenbeck and Jensen, 1998; Ataie-Ashtiani et al., 2002), (4) the difference of the initial distribution of the phases among experiments (Hollenbeck and Jensen, 1998; Bauters et al., 2000), and (5) the hydrophobicity of non-wetting grain used (e.g., organosilane-coated vs. Teflon grains in Ustohal et al. (1998)). We believe that our results are reasonable because drainage P_c-S curves are less sensitive to changes in the wettability than the imbibition path (Morrow, 1975). We could not optimize the imbibition P_c-S curves. Bradford and Leij (1995), Ustohal et al. (1998) and Bauters et al. (2000) showed that the imbibition P_c-S curves showed distinct trend regarding the degree of fractional-wet condition.

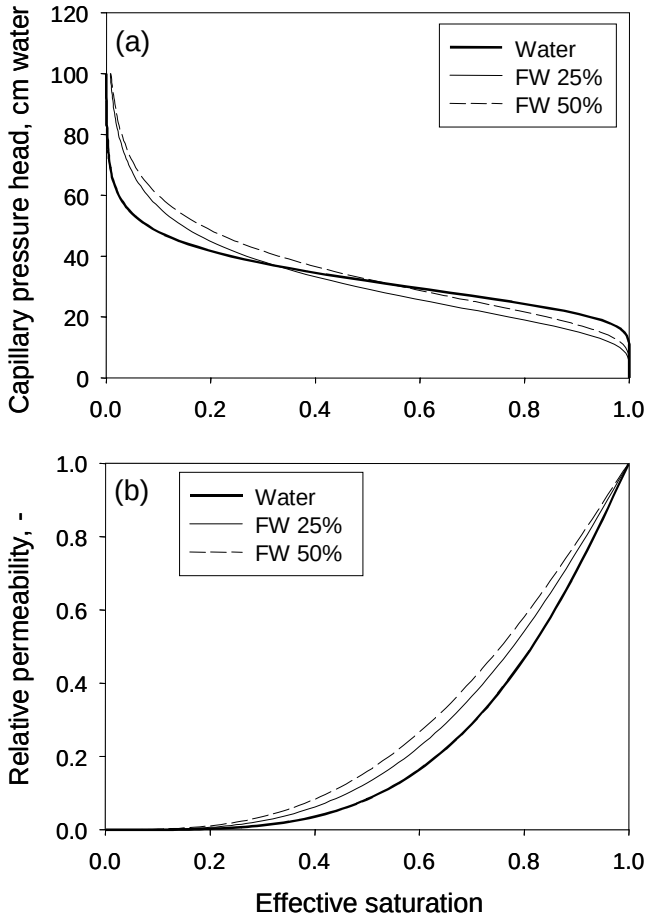

Figure 8-12: Results from multi-step outflow experiments and inverse modeling for medium sands as a function of wettability. The P-S curve for heterogeneous wetting conditions is different than those expected for a system with homogeneous wetting sand grains. The relative permeability in the fractional wetting system is higher than in a water wetting system due to the increased presence of water in larger pore spaces.

Figure 8-12 also shows k_r-S curves as affected by variable fractional-wet conditions. Demond and Roberts (1987) suggested in their review that the contact angle (especially between 49^o and 138^o) appears to have a large effect on the k_r-S curves for NAPL-water systems. However, the effect of fractional wettability on air-water k_r-S curves has not been investigated fully. In our study, the more fractional-wet media had a higher water k_r at a given saturation. This result is consistent with the reported experimental data (Donaldson and Thomas, 1971; Heaviside et al., 1987) and the numerical results of Bradford et al. (1997) for NAPL-water systems. Bradford et al. (1997) developed a k_r-S model resulting from modifying the original Burdine model to incorporate wettability variations. In their model, wetting and less wetting (non-wetting or intermediate) fluid pore classes are used to calculate k_r for water or NAPL. The wettability of the porous medium is used to determine the contributions of the pore classes to k_r. Their model predicted that an increase in the contact angle (or NAPL-wet fraction of a medium) would be accompanied by an increase in the water k_r and a decrease in the NAPL k_r.

Bradford et al. (1997) presented a procedure to estimate k_r values using the pore-size distribution and saturation independent (or dependent) contact angles. Fractional wettability systems can be referred to as saturation dependent contact angles. So, we followed the procedure of Bradford et al. (1997) to estimate the water k_r as a function of non-wetting solid fraction using the predicted P_c-S data and saturation dependent contact angle data. The pore-size distribution was estimated from the predicted water-wet P_c-S

curve and saturation dependent contact angles were obtained assuming zero of contact angle for the water wetting air-water system by

$$\cos(\Theta) = \frac{h_{c,fw}(S_{ew})}{h_{c,ww}(S_{ew})} \tag{8}$$

where the subscript *fw* and *ww* indicate fractional-wet and water-wet systems, respectively. The resulting predicted contact angles and k_r-S curves are shown in Figure 8-13. There was no distinct difference in predicted k_r-S curves for variable fractional-wet systems, indicating that Bradford et al. (1997) model could not explain the variation in k-S curves observed in our experimental results (Figure 8-12).

The increase of water k_r with increase of fractional-wet condition can be explained by the presence of non-wetting solids (Figure 8-14). In water-wet system, air moves in larger pores whereas water moves in smaller pores. In fractional-wet system with equal saturation of water and air, air moves into smaller pores near the non-wetting solids. So, a greater fraction of water moves in larger pores with higher conductivity. So, water relative permeability increases as the fraction of the non-wetting solids increases.

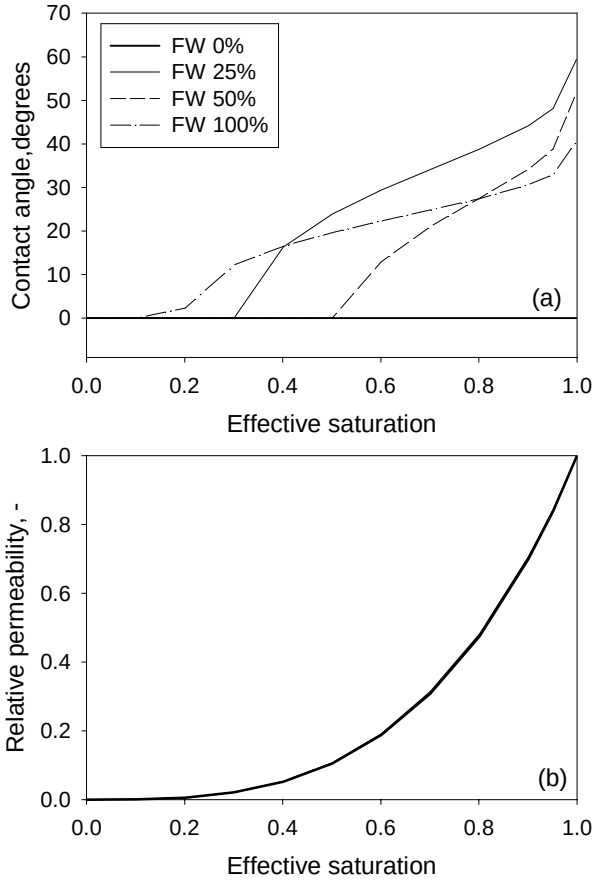

Figure 8-13: Contact angles and relative permeability functions predicted with the Bradford et al. (1997) model

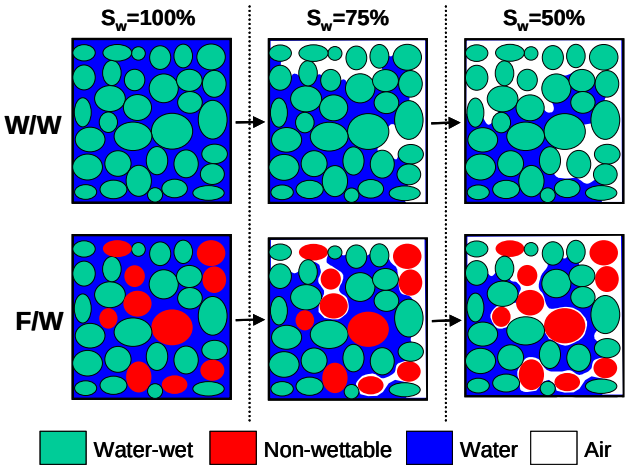

Figure 8-14: Schematic showing hypothetical distribution of air and water fluid during drainage path for water-wet and fractional-wet systems.

8.7 Development of Constitutive Relationships

Based on the observed importance of grain size and surface area observed in field sampling, work related to the development of constitutive relationships focused on estimating P-S curves from particle size data. These efforts utilized published data sets that provided sufficient particle size distribution data along with P-S data.

Basic properties such as the particle size distribution (PSD) and bulk density are widely available for many soil types and can be accurately and routinely determined in laboratories. Hence, formulation of soil hydraulic properties (i.e. capillary pressure and relative permeability (k-S-P)) entirely in terms of basic soil properties should be of considerable benefit. Translation of the PSD into a corresponding P-S curve has been accomplished using the concept that the pore-size distribution is directly related to the PSD (e.g. Arya and Paris, 1981; Haverkamp and Parlange, 1986; Arya et al., 1999). Relationships for k-S can also be computed directly from the PSD based on the assumption that soil pores can be represented by equivalent capillary tubes and that the water flow rate is a function of pore size (Arya et al., 1999). Again, the pore-size distribution is derived from the PSD. These translations of the PSD into corresponding air-water P-S and k-S curves in a soil can be used for estimating hydraulic properties of DNAPL-water system. To do this, the P-S curve of DNAPL-water system is estimated – with a range of success - from that of air-water system through scaling procedure using information of interfacial tension and contact angle. The k-S curve of air-water system could be scaled up to that of DNAPL-water system using information of viscosity ratio.

Therefore, the PSD data can give primary information for predicting DNAPL migration at the field site. However, estimating air-water P-S and k-S curves from the PSD in a soil depends heavily on details or measurement range of the PSD. For example, most PSD data measured at field sites generally have a range of particles >0.002 mm. However, some field site data have suggested the presence of a significant fraction of very fine or colloidal particles. Ignorance of this presence will affect an estimation of dry range of P-S and k-S curves of air-water system because the presence of colloids will change the pore-size distribution. Also, heterogeneity of colloidal particle deposition onto solid grains could also change surface charge properties, resulting in chemical heterogeneity (e.g. fractional wettability) as well as physical heterogeneity (e.g. the change of the pore-size distribution). Therefore, the information on interfacial tension and wettability change induced from colloidal accumulation onto porous media should be included into modeling efforts to predict air-water constitutive relationships from PSD and then DNAPL-water and three-phase relationships from air-water curves.

Figure 8-15 illustrates an example of prediction of water retention curves from the PSDs using the Arya-Paris model (1981, 1999) for specific real soil data from the SRS site. Neither water retention curves predicted using the PSDs matched measured data, indicating that prediction of water retention characteristic based on the assumption of random packing of all particle size does not adequately represent real soil packing condition. In a soil with fine particles (Fig. 8-15, 26-28 ft), the predicted water retention curve is characterized by a well-defined air-entry value, indicating narrow particle-size distribution and thus narrow pore-size distribution (Fig. 8-15 (a)). However, the real water retention data showed more broad pore-size distribution. We believe that this is due to heterogeneity of colloid deposition onto solid grains, making the pore size distribution more broad.

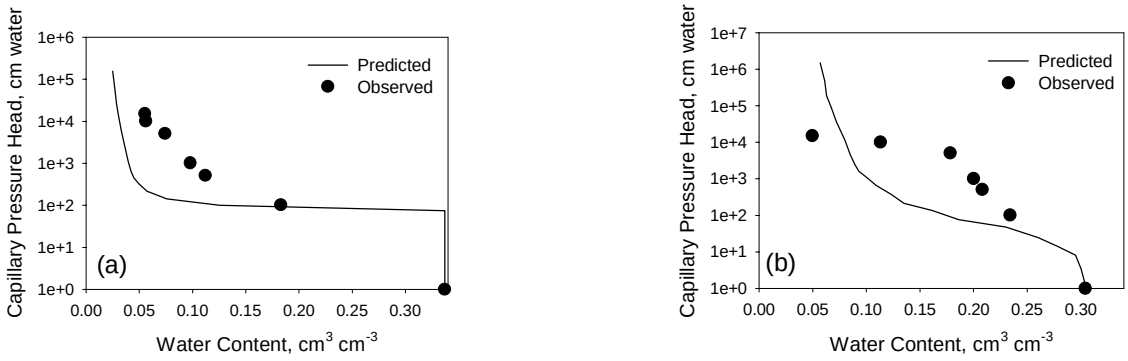

Figure 8-15: Comparison of experimental water retention curves for SRS soil with theoretical retention curves derived from particle size distribution measurements (Arya-Paris, 1999) (a) NSB-4 (26-28 ft) and (b) NSB-4 (16-18ft).

8.8 Conclusions

The fractal dimension and fractal coefficients determined here were used to describe the interface characteristics and calculate the entrapped interfacial areas. These conditions resulted in different interface characteristics when affected by micromodel orientation and interfacial tension. A method to determine microscopic interface lengths was given by Smith and Zhang (2000) using fractal analysis. The finger characteristics reported by Smith and Zhang (2000) as well as Chao et al. (2000) were observed.

The fractal dimension and fractal coefficients have been shown to change with different experimental conditions and can be used to describe such systems. The continuous phase interface length remained relatively constant when compared to the overall interface length. Thus indicating that surface tension is important in the resultant entrapped interfacial lengths during NWPI and WPI. During NWP more interfacial area would be available at lower interfacial tensions for the physicochemical processes of different remediation strategies. Alternatively, during WPI such remediation strategies will be more effective when used in high interfacial tension systems, with an increase in the interfacial areas.

Using multi-step outflow techniques, we estimated P_c-S-k_r parameters for air-aqueous phase systems with variable interfacial properties, mainly the change of surface tension and fractional wettability. To get variable surface tensions and fractional-wet systems, we used ethanol and mixtures of organosilane-coated sand, respectively. As expected, addition of ethanol strongly lowered h_c at a given S_{ew}. On the other hand, k_r-S curves were not affected by surface tension.

We found that the fractional-wet media did not affect significantly the drainage P_c-S-k_r curves. This finding confirms that drainage P_c-S curves are less sensitive to changes in the wettability than the imbibition path (Morrow, 1975). On the other hand, the more hydrophobic media had a higher water/aqueous phase k_r at a given saturation.

Our results provide a starting point for predicting the P_c-S-k_r functions for two-fluid systems as influenced by variable interfacial properties. To do these completely, we will test a wider range of interfacial properties (e.g. much lower surface tension).

References

Anderson, W.G., 1987. Wettability literature survey: IV. Effects of wettability on capillary pressure. J. Petr. Technol. 10, 1283-1300.

Anderson, R., G.Larson, C. Smith, 1991. Silicon compounds: Register and review. 5th Edition. Huls America Inc.

Arya, L.M., J.F. Paris. 1981. A physicoempirical model to predict the soil moisture characteristic from particle-size distribution and bulk density data. Soil Sci. Soc. Am. J. 45:1023-1030.

Arya, L.M., F.J. Leij, M.Th. van Genuchten, P.J. Shouse. 1999. Scaling parameter to predict the soil water characteristic from particle-size distribution data. Soil Sci. Soc. Am. J. 63:510-519.

ASTM, 1995. Standard test method for acid number of petroleum products by potentiometric titration. Designated D 664-95.

ASTM, 1991. Standard test method for interfacial tension of oil against water by the ring method. Designation D 971-91

Ataie-Ashtiani, B., S.M. Hassanizadeh, M.A. Celia, 2002. Effects of heterogeneities on capillary pressure-saturation-relative permeability relationships. J. Contam. Hydrol. 56, 175-192.

Bachmann, J., R. Horton, R.R. van der Ploeg, 2001. Isothermal and nonisothermal evaporation from four sandy soils of different water repellency. Soil Sci. Soc. Am. J. 65, 1599-1607.

Bauters, T.W.J., T.S. Steenhuis, D.A. DiCarlo, J.L. Nieber, L.W. Dekker, C.J. Ritsema, J.-Y. Parlange, R. Haverkamp, 2000. Physics of water repellent soils. J. Hydrol. 231-232, 233-243.

Beverung, C. J., C. J Radke, H. W. Blanch, 1999. Protein adsorption at the oil/water interface: characterization of adsorption kinetics by dynamic interfacial tension measurements. Biophysical Chemistry 81(1): 59-80.

BHI, 1996. *Design, Operations, and Maintenance of the Soil Vapor Extraction Systems for the 200 West Area Carbon Tetrachloride Expedited Response Action.* BHI-00365, Rev. 0, Bechtel Hanford, Inc., Richland, Washington.

Bradford, S.A., L.M. Abriola, F.J. Leij, 1997. Wettability effects on two- and three-fluid relative permeabilities. J. Contam. Hydrol. 28: 171-191.

Bradford, S.A., F.J. Leij, 1995. Fractional wettability effects on two- and three-fluid capillary pressure-saturation relations. J. Contam. Hydrol. 20: 89-109.

Briandet, R., T. Meylheuc, C.Maher, M.N. Bellon-Fontaine, 1999. Listeria monocytogenes Scott A: Cell Surface Charge, Hydrophobicity, and Electron Donor and Acceptor Characteristics under Different Environmental Growth Conditions. Appl. Envir. Microbiol. 65: 5328-5333

Bruss D. B, G. E. A. Wyld, 1957. Methyl isobutyl ketone as a wide-range solvent for titration of acid mixtures and nitrogen bases. Anal. Chem. 29: 232-235.

Celia, M.A., P. Binning, 1992. A mass conservative numerical solution for two-phase flow in porous media with application to unsaturated flow. Water Resour. Res. 28: 2819-2828.

Chang, W., Biggar, J., D. Neilson, 1994. Fractal description of wetting front instability in layered soil, *Water Resour. Res.* 30: 125-132.

Chao, W., J. Parlange, T. Steenhuis, 2000. An analysis of the movement of wetting and nonwetting fluids in homogeneous porous media, *Transport in Porous Media*. 41: 121-135.

Chen J, J.W. Hopmans, M.E. Grismer., 1999. Parameter estimation of two-fluid capillary pressure-saturation and permeability functions. Adv. Water Resour. 22: 479-493.

Chorover, J., G. Sposito, 1995. Dissolution behavior of kaolinitic tropical soils. Geochimica et Cosmochimica Acta. 59: 3109-3121.

Corey A.T., R.H. Brooks, 1999. The Brooks-Corey relationships. In: van Genuchten MTH, Leij FJ, Wu L, editors. Characterization and measurement of the hydraulic properties of unsaturated porous media. Riverside, CA: University of California, p.13-18.

Demond, A.H., P.V. Roberts, 1987. An examination of relative permeability relations for two-phase flow in porous media. Water Resour. Bull. 23: 617-628.

Demond, A.H., P.V. Roberts, 1991. Effects of interfacial forces on two-phase capillary pressure-saturation relationships. Water Resour. Res. 27: 423-437.

Denham, M.E., J.R. Kastner, K.M. Jerome, J. Santo Domingo, B.B. Looney, M.M. Franck, and J.V. Noonkester, 1999. Effects of Fenton's Reagent on Aquifer Geochemistry and Microbiology at the A/M Area, Savannah River Site, WSRC-TR-99-00428. Aiken, South Carolina 29808, Westinghouse Savannah River Company.

DiStefano, T.D., J.M. Gossett, and S.H. Zinder, 1992. Hydrogen as an Electron Donor for Dechlorination of Tetrachloroethene by an Anaerobic Mixed Culture. *Applied and Environmental Microbiology.* 58: 3622-3629.

Donaldson, E.C., R.D. Thomas, 1971. Microscopic observations of oil displacement in water-wet and oil-wet systems. SPE paper No. 3555, SPE Annual Meetings, New Orleans, LO.

Doty, T., 2003. The Role of Microorganisms on DNAPL Interfacial Properties and Distribution**,** Masters Thesis, Department Civil and Environmental Engineering, Clarkson University, Potsdam, NY.

Doty, T., K. Omrane, S.E. Powers, S.J. Grimberg (in preparation). The Role of PCE Degrading Microorganisms on DNAPL Interfacial Properties.

Dury, O., U. Fischer, R. Schulin, 1998. Dependence of hydraulic and pneumatic characteristics of soils on a dissolved organic compound, J. Contam. Hydrol. 33: 39-57.

Eddy-Dilek, C. A., B. B. Looney, J. Dougherty, T. C. Hazen, D. S. Kaback, 1991. *Characterization of the Geology, Geochemistry, Hydrology, and Microbiology of the In Situ Air Stripping Demonstration Site at the Savannah River Site.* Westinghouse Savannah River Co., Aiken, South Carolina. WSRC-RD-91-21. 118 pp. + app.

Eddy-Dilek, C. A., B. B. Looney, T. C. Hazen, R. L. Nichols, C. B. Fliermans, W. H. Parker, J. M. Dougherty, D. S. Kaback, J. L. Simmons, 1993. Post-test evaluation of the geology, geochemistry, microbiology, and hydrology of the in situ air stripping demonstration site at the Savannah River Site. Westinghouse Savannah River Company. Technical Report WSRC-TR-93-369.

Gephardt, P., R.G.E. Murray, W.A. Wood, N.R. Krieg, 1994. *Methods for General and Molecular Biology,* American Society for Microbiology, Washington, D.C.

Gossett, J. M., D. E. Fennell, S.H. Zinder, 1997. Comparison of Butyric Acid, Ethanol, Lactic Acid, and Propionic Acid as Hydrogen Donors for the Reductive Dechlorination of Tetrachloroethene. *Environ. Sci. Technol.* 31: 918-926.

Havercamp, R., J.Y. Parlange, 1986. Predicting the water-retention curve from a particle-size distribution: 1. Sandy soils without organic matter. Soil. Sci. 142: 325-339.

He, T., W. Tian, G. Zhang, G. Chen, Z. Zhang, 1998. Production of novel polyhydroxyalkanoates by pseudomonas stutzeri 1317 from glucose and soybean oil. Ferm Microbiology letters. 169: 45-49.

Heaviside, J., C.E. Brown, I.J.A. Gamble, 1987. Relative permeability for intermediate wettability reservoirs. SPE paper No. 16968. Dallas, TX.

Held, R. M. Celia, 2000. Modeling support of functional relationships between capillary pressure, saturation, interfacial area, and common lines, *Adv. Water Resour.* 24: 325-343.

Hirasaki, G. J., 1991. Wettability: Fundamentals and surface forces. SPE Form. Eval. 6: 217-226

Hoeiland, S. T., B.A. M. Blokhus, A. Skauge, 2001. The effect of crude oil acid fractions on wettability as studied by interfacial tension and contact angle. J. Sci. Eng. 30: 91-103.

Hollenbeck, K.J., K.H. Jensen, 1998. Experimental evidence of randomness and non-uniqueness in unsaturated outflow experiments designed for hydraulic parameter estimation. Water Resour. Res. 34: 595-602.

Hopkins, G. D., L. Semprini, P.L. McCarty, 1993. Microcosm and in situ field studies of enhanced biotransformation of trichloroethylene by phenol-utilizing microorganisms. Appl Environ Microbiol. 59: 2277-85

Hopmans, J.W., T. Vogel, P.D. Koblik, 1992. X-ray tomography of soil water distribution in one-step outflow experiments. Soil Sci Soc Am J. 56: 355-362.

Hopmans. J.W., M.E. Grismer, J. Chen, Y.P. Liu, B.K. Lien, 1998. Parameter estimation of two-fluid capillary pressure-saturation and permeability functions. EPA/600/R-98/046, National Risk Management Research Lab., Office of Research and Development, U.S. EPA, Cincinnati, OH.

Huertas, F. J., L. Chou et al., 1998. Mechanism of Kaolinite Dissolution at Room Temperature and Pressure: Part 1. Surface Speciation. Geochimica et Cosmochimica Acta. 62: 417-431.

Huling, S. G., J.W. Weaver, 1991. Dense Non Aqueous Phase Liquid. Ground water issue. EPA/540/4-91-002

Hurst, C.J., G.R. Knudsen, M.J. McInerney, L.D. Stetzenbach, M.V. Walter, 1996. Manual of Environmental Microbiology. ASM Press.

Jackson, D. G., T. Payne, et al., 1996. Estimating the Extent and Thickness of DNAPL within the A/M Area of the Savannah River Site (U). Aiken, South Carolina 29808, Westinghouse Savannah River Company.

Jackson, D. G., W. K. Hyde, et al., 1999. Characterization Activities to Determine the Extent of DNAPL in the Vadose Zone at the A-014 Outfall of A/M Area (U). Aiken, South Carolina 29808, Westinghouse Savannah River Company.

Keshavarz, E., S. Nakai, 1979. The relationship between hydrophobicity and interfacial tension of proteins. Biochimica et Biophysica Acta - Protein Structure. 576: 269-279

Kieffer, B., C. F. Jové, et al. 1999. An experimental study of the reactive surface area of the Fontainebleau sandstone as a function of porosity, permeability, and fluid flow rate. Geochimica et Cosmochimica Acta. 63: 3525-3534.

Klein, J., P. Dhurjati, 1995. Protein aggregation kinetics in an Escherishia coli strain overexpressing a *salmonella typhiurium* CheY Mutant gene. Appl. Envir. Microbiol. 61: 1220-1225.

Klute A, C. Dirksen, 1986. Conductivities and diffusivities of unsaturated soils. In: Klute A, editor. Methods of soil analysis, Part 1. 2nd ed. Agron. Monogr. 9. ASA and SSSA, Madison, WI. p.687-734

Kosugi K., 1996. Lognormal distribution model for unsaturated soil hydraulic properties. Water Resour Res. 32: 2697-2703.

Krumholz, L.R., R. Sharp, S. Fishbain, 1996. *A Freshwater Anerobe Coupling Acetate Oxidation to Tetrachloroethylene Dehalogenation.* App. Environ. Microbiol. 62: 4108-4113.

Kueper, B. H, E. O. Frind, 1988. An Overview of Immiscible Fingering in Porous Media, J. Contam. Hydrol. 2: 95-110.

Kueper, B. H., G. Farquhar, 1989. Experimental Observations of Multiphase Flow in Heterogeneous Porous Media, J. Contam. Hydrol. 5:83-95.

Langmuir, D., 1997. Aqueous Environmental Geochemistry. Upper Saddle River, NJ, Prentice-Hall, Inc.

Lefevre, G., M. Rocher, G. Braunegg, 1997. Effect of dissolved oxygen concentration on Poly(3-Hydroxybutyrate-co-Hydroxyvalerate) production by *Alcaligenes eutrophus.* Appl. Envir. Microbiol. 63: 827-833

Lenhard, R.J., J.C. Parker, 1987. Measurement and prediction of saturation-pressure relationships in three-phase porous media systems. J. Contam. Hydrol. 1: 407-424.

Leverett, M.C., 1941. Capillary behavior in porous solids. Trans. Am. Inst. Min. Metall. Pet. Eng. 142, 152-169.

Liu, H., J. Dane, 1996. A criterion for gravitational instability in miscible dense plumes, *J. Contam. Hydrol.* 23: 233-243.

Liu Y.P., J.W. Hopmans, M.E. Grismer, J.Y. Chen. 1998. Direct estimation of air-oil and oil-water capillary pressure and permeability relations from multi-step outflow experiments. J Contam Hydrol. 32: 223-245.

Looney, B. B., J. Rossabi, et al., 1992. Assessing DNAPL Contamination, A/M-Area, Savannah River Site: Phase I Results (U). Aiken, South Carolina 29808. Westinghouse Savannah River Company.

Lord, D.L., K. F. Hayes, A. H. Demond, A. Salehzadeh, 1997. Influence of Organic Acid Solution Chemistry on Subsurface Transport Properties, I. Surface and Interfacial Tension. Environ. Sci. Technol. 31: 2045-2051

Majid, M. I. A., D. H. Akmal, L. L. Few, A. Agustien, M. S. Toh, M. R. Samian, N. Najimudin, M. N. Azizan, 1999. Production of poly(3-hydroxybutyrate) and its copolymer poly(3-hydroxybutyrate-*co*-3-hydroxyvalerate) by *Erwinia* sp. USMI-20. International Journal of Biological Maromolecules. 25: 95-104.

Maloy, K., J. Feder, T. Jossang, 1985. Viscous fingering fractals in porous media, *Physical Review Letters*. 55: 2688-2691.

Mandelbrot, B.B., 1983. The Fractal Geometry of Nature. W.H. Freeman and Company, San Francisco, California.

McDougall, S., K. Sorbie, 1995. The impact of wettability on waterflooding: Pore-scale simulation, *SPE Reservoir Engineering.* 10: 208-213.

McDowell, C. J. 2002. Effects of Ethanol on the Migration and Distribution of gasoline in the Subsurface. Master thesis, Department of Civil and Environmental Engineering, Clarkson University, Potsdam, NY

Morrow, N.R., 1970. Irreducible wetting-phase saturations in porous media. Chem. Eng. Sci. 25: 1799-1815.

Nieber, J.L., T.W.J. Bauters, T.S. Steenhuis, J.-Y. Parlange, 2000. Numerical simulation of experimental gravity-driven unstable flow in water repellent sand. J. Hydrol. 231-232, 295-307.

Nittman, J., G. Daccord, H. Stanely, 1985. Fractal growth of viscous fingers: quantitative characterization of a fluid instability phenomenon. *Nature*, 314: 141-144.

Ogawa, S., P. Baveye, C. Boast, J-Y. Parlange, T. Steenhuis, 1999. Surface fractal characteristics of preferential flow patterns in field soils: evaluation and effect of image processing, *Geoderma*, 88: 109-136.

Oostrom, M., M. White, M. Brusseau, 2001. Theoretical estimation of free and entrapped nonwetting-wetting fluid interfacial areas in porous media, *Adv. Water Resour.* 24: 887-898.

Oxaal, U., M. Murat, F. Boger, A. Aharony, J. Feder, T. Jossang, 1987. Viscous fingering in percolation clusters, *Nature*, 329: 32-37.

Parker, J.C., Lenhard, R.J., Kuppusamy, T., 1987. A parametric model for constitutive properties governing multiphase flow in porous media. Water Resour. Res. 23, 618-624.

Pickett, J. B., W. P. Colven, et al., 1987. Environmental Information Document: M-Area Settling Basin and Vicinity. Aiken, South Carolina 29808. Savannah River Laboratory, E. I. duPont de Nemours & Company.

Prakash, S.T., S. K. Gupta, 2000. Effect of Carbon Source on PCE Dehalogenation. J.Environ. Engrg. 126: 622-628.

Marine, I. W., H. Bledsoe, 1984. Supplemental Technical Data Summary: M-Area Groundwater Investigation. Aiken, South Carolina 29808. Savannah River Laboratory, E. I. duPont de Nemours & Company.

Pankow, J. F., J. A. Cherry, 1996. Dense Chlorinated Solvents and Other DNAPLs in Groundwater. Waterloo Press, Portland, OR. pp522

Powers, S. E., W. H Anckner., T. F Seacord, 1996. Wettability of NAPL-conataminated sands. J. Environ. Eng. 122: 889-896.

Rijnaarts, H. H. M., W. Norde, J. Lyklema, A.J.B. Zehnder, 1995. The isoelectric point of bacteria as an indicator for the presence of cell surface polymers that inhibit adhesion. Colloid and Surfaces B. 4: 191-197.

Rimmer, A., J. Parlange, T. Steenhuis, C. Darnault, W. Condit, 1996. Wetting and nonwetting fluid displacements in porous media. *Transport in Porous Media*. 25: 205-215.

Rosemberg, M., 1991. Basic and applied aspects of microbial adhesion a the hydrocarbon: water interface. Critical reviews in microbiology. 18: 59-173.

Scheidegger, A., M. Borkovec, H. Sticher, 1992. Coating of silica sand with goethite: preparation and analytical identification. Geoderma, 58: 43-65.

Shackelford, J., S.J. Grimberg, 2001. Favorable Growth Conditions for TCE Bioremediation at the Savannah River Site. *Presented at* the Annual Summer Undergraduate Research Symposium, Clarkson University, Potsdam, NY.

Smatlak, C.R., J.M. Gossett, S.H. Zinder, 1996. Comparitive kinetics of hydrogen utilization for reductive dechlorination of tetrachloroethene and methanogenesis in an anaerobic enrichment culture. *Environ. Sci. Technol.* 30: 2850-2858.

Smith, J., Z. Zhang, 2000. Determining effective interfacial tension and predicting finger spacing for DNAPL penetration into water-saturated porous media. *J. Contam. Hydrol.* 48: 167-183.

Strom, R., D. Kaback, 1992. Groundwater Geochemistry of the Savannah River Site and Vicinity, WSRC-RP-92-450, Aiken, South Carolina, Westinghouse Savannah River Company.

Tung, K., J. Parlange, 1976. Note on the motion of long bubbles in closed tubes – Influence of surface tension, *Acta Mech*. 24: 313-317.

Ustohal, P., F. Stauffer, T. Dracos, 1998. Measurement and modeling of hydraulic characteristics of unsaturated porous media with mixed wettability. J. Contam. Hydrol. 33: 5-37.

van der Vegt, W., W. Norde, H. C. van der Mei, H. J. Busscher, 1996. Kinetics of Interfacial Tension Changes during Protein Adsorption from Sessile Droplets on FEP–Teflon. Interface Science. 179: 57-65.

Van Schie P.M, M. Fletcher, 1999. Adhesion of Biodegradative Anaerobic Bacteria to Solid Surfaces. 65: 5082–5088

Vogel, T. M., P. L. McCarthy, 1985. Biotransformation of Tetrachloroethylene to Trichloroethylene, Dichloroethylene, Vinyl Chloride, and Carbon Dioxide under Methanogenic Conditions. *App. Environ. Microbiol.* 49: 1080-1083.

Warfel, M., 1998. Characterization of Particles from Wastewater and Sludge Treatment Facilities by Size and Morphology. *Thesis for the degree of Masters of Science.* Cornell University, Ithaca NY.

White, A. F., A. E. Blum, et al., 1996. Chemical Weathering Rates of a Soil Chronosequence on Granitic Alluvium: I. Quantification of Mineralogical and Surface Area Changes and Calculation of Primary Silicate Reaction Rates. Geochimica et Cosmochimica Acta. 60: 2533-2550.

Wildenschild, D., J.W. Hopmans, J. Šimůnek, 2001. Flow rate dependence of soil hydraulic characteristics. Soil Sci Soc Am J. 65: 35-48.

Xie, Z., J. V. Walther, 1992. Incongruent dissolution and surface area of kaolinite. Geochimica et Cosmochimica Acta, 56: 3357-3363.

Yang, Y., P. L. McCarthy, 1998. Competition for Hydrogen within a Chlorinated Solvent Dehalogenating Anaerobic Mixed Culture. *Environ. Sci. Technol.* 32: 3591-3597.

Yu, L. N.C.Wardlaw, 1985. Mechanisms of nonwetting phase trapping during imbibition at slow rates, *Journal of Colloidal and Interfacial Science* 109: 473-485.

Zhang, L., L. Lan, S. Zhao, J. Yu, 2002. Studies of Synergism/Antagonism for Lowering Dynamic Interfacial Tensions in Surfactant/Alkali/Acidic Oil Systems, Part 2: Synergism/Antagonism in Binary Surfactant Mixtures. J. Coll. Inter. Sci. 251: 166–171

Zheng. J., S. E. Powers, 1999. Organic bases and their impact on wettability. J. Contam. Hydrol. 39: 161-181.

Zheng, J., S. Behrens, M. Borkovec, S.E. Powers, 2001. Predicting the Wettability of Quartz Surfaces Exposed to Dense Non-aqueous Phase Liquids. *Environ. Sci. Technol*. 35: 2207-2213.

Zheng, J., S.E. Powers, 2003. Identifying the Effects of Polar Constituents in Coal-Derived DNAPLs on Interfacial Tension. *Environ. Sci. Technol*. in press.